GENIUS

a Supersensitive Germanium Detector System for Rare Events

H.V. Klapdor–Kleingrothaus, L. Baudis, G. Heusser, B. Majorovits,
H. Päs
Max–Planck–Institut für Kernphysik, Heidelberg, Germany

August 1999

The GENIUS collaboration includes groups from:
MPIK Heidelberg, Germany; Inst. of Nucl. Research, Kiev, Ukraine; Physik. Techn. Bundesanstalt, Braunschweig, Germany; Internat. Center for Theoret. Physics, Trieste, Italy; JINR Dubna, Russia; Inst. of Radiophys. Research, Nishnij Novgorod, Russia; Dep. of Physics, Northeastern Univ. Boston, USA; Dep. of Physics, Univ. of Maryland, USA; Los Alamos Nat. Lab., USA; Dep. de Fisica Teorica, Univ. of Valencia, Spain; Dep. of Physics, Texas A&M Univ., USA

Spokesman of the Collaboration: H. V. Klapdor–Kleingrothaus

MPI-Report MPI-H-V26-1999

The GENIUS Collaboration

Status September 1999

H. V. Klapdor–Kleingrothaus*,L. Baudis, A. Dietz, G. Heusser, St. Kolb, B. Majorovits, H. Päs, F. Schwamm, H. Strecker
Max–Planck–Institut für Kernphysik, Heidelberg, Germany

O.A. Ponkratenko, V.I. Tretyak, Yu.G. Zdesenko
Institute of Nuclear research, Kiev, Ukraine

V. Alexeev, A. Balysh, A. Bakalyarov, S. T. Belyaev, V. I. Lebedev, S. Zhukov
Kurchatov Institute, Moscow, Russia

U. Keyser, A. Paul, S. Röttger, A. Zimbal
Physikalisch-Technische Bundesanstalt, Braunschweig, Germany

A. Yu. Smirnov
Internat. Center for Theoretical Physics, Trieste, Italy

V. Bednyakov
Joint Institute for Nuclear Research, Dubna, Russia

I.V. Krivosheina, V. Melnikov
Institute of Radiophysical Research, Nishnij Novgorod, Russia

P. Nath
Department of Physics, Northeastern University, Boston, USA

R.N. Mohapatra
Department of Physics, University of Maryland, USA

J.W.F Valle
Departamento de Fisica Teorica, University of Valencia, Spain

R. Arnowitt
Department of Physics, Texas A&M University, USA

* Spokesman of the Collaboration

1. The New Physics Potential of GENIUS

1.1. Introduction

Two outstanding problems in contemporary astro- and particle physics are the nature of the dark matter in the Universe and the question for the neutrino mass. There is compelling evidence on all cosmological scales that the dominant form of matter is nonbaryonic [Kol94]. Attractive candidates for nonbaryonic dark matter are relic elementary particles left over from the big bang, the three most promising being neutrinos, axions and neutralinos [Jun96].

There is significant evidence from theories of structure formation against neutrinos as the bulk of dark matter. A mixed hot plus cold dark matter scenario still gives the better fit to the CMB and LSS-data [Gaw98]. Recently ΛCDM scenarios have become the most attractive ones [Tur99].

To adress both issues we propose the GENIUS experiment [Kla98, Kla98b]. The optimal locations would be the Gran Sasso or WIPP underground laboratories. GENIUS, using ionization in a Ge detector as detection technique, would operate naked Ge crystals in ultrapure liquid nitrogen. The aim is to reach the background level of 10^{-3} events/kg y keV in the low energy region, thus to cover most of the parameter space predicted for neutralinos in the MSSM, and to be sensitive to the low-energy pp and ^{7}Be solar neutrino flux. In the energy region of the $0\nu\beta\beta$ -decay of ^{76}Ge the goal is to reach a count rate of 0.3 events/t y keV, thus testing the effective Majorana neutrino mass down to 0.01 eV for one ton of enriched ^{76}Ge (0.001 eV for ten tons). While for dark matter search only 100 kg of natural Ge are needed as detectors, an amount of the order of one ton of (natural or enriched) Ge would allow to observe for the first time pp neutrinos in a real-time measurement.

In addition to the unique information on neutrino masses and mixings obtainable, GENIUS would allow also a breakthrough into the multi-TeV range for many other beyond standard models of particle physics, such as supersymmetry (R-parity breaking, sneutrino mass), compositeness, right-handed W boson mass, test of special relativity and equivalence principle in the neutrino sector, and others, competitive to corresponding research at future high-energy colliders.

1.2. Direct Dark Matter Detection

1.2.1. Three dark matter problems There is evidence on all cosmological scales that most of the matter in our Universe is dark. The quantity and composition of dark matter is of fundamental importance in cosmology.

We know of three so-called dark matter problems at present: the bulk of baryonic matter is dark; the dominant form of matter is nonbaryonic; an

additional dark, exotic form of energy contributes about 60% to the critical density Ω_0.

A precise determination of the universal baryon density is provided by the big-bang nucleosynthesis (BBN). Comparison of the measured primeval deuterium abundance with its big-bang prediction yields a baryon density of $\Omega_B h^2 = 0.019 \pm 0.0012$ [Bur99a]. However, clusters of galaxies account only for about 10% of the baryons [Per92]. Promising candidates for the dark baryons are so-called MACHOS. The search for MACHOs in the halo of our own galaxy, in form of planets, white and brown dwarfs or primordial black holes, exploits the gravitational microlensing effect, the temporary brightening of a background star as an unseen object passes close to the line of sight. For several years two groups are monitoring the brightness of millions of stars in the Magellanic clouds, the MACHO [Alc97] and the EROS [ERO98] collaborations. Several candidates have already been detected. If interpreted as dark matter they would make up half the amount needed in the galactic halo. The most probable mass of these candidates, which can be inferred from the duration of a stars brightening together with the lense distance, is about half the solar mass. However, no stellar candidate seems able to explain the observations. Measurements of carbon abundances in Lyman α forest lines speak against white dwarfs, even if their masses lie in the expected region [Fre99]. The possibility remains, that MACHOs are an exotic form of baryonic matter, like primordial black holes, or that they are not located in the halo of our galaxy [Gri99]. Two events which have been discovered in the direction of the Small Magellanic Cloud underline this hypothesis; both lenses are stars within the satellite galaxy itself [Mon99].

Clusters of galaxies provide very reliable methods of estimating the total matter density [Whi93]. They are the largest observed structures, which in part already attained hydrostatic equilibrium. The relative amount of baryons and dark matter within their hydrostatic region provides a measure of the cosmic mix of these components. The baryonic component of rich clusters is dominated by the X-ray emitting intracluster gas. Using the cluster baryon fraction determined from X-ray measurements and assuming that clusters provide a fair sample of matter in the Universe, a matter density of about a third of the critical density (i.e. a flat Universe) is inferred [Evr98].

There are many other methods of inferring the total matter density, involving different physics.

For example, compelling evidence for both baryonic and nonbaryonic dark matter comes from observation of the rotation curves of galaxies. In particular the rotation curves of dwarf spirals are completely dark matter dominated [Bur99]. Also distant field galaxies, which are much younger than nearby galaxies are entirely embedded in dark halos [Fuc99]. This is

indeed expected from theories of galaxy cosmogony, where the dark matter haloes themselves are thought to be the sites of galaxy formation.

On the other side, there is strong evidence from structure formation that the total matter density, Ω_M is significantly greater then the density of baryons, Ω_B [Dod96].

Evidence for an additional dark, smoothly distributed form of energy comes from observation of distant supernovae of type Ia. By measuring the deviation of the Hubble law from linearity at high redshifts, the acceleration or deceleration of the expansion can be determined. Objects with well understood properties, which can be observed up to very large distance (standard candles) are type Ia supernovae, thermonuclear explosions of white dwarfs in binary systems. Two groups succeeded in measuring distances to some 50 supernovae type Ia [Per98, Rie98]. The measurements indicate that the Universe is speeding up, the simplest explanation being a so-called cosmological constant, a smooth contribution to the energy density of the Universe, which cannot clump. Such a contribution is also supported by inflation, since the dynamically determined matter density ($\Omega_M \simeq 0.4$) is too low to yield the predicted flat Universe ($\Omega_0 = 1$).

A summary of the matter/energy composition of the Universe is shown in Fig. 1 (from [Tur99]).

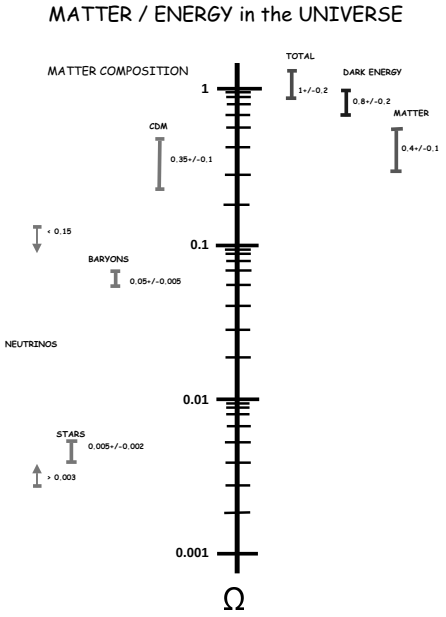

Figure 1. Summary of an overall accounting of matter and energy in the Universe, from [Tur99]

1.2.2. Nonbaryonic dark matter candidates From the nonbaryonic dark matter candidates proposed in the 1980s, only WIMPs (weakly interacting massive particles) and axions survived [Kam99]. WIMPs, which arise in supersymmetric or other theories beyond the standard model of particle physics, were in thermal equilibrium with other particles during the early phase of the Universe. Their abundance depends only on their annihilation cross section, but not on the WIMP mass. Their annihilation cross section must be in the order of a typical weak interaction should their abundance be of cosmological relevance today. If supersymmetry is realized in nature on the required energy scale, then the lightest supersymmetric particle (LSP), the neutralino, shows exactly the properties of a WIMP [Kam99].

Axions, the other leading dark matter particle candidates, were postulated two decades ago to explain why the strong interaction conserves the CP-symmetry, which is violated in the standard model. Axions could have been produced during the QCD phase transition; their masses are constrained by experimental searches, astrophysical and cosmological arguments to the order of 10^{-5} eV. Since axions couple to two photons, they can be detected by stimulating their conversion to photons in a cavity permeated by a strong static magnetic field [Sik83]. In order to cover a wide mass range the cavity must be tuned to different frequencies. Two pilot experiments in Brookhaven [Pan87] and Florida [Hag90] already demonstrated the feasibility of the cavity detection method; the second generation experiments presently under way at the Lawrence Livermore National Laboratory [Bib99] and at the Kyoto University [Mat94] will have a sensitivity which is sufficient to discover axions if they populate the galactic halo.

Besides these dark matter candidates, another class of candidates, the so-called superheavy dark matter, emerged. If one gives up the assumption, that the particle was in thermal equilibrium in the early universe, then its present abundance is no longer determined by the annihilation cross section and much heavier particles, so-called WIMPZILLAs, are allowed [Kol99]. There are two necessary conditions for WIMPZILLAs, they must be stable, or at least have a lifetime much greater than the age of the universe and their interaction rate must be sufficiently weak such that thermal equilibrium with the primordial plasma was never obtained. For this, the particle must be extremely massive, of the order of the Hubble parameter at the end of inflation and the annihilation rate per particle must be smaller than the expansion rate of the Universe [Kol99].

Another kind of heavy particles, which could form a natural dark matter candidate, are stable baryonic Q-balls [Kus99]. They are predicted by supersymmetric models and could have been produced during the baryogenesis epoch. In this scenario, the baryonic matter and the dark matter are produced in the same process, therefore it is easy to understand why

the observed abundances of these are in the same order of magnitude. The way to detect Q-balls depends on their ability to pick up electric charge as they travel through ordinary matter. Electrically charged superballs would loose their energy in atomic collisions, their expected signature is similar to those of nuclearites, which are searched for in the MACRO experiment. Non observation of these gives a lower limit on the baryon number of dark matter Q-balls of 10^{21}. The signature of electrically neutral Q-balls are similar to those expected from GUT-monopoles, the lower limit from the Baikal experiment on their baryonic charge is 10^{23}. These limits will be improved by future experiments, like AMANDA or ANTARES. However for covering the entire cosmologically interesting range a detector with an are of several square kilometers would be needed [Kus99].

1.2.3. Status of the direct search for WIMPs If WIMPs populate the halo of our galaxy they could be detected directly in low background laboratory experiments or indirectly through their annihilation products in the halo, the centre of the Sun or Earth. The goal of the direct detection experiments is to look for the elastic scattering of a WIMP off nuclei in a low-background detector. The recoil nucleus looses its energy through ionization and thermal processes. The methods to detect this energy loss span from scintillators, ionization detectors, bolometers to superheated droplet or superconducting granular detectors.

The deposited energy for neutralinos with masses between 10 GeV and 1 TeV is below 100 keV [Jun96]. For a standard halo comprised of WIMPs with a Maxwellian velocity distribution characterized by $v_{rms} = 270$ km/s and a mass density of 0.4 GeV/cm^2, the expected event rates are well below 1 event per kilogramm target material and day [Jun96]. This makes any experimental attempt to directly detect neutralinos a great technical challenge, requiring a large detector mass, a low energy threshold, a low background and/or an effective background discrimination technique.

Direct detection experiments operating so far have reached sensitivities low enough to enter the parameter space predicted for neutralinos in the MSSM. The best current limits on WIMP-nucleon cross section come from the DAMA NaI experiment [Ber98], from the Heidelberg-Moscow experiment [HM98] and from CDMS [Ake98] (see Figure 5).

The Stanford CDMS (Cold Dark Matter Search) experiment [Gai98] uses thermal detectors of ultrapure germanium and silicon which are operated at a temperature of 20 mK. The simultaneous measurement of both ionization and phonon signals allows the discrimination of a nuclear recoil event from an electron interaction. This represents a very effective background suppression method. For the moment the experiment is located at the Stanford Underground Facility, 10.6 m below ground, where it is

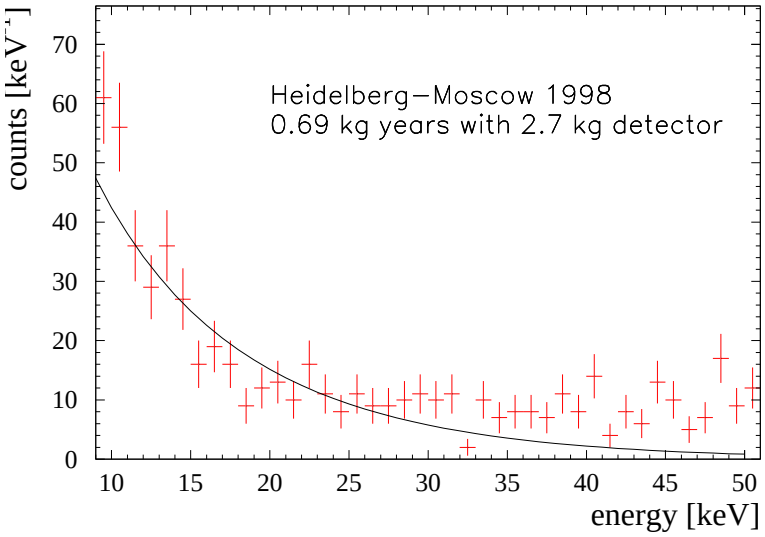

Figure 2. Total measured spectrum with one enriched ^{76}Ge detector of the Heidelberg-Moscow experiment after an exposure of 0.69 kg yr and a theoretical spectrum for a 100 GeV WIMP.

planned to obtain an exposure of 100 kg d with two silicon and four germanium devices. For the future it is planned to operate the detector in the Soudan Mine with 2000 mwe overburden, which will reduce the muon flux by five orders of magnitude and thus reduce the cosmogenic activities and the neutron background. Fig. 5 shows the expected sensitivity at the Stanford site and at the Soudan site.

The DAMA experiment is running 115.5 kg NaI detectors in the Gran Sasso Underground Laboratory [Ber97a]. The high obtainable statistic opens the possibility to look for a WIMP signature, as a variation of the event rate due to the movement of the Sun in the galactic halo and the Earth rotation around the Sun. The analysis of about 54 kg yr in terms of a WIMP annual modulation signature favours a positive signal, the allowed region of WIMP masses and cross sections is well embedded in the minimal supersymmetric parameter space predicted for neutralinos [Ber98a, Bot98]. However, a further confirmation by DAMA and by other experiments must be awaited.

The Heidelberg-Moscow [HM97] and HDMS (Heidelberg Dark Matter Search) [Bau97] experiments are both located in the Gran Sasso Laboratory, where the muon component of the cosmic rays is reduced to one part

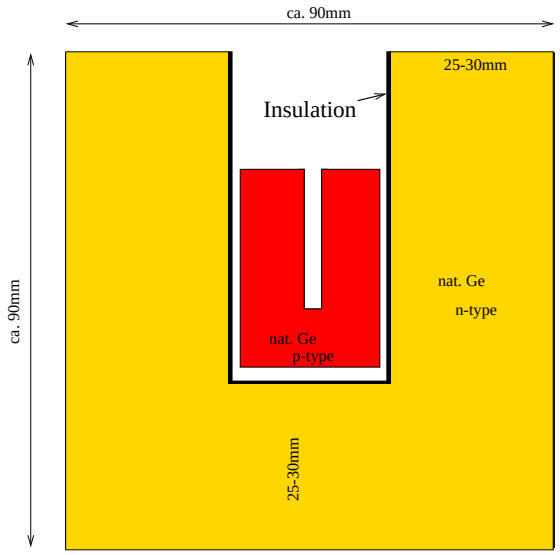

Figure 3. Schematic figure of the HDMS detector.

in a million. The Heidelberg-Moscow experiment, which also searches for the neutrinoless double beta decay in enriched ^{76}Ge, gives at present the most stringent limits on WIMP-nucleon cross section on spin-independent interactions for using raw data without pulse shape analysis [HM98]. Fig. 2 shows the measured spectrum with one enriched ^{76}Ge detector after an exposure of 0.69 kg yr and a calculated WIMP spectrum for a 100 GeV WIMP.

HDMS, which is a dedicated dark matter experiment [Bau97], aims to improve this limit by one order of magnitude. As in the Heidelberg-Moscow experiment, the aim is to look for a small ionization signal inside a high purity Ge crystal. The actual dark matter target, a 200 g crystal made of natural Ge, is surrounded by a well-type Ge crystal (see Fig. 3).

The outer detector acts as an effective veto against multiple scattered photons, allowing to suppress the background originating from the latter by a factor 6-10. The HDMS prototype (see Fig. 4) started to measure in April 1998, while the full HDMS experiment (inner crystal made of enriched ^{73}Ge and a new cryostat system of selected copper) will start measuring in the course of the year 2000. With the expected sensitivity (see Fig. 5) it

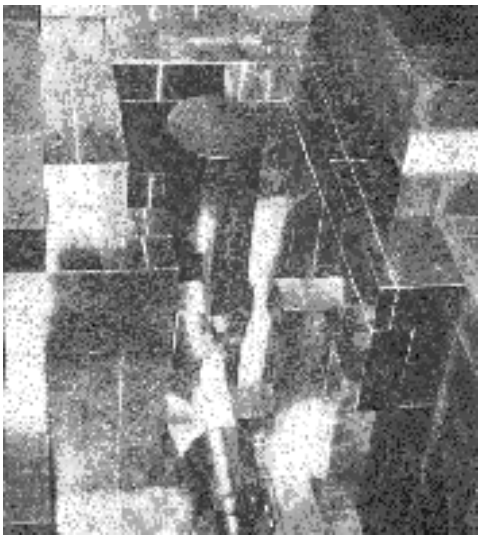

Figure 4. The HDMS detector during its installation in the Gran Sasso Laboratory.

will be able to test, like CDMS, the complete DAMA evidence region.

1.2.4. GENIUS as a dark matter detector For an almost complete covering of the MSSM parameter space, an increase in sensitivity by more than three orders of magnitude relative to running experiments is required.

The GENIUS experiment could accomplish this task by operating about 40 'naked' natural Ge detectors (100 kg) in a tank of ultrapure liquid nitrogen. The idea is to increase the target mass to 100 kg while decreasing at the same time the absolute background by a considerable amount.

The final goal would be to reach a background level of 10^{-3} events/kg y keV in the energy region relevant for dark matter searches.

The energy threshold would be about 11 keV, the energy resolution being better than 0.3 %. With 100 kg of target material, GENIUS could also look for a WIMP signature in form of an annual modulation of the WIMP-signal.

A comparable sensitivity can be reached in principle only by LHC. An advantage of GENIUS is that it will be particulary sensitive in regions of large tanβ in the minimal SUGRA space, where conventional signals for supersymmetry in collider experiments are difficult to detect. Thus, if the parameter tanβ is large, then the first direct evidence for supersymmetry could come from GENIUS, rather than from collider searches for sparticles [Bae97]. But also if SUSY will be detected by collider experiments, it would

still be fascinating - and necessary - to verify the existence and properties of neutralino dark matter.

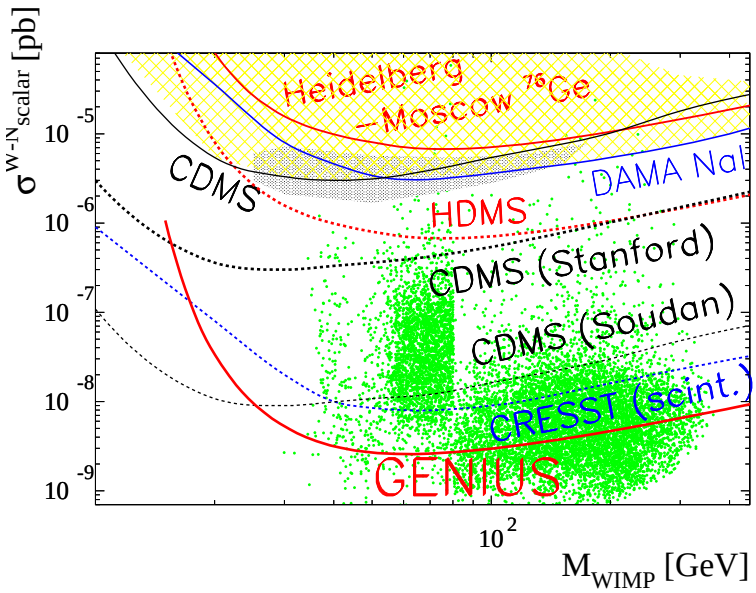

Figure 5. WIMP–nucleon cross section limits as a function of the WIMP mass. The hatched region is excluded by the Heidelberg–Moscow [HM98] and the DAMA experiment [Ber98], the dashed lines are expectations for recently started or future experiments, like HDMS [Bau97], CDMS [Ake98] and CRESST [Bue96]. The filled contour represents the 2σ evidence region of the DAMA experiment [Ber98a]. The solid fat line denotes the expectation for the GENIUS project with a background level of 0.01 counts/(keV kg y), an energy threshold of 11 keV and an exposure of 300 kg yr. The experimental limits are compared to expectations (scatter plot) for WIMP–neutralinos calculated in the MSSM framework with non–universal scalar mass unification [Bed97c].

Fig. 5 shows a comparison of existing constraints and future sensitivities of cold dark matter experiments, together with the theoretical expectations for neutralino scattering rates [Bed97b]. Obviously, GENIUS could easily cover the range of positive evidence for dark matter recently claimed by DAMA [Ber97b, Bot97]. It would also be by far more sensitive than all other dark matter experiments at present under construction or proposed, like the cryogenic experiment CDMS. Furthermore, obviously GENIUS will be the only experiment, which could seriously test the MSSM predictions over a large part of the SUSY parameter space. In this way, GENIUS

could compete even with LHC in the search for SUSY, see for example the discussion in [Bae97]. It is important to note, that GENIUS could reach the sensitivity shown in Fig. 5 with only 100 kg of *natural* Ge detectors in a measuring time of three years [Kla98d].

1.3. Double Beta Decay

Strong hints for neutrino masses are given by the atmospheric and solar neutrino data, in particular by the SuperKamiokande confirmation of the atmospheric neutrino deficit [SK98]. However, neutrino oscillation experiments can measure only neutrino mass differences. In view of the SuperKamiokande data and of the dark matter problem, a determination of the absolute neutrino mass scale should become a high priority. A method for measuring the Majorana neutrino mass is provided by neutrinoless double beta decay, at the same time a unique method of discerning between a Majorana and a Dirac neutrino. The current most stringent experimental limit on the effective Majorana neutrino mass, $\langle m \rangle$ <0.2 eV, comes from the Heidelberg-Moscow experiment [Bau99a]. Future planned experiments, like NEMO or Kamland will, like the Heidelberg-Moscow experiment, improve this limit at best by a factor of two. Fig. 20 gives the present status of the at present most sensitive double beta experiments and of future plans.

For a significant step beyond this limit, much higher source strenghts and lower background levels are needed. This goal could be accomplished by the GENIUS experiment operating 300 detectors made of enriched ^{76}Ge, (1 ton) in a liquid nitrogen shielding (see Fig. 6).

GENIUS would search for the $0\nu\beta\beta$ -decay in ^{76}Ge, at the Q-value of 2038.56 $\pm$ 0.32 keV [Hyk91]. The aim is to reach the sensitivity of $\langle m \rangle$ <0.01 eV after one year of measuring time. In an extended version using 10 tons of ^{76}Ge, a sensitivity of 0.001 eV could be reached. Already the first step will have striking influence on presently discussed neutrino mass scenarios. The potential of GENIUS would also allow a breakthrough into the multi TeV range for many beyond standard models. It will give information on supersymmetry (R-parity breaking, sneutrino mass), leptoquarks (leptoquark -Higgs coupling or leptoquark mass), compositeness, right-handed W boson mass, test of special relativity and equivalence principle in the neutrino sector and others, competitive to corresponding results from future high-energy colliders. The sensitivity of GENIUS in the neutrino sector would be larger than of many present terrestrial neutrino oscillation experiments and would provide complementary informations to those planned for the future. GENIUS with one ton would be able to check the LSND indication for neutrino oscillations and GENIUS with ten tons could probe directly the large angle solution of the solar neutrino problem. For an almost degenerate neutrino mass scenario it could even probe the small angle solution of the solar neutrino problem. This potential has been

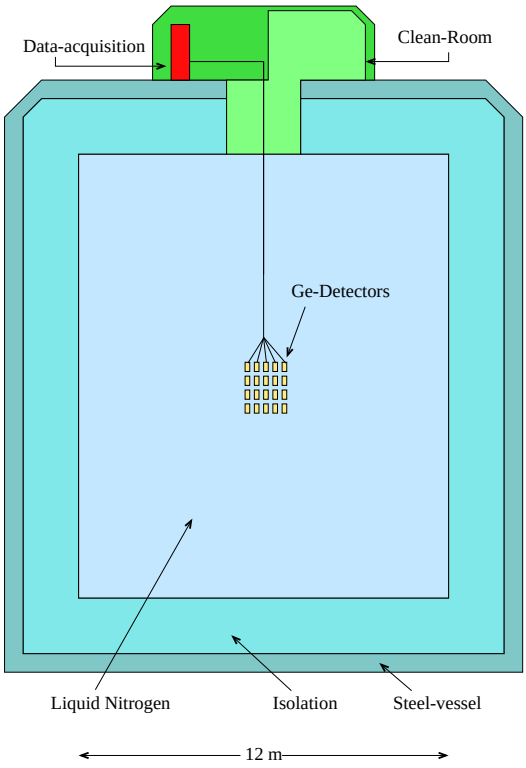

Figure 6. Schematic view of the GENIUS experiment.

descibed recently in various papers [Kla98b, Kla97c, Pan99, Kla98f]. In the following subsubsections we give a short background of the general potential of double beta decay, a report of the status of double beta experiments, proposals and results, and an outline of the potential of GENIUS for investigation of neutrino masses and mixings and of other beyond standard model physics.

1.3.1. General new physics potential of double beta decay Double beta decay can occur in several decay modes (Fig. 7):

$$ {}^{A}_{Z}X \rightarrow {}^{A}_{Z+2}X + 2e^- + 2\overline{\nu}_e \quad (1) $$

$$ {}^{A}_{Z}X \rightarrow {}^{A}_{Z+2}X + 2e^- \quad (2) $$

$$ {}^{A}_{Z}X \rightarrow {}^{A}_{Z+2}X + 2e^- + \phi \quad (3) $$

$$ {}^{A}_{Z}X \rightarrow {}^{A}_{Z+2}X + 2e^- + 2\phi \quad (4) $$

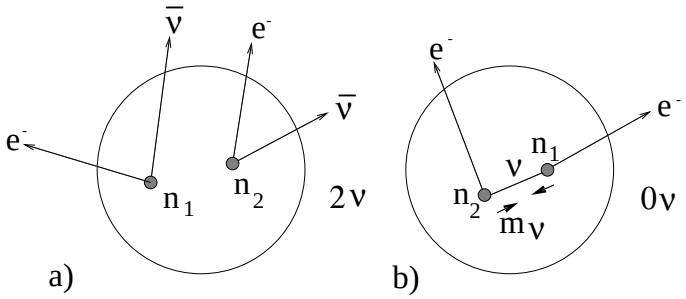

Figure 7. Schematic representation of 2ν and 0ν double beta decay.

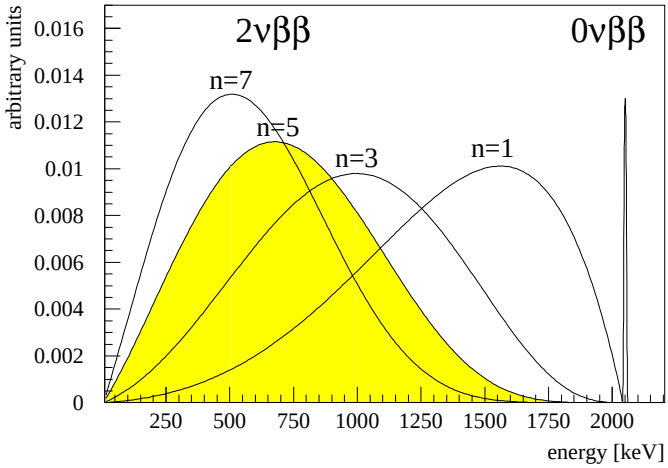

Figure 8. Spectral shapes of the different modes of double beta decay, denotes the spectral index, n=5 for $2\nu\beta\beta$ decay

the last three of them violating lepton number conservation by $\Delta L = 2$. For the neutrinoless mode (2) we expect a sharp line at $E = Q_{\beta\beta}$, for the two–neutrino mode and the various Majoron–accompanied modes classified by their spectral index, continuous spectra (see Fig. 8). Important for particle physics are the decay modes (2)–(4).

Figure 9 gives the Feynman graphs of the neutrinoless double beta decay mode triggered by the exchange of a neutrino. The neutrinoless mode (2) needs not be necessarily connected with the exchange of a virtual neutrino or sneutrino. *Any* process violating lepton number can in principle lead to a process with the same signature as usual $0\nu\beta\beta$ decay. It may be triggered by exchange of neutralinos, gluinos, squarks, sleptons, leptoquarks,... (see below and [Kla98b, Päs97, Päs99]). Fig. 10 gives the graph of the general

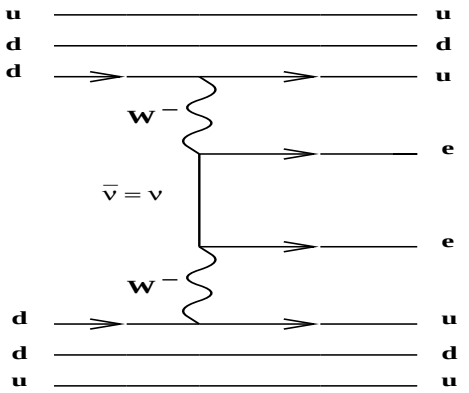

Figure 9. Feynman graph for neutrinoless double beta decay triggered by exchange of a left–handed light or heavy neutrino

neutrinoless double beta decay mode.

This gives rise to the broad potential of double beta decay for testing or yielding restrictions on quantities of beyond standard model physics (Table

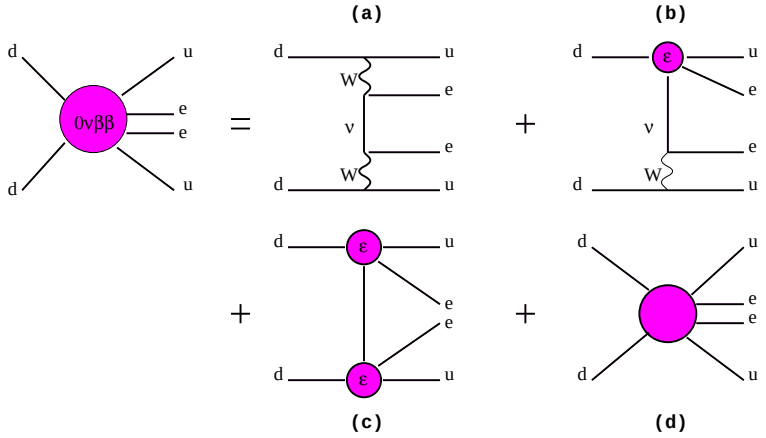

Figure 10. Feynman graphs of the general double beta decay rate: The contributions (a)-(c)correspond to the long range part, the contribution d) is the short range part.

Observ.	Restrictions	Topics investigated
0ν:	via ν exchange:	Beyond the standard model and SU(5)
	Neutrino mass	model; early universe, matter–antimatter
	Light Neutrino	asymmetry, Dark matter
	Heavy Neutrino	L–R –symmetric models (e.g. SO(10)), compositeness
	Test of Lorentz invariance and equivalence principle	
	Right handed weak currents	$V+A$ interaction, $W_R^{\pm}$ masses
	via photino, gluino, zino (gaugino) or sneutrino exchange:	SUSY models: Bounds for parameter space beyond the range of accelerators
	R-parity breaking, sneutrino mass	
	via leptoquark exchange	leptoquark masses and models
	leptoquark-Higgs interaction	
$0\nu\chi$:	existence of the Majoron	Mechanism of (B-L) breaking -explicit -spontaneous breaking of the local/global B-L symmetry new Majoron models

Table 1. $\beta\beta$ decay and particle physics

1).

There is, however, a generic relation between the amplitude of $0\nu\beta\beta$ decay and the $(B-L)$ violating Majorana mass of the neutrino. It has been recognized about 15 years ago [Sch81] that if any of these two quantities vanishes, the other one vanishes, too, and vice versa, if one of them is non–zero, the other one also differs from zero. This Schechter-Valle-theorem is valid for any gauge model with spontaneously broken symmetry at the weak scale, independent of the mechanism of $0\nu\beta\beta$ decay. A generalisation of this theorem to supersymmetry has been given recently [Hir97a, Hir98b]. This theorem claims for the neutrino Majorana mass, the $B-L$ violating mass of the sneutrino and neutrinoless double beta decay amplitude: If one of them is non–zero, also the others are non–zero and vice versa, independent of the mechanisms of $0\nu\beta\beta$ decay and (s-)neutrino mass generation. This theorem connects double beta research with new processes potentially observable at future colliders like NLC (next linear collider) [Hir97a, Hir98a].

1.3.1.1 Neutrino mass Neutrino physics has entered an era of new actuality in connection with several possible indications of physics beyond the standard model (SM) of particle physics: A lack of solar (^7Be) neutrinos, an atmospheric ν_μ deficit and mixed dark matter models could all be explained simultaneously by non–vanishing neutrino masses. Recent GUT models, for example an extended SO(10) scenario with S_4 horizontal symmetry could

explain these observations by requiring degenerate neutrino masses of the order of 1 eV [Lee94, Moh94, Pet94, Ioa94, Fri95, Moh95] [Pet96, Val96]. For an overview see [Smi96, Moh97a]. More recent theoretical discussions are given in [Kla2000, Adh98, Min97, Giu99, Ma99, Vis99, Bil99].

From all this work it is clear that double beta decay experiments have come into some key position, since the predictions of or assumptions in such scenarios start now to become testable partly already by the most advanced present experiments like the Heidelberg-Moscow experiment.

Neutrinoless double beta decay can be triggered by exchange of a light or heavy left-handed Majorana neutrino (see Fig. 9). For exchange of a heavy *right*–handed neutrino see below. The propagators in the first and second case show a different m_ν dependence: Fermion propagator $\sim \frac{m}{q^2-m^2} \Rightarrow$

$$a) \quad m \ll q \rightarrow \sim m \quad 'light' \ \ neutrino \tag{5}$$

$$b) \quad m \gg q \rightarrow \sim \frac{1}{m} \quad 'heavy' \ \ neutrino \tag{6}$$

The half–life for $0\nu\beta\beta$ decay induced by exchange of a light neutrino is given by [Mut88]

$$[T^{0\nu}_{1/2}(0^+_i \rightarrow 0^+_f)]^{-1} = C_{mm}\frac{\langle m_\nu \rangle^2}{m_e^2} + C_{\eta\eta}\langle\eta\rangle^2 + C_{\lambda\lambda}\langle\lambda\rangle^2 + C_{m\eta}\frac{m_\nu}{m_e}$$

$$+ C_{m\lambda}\langle\lambda\rangle\frac{\langle m_\nu\rangle}{m_e} + C_{\eta\lambda}\langle\eta\rangle\langle\lambda\rangle \tag{7}$$

or, when neglecting the effect of right–handed weak currents, by

$$[T^{0\nu}_{1/2}(0^+_i \rightarrow 0^+_f)]^{-1} = C_{mm}\frac{\langle m_\nu \rangle^2}{m_e^2} = (M^{0\nu}_{GT} - M^{0\nu}_F)^2 G_1 \frac{\langle m_\nu\rangle^2}{m_e^2} \tag{8}$$

where G_1 denotes the phase space integral, $\langle m_\nu \rangle$ denotes an effective neutrino mass

$$\langle m_\nu \rangle = \sum_i m_i U^2_{ei}, \tag{9}$$

respecting the possibility of the electron neutrino to be a mixed state (mass matrix not diagonal in the flavor space)

$$|\nu_e\rangle = \sum_i U_{ei}|\nu_i\rangle \tag{10}$$

For Majorana neutrinos, U is given by

$$\begin{pmatrix} c_{12}c_{13} & s_{12}c_{13}e^{-i\delta_{12}} & s_{13}e^{-i\delta_{13}} \\ -s_{12}c_{23}e^{i\delta_{12}} - c_{12}s_{23}s_{13}e^{i(\delta_{13}+\delta_{23})} & c_{12}c_{23} - s_{12}s_{23}s_{13}e^{i(\delta_{23}+\delta_{13}-\delta_{12})} & s_{23}c_{13}e^{i\delta_{23}} \\ s_{12}s_{23}e^{i(\delta_{23}+\delta_{13})} - c_{12}c_{23}s_{13}e^{i(\delta_{23}+\delta_{13})} & -c_{12}s_{23}e^{i\delta_{23}} - s_{12}c_{23}s_{13}e^{i(\delta_{13}-\delta_{12})} & c_{23}c_{13} \end{pmatrix}, \tag{11}$$

where $s_{ij} = sin\theta_{ij}, c_{ij} = cos\theta_{ij}$ and δ is a CP violating phase. For a given neutrino oscillation pattern the absolute ν masses are not fixed, adding an arbitrary m_0

$$m_i \rightarrow m_i + m_0 \tag{12}$$

does not change the oscillation probabilities, but the $0\nu\beta\beta$ rate. This means the oscillation pattern does not restrict the effective Majorana mass. Thus neutrinoless double beta decay is a indispensable crucial check of neutrino mass models.

The effective mass $\langle m_\nu \rangle$ could be smaller than m_i for all i for appropriate CP phases of the mixing coefficiants U_{ei} [Wol81]. In general not too pathological GUT models yield $m_{\nu_e} = \langle m_{\nu_e} \rangle$ (see [Lan88]).

η,λ describe an admixture of right–handed weak currents, and $M^{0\nu} \equiv M^{0\nu}_{GT} - M^{0\nu}_{F}$ denote nuclear matrix elements.

Nuclear matrix elements: A detailed discussion of $\beta\beta$ matrix elements for neutrino induced transitions including the substantial (well–understood) differences in the precision with which 2ν and $0\nu\beta\beta$ rates can be calculated, can be found in [Gro90, Mut88, Mut89] [Sta90, Kla98a, Kla98b].

1.3.1.2 Supersymmetry Supersymmetry (SUSY) is considered as prime candidate for a theory beyond the standard model, which could overcome some of the most puzzling questions of today's particle physics (see, e.g. [Hab93, Moh92, Kan97]). Generally one can add the following R–parity violating terms to the usual superpotential [Hal84].

$$W_{\not R_P} = \lambda_{ijk} L_i L_j \overline{E}_k + \lambda^{'}_{ijk} L_i Q_j \overline{D}_k + \lambda^{''} \overline{U}_i \overline{D}_j \overline{D}_k, \tag{13}$$

where indices i, j, k denote generations. L,Q denote lepton and quark doublet superfields and $\overline{E}, \overline{U}, \overline{D}$ lepton and up, down quark singlet superfields. Terms proportional to λ, $\lambda^{'}$ violate lepton number, those proportional to $\lambda^{''}$ violate baryon number. From proton decay limits it is clear that both types of terms cannot be present at the same time in the superpotential. On the other hand, once the $\lambda^{''}$ terms being assumed to be zero, λ and $\lambda^{'}$ terms are not limited. $0\nu\beta\beta$ decay can occur within the $\not R_p$ MSSM through Feynman graphs such as those of Fig. 11 In lowest order there are alltogether six different graphs of this kind. [Hir95a, Hir95b, Hir96c]. Thus $0\nu\beta\beta$ decay can be used to restrict R–parity violating SUSY models [Hir95a, Hir96d, Moh91, Hir95b, Moh86a]. From these graphs one derives [Hir95a] under some assumptions

$$[T^{0\nu}_{1/2}(0^+ \rightarrow 0^+)]^{-1} \sim G_{01} (\frac{\lambda^{\prime 2}_{111}}{m^4_{\tilde{q},\tilde{e}} m_{\tilde{g}\chi}} M)^2 \tag{14}$$

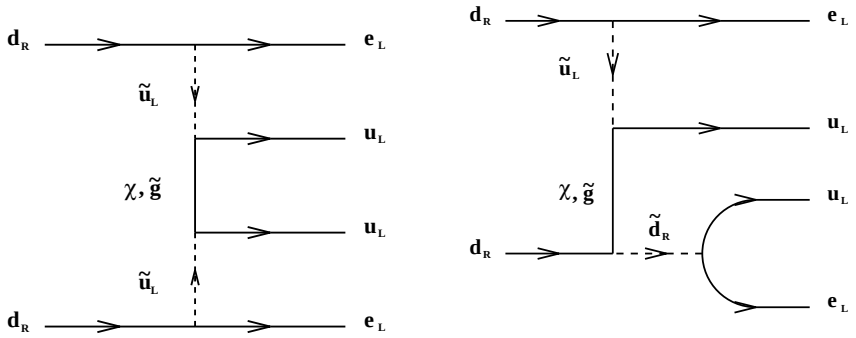

Figure 11. Examples of Feynman graphs for $0\nu\beta\beta$ decay within R–parity violating supersymmetric models (from [Hir95a]).

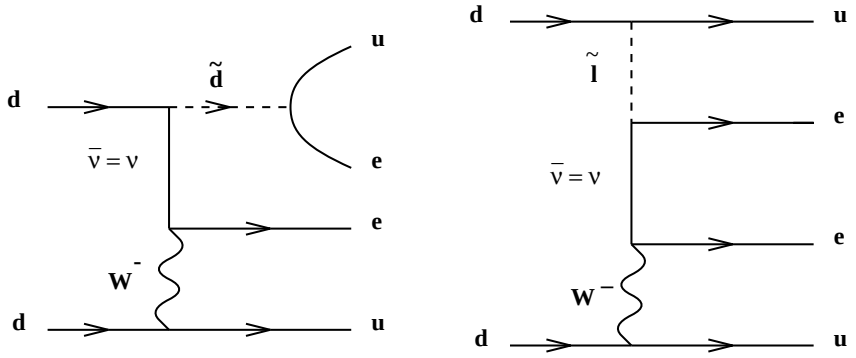

Figure 12. (left) Feynman graph for the mixed SUSY-neutrino exchange mechanism of $0\nu\beta\beta$ decay. R-parity violation occurs through scalar quark exchange. (right) As left figure, but for scalar lepton exchange (from [Hir96]).

where G_{01} is a phase space factor, $m_{\tilde{q}\tilde{e}\tilde{g}\chi}$ are the masses of supersymmetric particles involved: squarks, selectrons, gluinos, or neutralinos. λ'_{111} is the strength of an R–parity breaking interaction (eq. 11), and M is a nuclear matrix element. For the matrix elements and their calculation (see [Hir96d]).

It is also worthwile to notice that $0\nu\beta\beta$ decay is not only sensitive to $\lambda^{'}_{111}$. Taking into account the fact that the SUSY partners of the left and right–handed quark states can mix with each other, one can derive limits on different combinations of $\lambda^{'}$ [Hir96a, Moh96b, Bab95, Päs99b] (see Fig. 12). The dominant diagram of this type is the one where the exchanged scalar particles are the $\tilde{b} - \tilde{b}^C$ pair. Under some assumptions (e.g. the MSSM mass parameters to be approximately equal to the "effective" SUSY

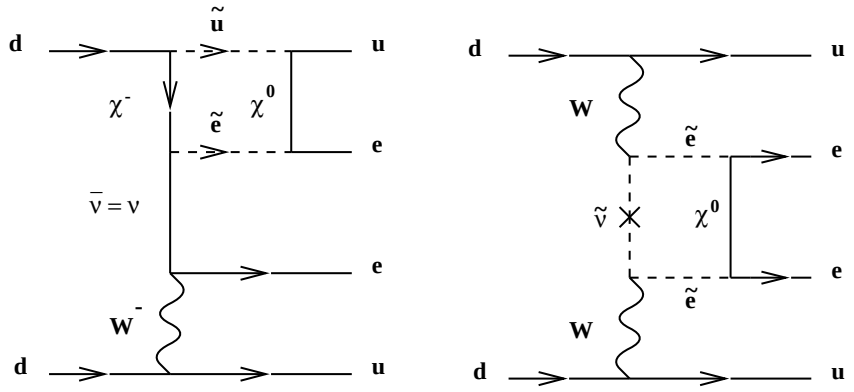

Figure 13. Examples of R_P conserving SUSY contributions to $0\nu\beta\beta$ decay (from [Hir97a]).

breaking scale Λ_{SUSY}), one obtains [Hir96a]

$$\lambda^{'}_{11i} \cdot \lambda^{'}_{1i1} \leq \epsilon^{'}_{i} \Big(\frac{\Lambda_{SUSY}}{100GeV} \Big)^3 \tag{15}$$

and

$$\Delta_n \lambda^{'}_{311} \lambda_{n13} \leq \epsilon \Big(\frac{\Lambda_{SUSY}}{100GeV} \Big)^3 \tag{16}$$

Further constraints on R parity violating Supersymmetry may be obtained directly from the neutrino mass bound [Bha99]. Products of trilinear couplings λ and/or λ' may generate a complete neutrino mass matrix through one-loop self-energy graphs [Dim87, Dre98]. Let us first consider the effects of the λ' interactions. The relevant part of the Lagrangian can be written as

$$-\mathcal{L}_{\lambda'} = \lambda'_{ijk} \left[\bar{d}_k P_L \nu_i \tilde{d}_{jL} + \bar{\nu}^c_i P_L d_j \tilde{d}^*_{kR} \right] + \text{ h.c.} \tag{17}$$

Majorana mass terms for the left-handed neutrinos, given by

$$\mathcal{L}_M = -\frac{1}{2} m_{\nu_{ii'}} \bar{\nu}_{Li} \nu^c_{Ri'} + \text{ h.c.}, \tag{18}$$

are generated at one loop. Fig. 14 shows the corresponding diagrams. The induced masses are given by

$$m_{\nu_{ii'}} \simeq \frac{N_c \lambda'_{ijk} \lambda'_{i'kj}}{16\pi^2} m_{d_j} m_{d_k} \left[\frac{f(m^2_{d_j}/m^2_{\tilde{d}_k})}{m_{\tilde{d}_k}} + \frac{f(m^2_{d_k}/m^2_{\tilde{d}_j})}{m_{\tilde{d}_j}} \right], \tag{19}$$

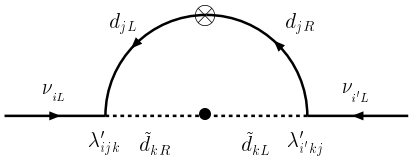

(a)

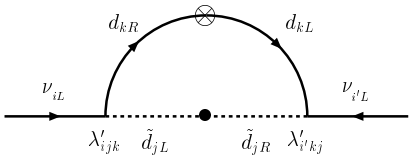

(b)

Figure 14**.** The λ'-induced one loop diagrams contributing to Majorana masses for the neutrinos.

where $f(x) = (x \ln x - x + 1)/(x - 1)^2$. Here, m_{d_i} is the down quark mass of the ith generation inside the loop, $m_{\tilde{d}_i}$ is an average of $\tilde{d}_{Li}$ and $\tilde{d}_{Ri}$ squark masses, and $N_c = 3$ is the colour factor. In deriving Eq. (19), it was assumed that the left-right squark mixing terms in the soft part of the Lagrangian are diagonal in their physical basis and proportional to the corresponding quark masses, *i.e.* $\Delta m^2_{\rm LR}(i) = m_{d_i} m_{\tilde{d}_i}$. With λ-type interactions, one obtains exactly similar results as above. The quarks and squarks in these equations will be replaced by the leptons and sleptons of the corresponding generations. The colour factor $N_c = 3$ and Q_d would be replaced by 1 and Q_e, respectively. Among the different entries of the flavour space mass matrix, only the ee-term has a *direct experimental* bound obtained from neutrinoless double-beta decay.

For an overview on our knowledge on λ'_{ijk} from other sources we refer to [Kol97, Bha97, Bha99].

Also R–parity *conserving* softly broken supersymmetry can give contributions to $0\nu\beta\beta$ decay, via the $B - L$–violating sneutrino mass term, the latter being a generic ingredient of any weak–scale SUSY model with a Majorana neutrino mass [Hir97a, Hir98a]. These contributions are realized at the level of box diagrams [Hir98a] (Fig. 13). The $0\nu\beta\beta$ half-life for

contributions from sneutrino exchange is found to be [Hir98a]

$$[T^{0\nu\beta\beta}_{1/2}]^{-1} = G_{01}\frac{4m_p^2}{G_F^4}\Big|\frac{\eta^{SUSY}}{m^5_{SUSY}}M^{SUSY}\Big|, \tag{20}$$

where the phase factor G_{01} is tabulated in [Doi85], η^{SUSY} is the effective lepton number violating parameter, which contains the $(B-L)$ violating sneutrino mass $\tilde{m}_M$ and M^{SUSY} is the nuclear matrix element [Hir96e].

1.3.1.3 Left–Right symmetric theories – Heavy neutrinos and right–handed W Boson Heavy *right–handed* neutrinos appear quite naturally in left–right symmetric GUT models. Since in such models the symmetry breaking scale for the right–handed sector is not fixed by the theory, the mass of the right–handed W_R boson and the mixing angle between the mass eigenstates W_1, W_2 are free parameters. $0\nu\beta\beta$ decay taking into account contributions from both, left– and right–handed neutrinos have been studied theoretically by [Hir96e, Doi93]. The former gives a more general expression for the decay rate than introduced earlier by [Moh86b].

The amplitude will be proportional to (see Fig. 15)[Hir96e]

$$\Big(\frac{m_{W_L}}{m_{W_R}}^4\Big)\Big(\frac{1}{m_N}+\frac{m_N}{m^2_{\Delta^{--}_R}}\Big) \tag{21}$$

Eq. 21 and the experimental lower limit of $0\nu\beta\beta$ decay leads to a constraint limit within the 3–dimensional parameter space ($m_{W_R} - m_N - m_{\Delta^{--}_R}$).

1.3.1.4 Compositeness Although so far there are no experimental signals of a substructure of quarks and leptons, there are speculations that at some higher energy ranges beyond 1 TeV or so there might exist an energy scale Λ_C at which a substructure of quarks and leptons (preons) might become visible [Pan96, Moh92, Sou92, Pan99] (Fig. 16).

A possible low energy manifestation of compositeness could be neutrinoless double beta decay, mediated by a composite heavy Majorana neutrino, which then should be a Majorana particle (Fig. 17).

Recent theoretical work shows (see [Pan96, Tak96, Pan97a, Tak97, Pan99]) that the mass bounds for such an excited neutrino which can be derived from double beta decay are at least of the same order of magnitude as those coming from the direct search of excited states in high energy accelerators (see also subsection 1.3.2).

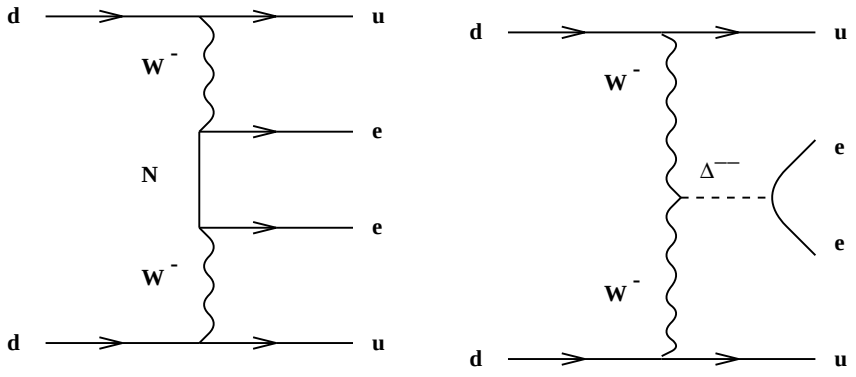

Figure 15. Left: Heavy neutrino exchange contribution to neutrinoless double beta decay in left-right symmetric models, and Right: Feynman graph for the virtual exchange of a double-charged Higgs boson (from [Hir96d]).

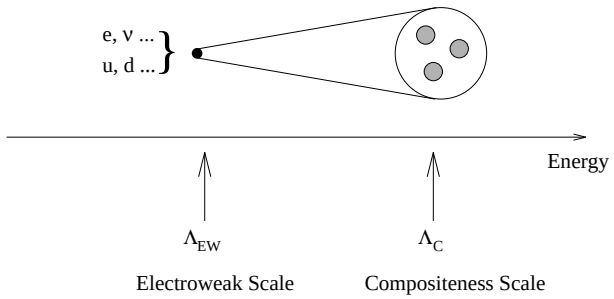

Figure 16. The idea of compositeness. At a (still unknown) energy scale Λ_C quarks and leptons might show an internal structure

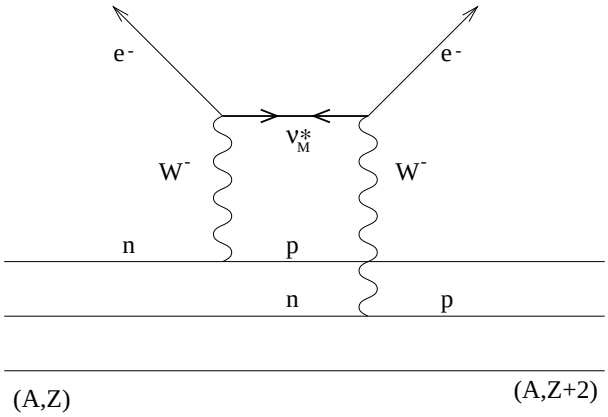

Figure 17. Neutrinoless double beta decay (ΔL = +2 process) mediated by a composite heavy Majorana neutrino.

1.3.1.5 Majorons The existence of new bosons, so–called Majorons, can play a significant role in new physics beyond the standard model, in the history of the early universe, in the evolution of stellar objects, in supernovae astrophysics and the solar neutrino problem [Geo81, Fri88, Kla92]. In many theories of physics beyond the standard model neutrinoless double beta decay can occur with the emission of Majorons

$$2n \rightarrow 2p + 2e^- + \phi \tag{22}$$

$$2n \rightarrow 2p + 2e^- + 2\phi. \tag{23}$$

To avoid an unnatural fine–tuning in recent years several new Majoron models were proposed [Bur93, Bam95b, Car93], where the term Majoron denotes in a more general sense light or massless bosons with couplings to neutrinos.

The main novel features of these "New Majorons" are that they can carry leptonic charge, that they need not be Goldstone bosons and that emission of two Majorons can occur. The latter can be scalar–mediated or fermion–mediated. For details we refer to [Päs96, Bur96].

The half–lifes are according to [Moh88, Doi85] in some approximation given by

$$[T_{1/2}]^{-1} = | < g_\alpha > |^2 \cdot |M_\alpha|^2 \cdot G_{BB_\alpha} \tag{24}$$

for $\beta\beta\phi$-decays, or

$$[T_{1/2}]^{-1} = | < g_\alpha > |^4 \cdot |M_\alpha|^2 \cdot G_{BB_\alpha} \tag{25}$$

for $\beta\beta\phi\phi$–decays. The index α indicates that effective neutrino–Majoron coupling constants g, matrix elements M and phase spaces G differ for different models.

Nuclear matrix elements: There are five different nuclear matrix elements. Of these M_F and M_{GT} are the same which occur in $0\nu\beta\beta$ decay. The other ones and the corresponding phase spaces have been calculated for the first time by [Päs96, Hir96c]. The calculations of the matrix elements show that the new models predict, as consequence of the small matrix elements, very large half–lives and that unlikely large coupling constants would be needed to produce observable decay rates (see [Päs96, Hir96c]).

1.3.1.6 Sterile neutrinos Introduction of sterile neutrinos has been claimed to solve simultaneously the conflict between dark matter neutrinos, LSND and supernova nucleosynthesis [Pel95] and light sterile neutrinos are part of popular neutrino mass scenarios for understanding the various hints for neutrino oscillations and [Moh96a, Moh97a, Moh97b]. Neutrinoless double beta decay can also investigate several effects of *heavy* sterile neutrinos [Bam95a] (Fig. 18).

If we assume having a light neutrino with a mass $\ll$ 1 eV, mixing with a much heavier (m $\geq$ 1 GeV) sterile neutrino can yield under certain conditions a detectable signal in current $\beta\beta$ experiments.

1.3.1.7 Leptoquarks Interest on leptoquarks (LQ) has been renewed during the last few years since ongoing collider experiments have good prospects for searching these particles [Buc87]. LQs are vector or scalar particles carrying both lepton and baryon numbers and, therefore, have a well distinguished experimental signature. Direct searches of LQs in deep inelastic ep-scattering at HERA [H196] placed lower limits on their mass $M_{LQ} \geq 225 - 275$ GeV, depending on the LQ type and couplings.

To consider LQ phenomenology in a model-independent fashion one usually follows some general principles in constructing the Lagrangian of the LQ interactions with the standard model fields. In order to obey the stringent constraints from (c1) helicity-suppressed $\pi \rightarrow e\nu$ decay, from (c2) FCNC processes and from (c3) proton stability, the following assumptions are commonly adopted: (a1) LQ couplings are chiral, (a2) LQ couplings are generation diagonal, and (a3) there are no diquark couplings.

Recently, however, it has been pointed out [Hir96b] that possible LQ-Higgs interactions spoil assumption (a1): Even if one assumes LQs to be chiral at some high energy scale, LQ-Higgs interactions introduce after electro-weak symmetry breaking mixing between LQ states with different chirality. Since there is no fundamental reason to forbid such LQ-Higgs

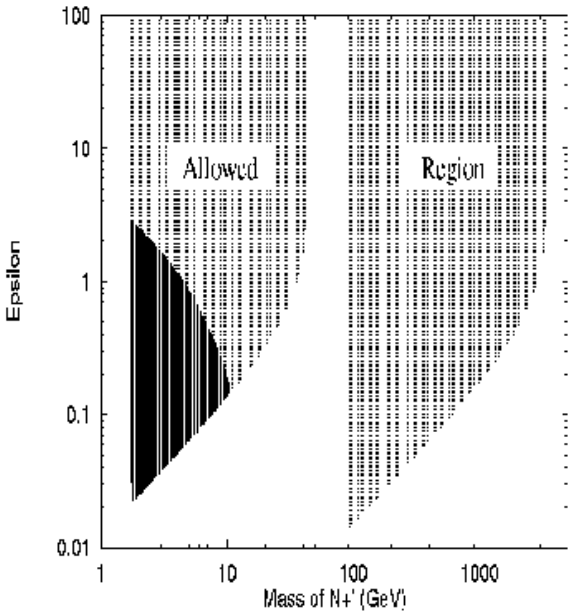

Figure 18. Regions of the parameter space ($\epsilon - M_{N'_+}$)plane yielding an observable signal (shaded areas) (from [Bam95a]). Darker area: 'natural' region, lighter shaded: Finetuning needed, to keep m_{ν_e} below 1 eV. $M_{N'_+}$: mass eigenstate, ϵ: strength of lepton number violation in mass matrix

interactions, it seems difficult to get rid of the unwanted non-chiral interactions in LQ models.

In such LQ models there appear contributions to $0\nu\beta\beta$ decay via the Feynman graphs of Fig.19. Here, S and V^μ stand symbolically for scalar and vector LQs, respectively. The half–life for $0\nu\beta\beta$ decay arising from leptoquark exchange is given by [Hir96b]

$$T^{0\nu}_{1/2} = |M_{GT}|^2 \frac{2}{G_F^2}[\tilde{C}_1 a^2 + C_4 b_R^2 + 2C_5 b_L^2]. \tag{26}$$

with $a = \frac{\epsilon_S}{M_S^2} + \frac{\epsilon_V}{M_V^2}$, $b_{L,R} = \frac{\alpha_S^{(L,R)}}{M_S^2} + \frac{\alpha_V^{(L,R)}}{M_V^2}$, $\tilde{C}_1 = C_1 \left(\frac{\mathcal{M}_1^{(\nu)}/(m_e R)}{M_{GT} - \alpha_2 M_F} \right)^2$.

For the definition of the C_n see [Doi85] and for the calculation of the matrix element $\mathcal{M}_1^{(\nu)}$ see [Hir96b]. This allows to deduce information on leptoquark masses and leptoquark–Higgs couplings (see subsection 1.3.2).

1.3.1.8 Special Relativity and Equivalence Principle Special relativity and the equivalence principle can be considered as the most basic foundations of

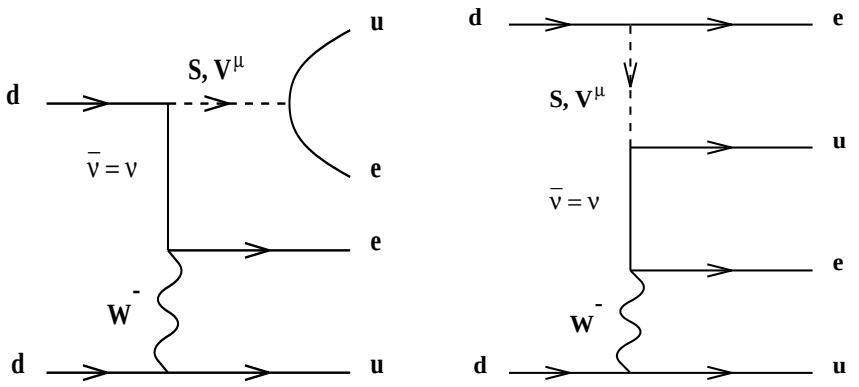

Figure 19. Examples of Feynman graphs for $0\nu\beta\beta$ decay within LQ models. S and V^μ stand symbolically for scalar and vector LQs, respectively (from [Hir96a]).

the theory of gravity. Many experiments already have tested these principles to a very high level of accuracy [Hug60] for ordinary matter - generally for quarks and leptons of the first generation. These precision tests of local Lorentz invariance – violation of the equivalence principle should produce a similar effect [Wil92] – probe for any dependence of the (non–gravitational) laws of physics on a laboratory's position, orientation or velocity relative to some preferred frame of reference, such as the frame in which the cosmic microwave background is isotropic.

A typical feature of the violation of local Lorentz invariance (VLI) is that different species of matter have a characteristical maximum attainable speed. This can be tested in various sectors of the standard model through vacuum Cerenkov radiation [Gas89b], photon decay [Col97], neutrino oscillations [Gla97, Gas89a, Hal91, Hal96, But93] and $K-$physics [Ham98, Goo61]. These arguments can be extended to derive new constraints from neutrinoless double beta decay [Kla98f].

The equivalence principle implies that spacetime is described by unique operational geometry and hence universality of the gravitational coupling for all species of matter. In the recent years there have been attempts to constrain a possible amount of violation of the equivalence principle (VEP) in the neutrino sector from neutrino oscillation experiments [Gas89a, Hal91, Hal96, But93]. However, these bounds do not apply when the gravitational and the weak eigenstates have small mixing. In a recent paper [Kla98f] a generalized formalism of the neutrino sector has been given to test the VEP and it has been shown that neutrinoless double beta

decay also constrains the VEP. VEP implies different neutrino species to suffer from different gravitational potentials while propagating through the nucleus and hence the effect of different eigenvalues doesn't cancel for the same effective momentum. The main result is that neutrinoless double beta decay can constrain the amount of VEP even when the mixing angle is zero, *i.e.*, when only the weak equivalence principle is violated, for which there does not exist any bound at present.

1.3.2 Double Beta Decay Experiments: Present Status and Results

1.3.2.1 Present Experiments and Proposals Fig. 20 shows an overview over measured $0\nu\beta\beta$ half–life limits and deduced mass limits. The largest sensitivity for $0\nu\beta\beta$ decay is obtained at present by active source experiments (source=detector), in particular ^{76}Ge [Kla98a, Kla98b, Bau99a].

Only a few of the present most sensitive experiments may probe the neutrino mass in the next years into the sub–eV region, the Heidelberg–Moscow experiment being the by far most advanced and most sensitive one, see Fig. 20.

Figs. 20 show in addition to the present status the future perspectives of the main existing $\beta\beta$ decay experiments and includes some ideas for the future which have been published. The best presently existing limits besides the HEIDELBERG-MOSCOW experiment (light-shaded bars in Fig. 20), have been obtained with the isotopes: ^{48}Ca [You95], ^{82}Se [Ell92], ^{100}Mo [Als89], ^{116}Cd [Dan95], ^{130}Te [Ale94], ^{136}Xe [Vui93] and ^{150}Nd [Moe94]. These and other double beta decay setups presently under construction or partly in operation such as NEMO [NEM94, Bar97], the Gotthard ^{136}Xe TPC experiment [Joer94], the ^{130}Te cryogenic experiment [Ale94], a new ELEGANT ^{48}Ca experiment using 30 g of ^{48}Ca [Kum96], a hypothetical experiment with an improved UCI TPC [Moe94] assumed to use 1.6 kg of ^{136}Xe, etc., will not reach or exceed the ^{76}Ge limits. The goal 0.3 eV aimed at for the year 2004 by the NEMO experiment (see [Piq96, Bar97] and Fig. 20) may even be very optimistic if claims about the effect of proton-neutron pairing on the $0\nu\beta\beta$ nuclear matrix elements by [Pan96b] will turn out to be true, and also if the energy resolution will not be improved considerably (see Fig. 1 in [Tre95]). Therefore, the conclusion given by [Bed97c] concerning the future SUSY potential of NEMO has no serious basis. As pointed out by Raghavan [Rag94], even use of an amount of about 200 kg of enriched ^{136}Xe or 2 tons of natural Xe added to the scintillator of the KAMIOKANDE detector or similar amounts added to BOREXINO (both primarily devoted to solar neutrino investigation) would hardly lead to a sensitivity larger than the present ^{76}Ge experiment. This idea is going to be realized at present by the KAMLAND experiment [Suz97].

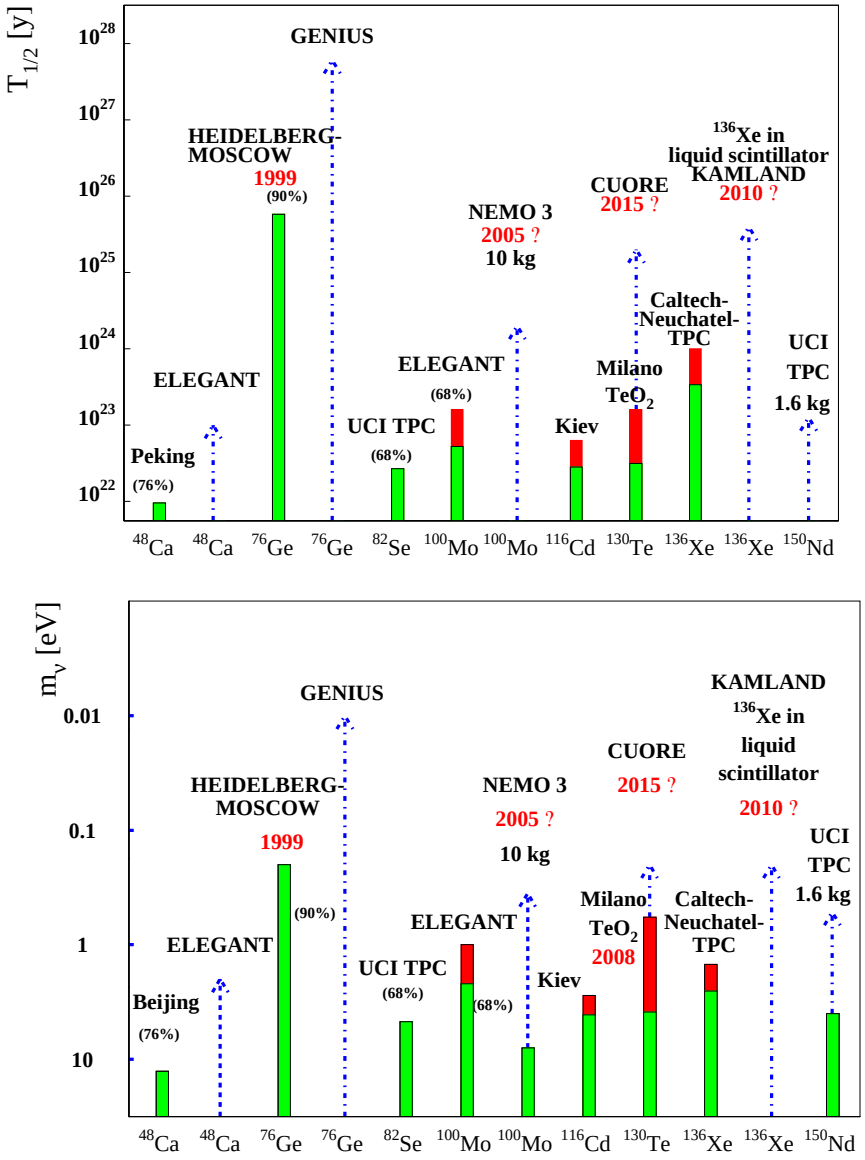

Figure 20. Present situation, 1999, and expectation for the near future and beyond, of the most promising $\beta\beta$-experiments concerning accessible half life (upper) and neutrino mass limits (lower). The light-shaded parts of the bars correspond to the present status, the dark parts of the bars to expectations for running experiments, dashed lines to experiments under construction and dash-dotted lines to proposed experiments.

It is obvious from Fig. 20 that *none* of the present experimental approaches, or plans or even vague ideas has a chance to surpass the border of 0.1 eV for the neutrino mass to lower values (see also [Nor97]). At present there is only one way visible to reach the domain of lower neutrino masses, suggested by [Kla98a] and meanwhile investigated in some detail concerning its experimental realization and physics potential in [Kla97c, Hel97, Kla98b, Kla98c, Bau99a, Kla2000].

1.3.2.2 Present limits on beyond standard model parameters from double beta decay The sharpest limits from $0\nu\beta\beta$ decay are presently coming from the Heidelberg–Moscow experiment [Kla87, Kla98b, Kla99a, Bau99a]. They will be given in the following. With five enriched (86% of ^{76}Ge) detectors of a total mass of 11.5 kg taking data in the Gran Sasso underground laboratory, and with a background of at present 0.06 counts/kg year keV in the region of the Q–value, the experiment has reached its final setup and is now exploring the sub–eV range for the mass of the electron neutrino. Fig. 21 shows the spectrum taken in a measuring time of 24 kgy with pulse shape analysis.

Half-life of neutrinoless double beta decay The deduced half-life limit for $0\nu\beta\beta$ decay is using the method proposed by [PDG98]

$$T^{0\nu}_{1/2} > 1.1 \cdot 10^{25} y \;\; (90\% C.L.) \tag{27}$$

$$> 1.6 \cdot 10^{25} y \;\; (68\% C.L.). \tag{28}$$

from the full data set with 49 kg yr and:

$$T^{0\nu}_{1/2} > 1.8 \cdot 10^{25} y \;\; (90\% C.L.) \tag{29}$$

$$> 3.0 \cdot 10^{25} y \;\; (68\% C.L.). \tag{30}$$

from the data with pulse shape analysis with a total exposure of 31 kg yr.

Neutrino mass

Light neutrinos: The upper limit of an (effective) electron neutrino Majorana mass, deduced from the data with pulse shape analysis, is, with the matrix element from [Sta90]

$$\langle m_\nu \rangle < 0.36 eV \;\; (90\% C.L.) \tag{31}$$

$$< 0.28 eV \;\; (68\% C.L.) \tag{32}$$

This is the sharpest limit for a Majorana mass of the electron neutrino so far. With these values the Heidelberg–Moscow experiment starts to take

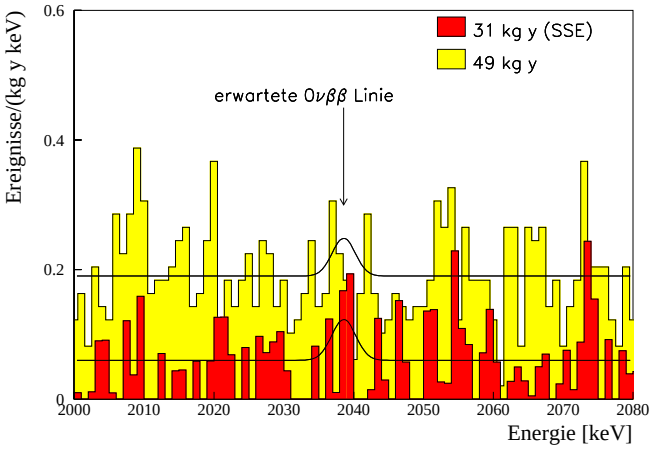

Figure 21. Integral spectrum in the region of interest after subtraction of the first 200 days of measurement of each detector, leaving 49 kg yr and 31 kg y of measuring time without and with pulse shape analysis respectively. The solid curves correspond to the signal excluded with $90\% C.L.$ (with $T^{0\nu}_{1/2} \geq 1.1 \times 10^{25}$ yr, 90% C.L. and $T^{0\nu}_{1/2} \geq 1.8 \times 10^{25}$ yr, 90% C.L.)

striking influence on presently discussed neutrino mass scenarios, which arose in connection with the recent Superkamiokande results on solar and atmospheric neutrinos. We mention a few examples:

The new $0\nu\beta\beta$ result excludes already now simultaneous 3ν solutions for hot dark matter, the atmospheric neutrino problem and the small mixing angle MSW solution [Adh98]. This means that Majorana neutrinos are ruled out, if the small mixing angle solution of the solar neutrino problem is borne out – if we insist on neutrinos as hot dark matter candidates. According to [Min97] degenerate neutrino mass schemes for hot dark matter, solar and atmospheric anomalies and CHOOZ are already now excluded (with 68 % C.L.) for the small *and* large mixing angle MSW solutions (without unnatural finetuning). If starting from recent dark matter models [Pri98] including in addition to cold and hot dark matter also a cosmological constant $\Lambda \neq 0$, these conclusions remain also valid, except for the large angle solution which would not yet be excluded by $0\nu\beta\beta$ decay (see [Kla2000]).

According to [Bar98] simultaneous 3ν solutions of solar and atmospheric neutrinos, LSND and CHOOZ (no hot dark matter!) predict $\langle m_\nu \rangle \simeq 1.5eV$ for the degenerate case ($m_i \simeq 1eV$) and $\langle m \rangle \simeq 0.14eV$ for the hierarchical case. This means that the first case is being tested already by the present Heidelberg–Moscow result. A model producing the neutrino masses based

on a heavy scalar triplet instead of the seesaw mechanism derives from the solar small angle MSW allowed range of mixing, and accomodating the atmospheric neutrino problem, $\langle m_\nu \rangle$ =0.17-0.31 eV [Ma99]. Also this model is already close to be disfavored. Looking into 4-neutrino scenarios, according to [Giu99] there are only two schemes with four neutrino mixing that can accomodate the results of *all* neutrino oscillation experiments (including LSND). In the first of the schemes, where $m_1 < m_2 \ll m_3 < m_4$, with solar (atmospheric) neutrinos oscillating between m_3 and m_4 (m_1 and m_2), and $\Delta m^2_{LSND} = \Delta m^2_{41}$, the HEIDELBERG–MOSCOW $0\nu\beta\beta$ bound excludes [Giu99] the small mixing angle MSW solution of the solar neutrino problem, for both $\nu_e \to \nu_\tau$, and $\nu_e \to \nu_s$ transitions. Including recent astrophysical data yielding $N_\nu^{BBN} \leq 3.2$ (95 % C.L.) [Bur99a], the oscillations of solar neutrinos occur mainly in the $\nu_e \to \nu_s$ channel, and *only* the small angle solutions is allowed by the fit of the solar neutrino data [Bah98a, Fuk99]. This means that $0\nu\beta\beta$ excludes the whole first scheme.

In the second scheme $m_1 < m_2 \ll m_3 < m_4$, with solar (atmospheric) neutrinos oscillating between m_1 and m_2 (m_3 and m_4), the present neutrino oscillation experiments indicate an effective Majorana mass of $7 \cdot 10^{-4} eV \leq |\langle m \rangle| \leq 2 \cdot 10^{-2} eV$. This could eventually be measured by GENIUS (see below). For a similar recent analysis see [Bil99]. For further detailed analyses of neutrino mass scenarios in the light of present and future neutrino experiments including double beta decay we refer to [Kla2000].

Superheavy neutrinos: For a superheavy *left*–handed neutrino we deduce [HM95, Bel96, Bel98] exploiting the mass dependence of the matrix element (for the latter see [Mut89]) a lower limit (see also Fig. 36)

$$\langle m_H \rangle \geq 9 \cdot 10^7 GeV. \tag{33}$$

Assuming the bound on the mixing matrix, $U^2_{ei} < 5 \cdot 10^{-3}$ [Bel98], and assuming no cancellation between the involved states, this limit implies a bound on the mass eigenstate

$$M_i > 4.5 \cdot 10^5 GeV. \tag{34}$$

Right–handed W boson For the right–handed W boson we obtain (see Fig. 22) a lower limit of

$$m_{W_R} \geq 1.4 TeV \tag{35}$$

(see [Hir96e, Kla98e]).

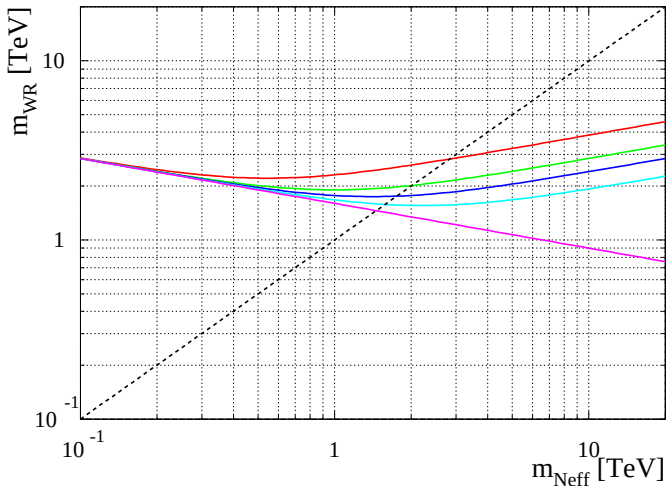

Figure 22. Limits on the mass of the right-handed W-boson from neutrinoless double beta decay (full lines) and vacuum stability (dashed line). The five full lines correspond to the following masses of the doubly charged higgs, $m_{\Delta^{--}}$: 0.3, 1.0, 2.0, 5.0 and ∞ [TeV] downward (from [Hir96e]).

SUSY parameters – R–parity breaking and sneutrino mass The constraints on the parameters of the minimal supersymmetric standard model with explicit R–parity violation deduced [Hir95a, Hir96d, Hir96a] from the $0\nu\beta\beta$ half–life limit are more stringent than those from other low–energy processes and from the largest high energy accelerators (Fig. 23). The limits are

$$\lambda^{'}_{111} \leq 4 \cdot 10^{-4} \Big(\frac{m_{\tilde{q}}}{100GeV}\Big)^2 \Big(\frac{m_{\tilde{g}}}{100GeV}\Big)^{\frac{1}{2}} \tag{36}$$

with $m_{\tilde{q}}$ and $m_{\tilde{g}}$ denoting squark and gluino masses, respectively, and with the assumption $m_{\tilde{d_R}} \simeq m_{\tilde{u}_L}$. This result is important for the discussion of new physics in the connection with the high–Q^2 events seen at HERA. It excludes the possibility of squarks of first generation (of R–parity violating SUSY) being produced in the high–Q^2 events [Cho97, Alt97, Hir97b].

We find further [Päs99b]

$$\lambda^{'}_{113}\lambda^{'}_{131} \leq 3 \cdot 10^{-8} \tag{37}$$

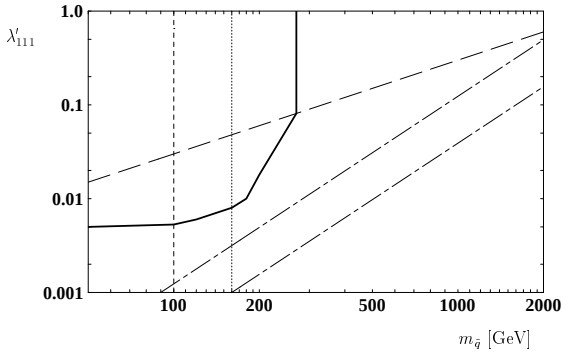

Figure 23. Comparison of limits on the R–parity violating MSSM parameters from different experiments in the λ'_{111}–$m_{\tilde{q}}$ plane. The ashed line is the limit from charged current universality according to [Bar89]. The vertical line is the limit from the data of Tevatron [Roy92]. The thick full line is the region which might be explored by HERA [But93a]. The two dash–dotted lines to the right are the limits obtained from the half–life limit for $0\nu\beta\beta$ decay of ^{76}Ge, for gluino masses of (from left to right) $m_{\tilde{g}}$ =1TeV and 100 GeV, respectively. The regions to the upper left of the lines are forbidden. (from [Hir95])

$$\lambda^{'}_{112}\lambda^{'}_{121} \leq 1 \cdot 10^{-6}. \tag{38}$$

The constraints on coupling products derived from the double beta decay neutrino mass limit [Bha99] are presented in tab. 2. As is obvious from the table, the double beta decay neutrino mass limits improve previous bounds on products of R–parity violating couplings by 1-5 orders of magnitude.

For the $(B-L)$ violating sneutrino mass $\tilde{m}_M$ the following limits are obtained [Hir98b]

$$\tilde{m}_M \leq 1.3\Big(\frac{m_{SUSY}}{100GeV}\Big)^{\frac{3}{2}} GeV, \quad \chi \simeq \tilde{B} \tag{39}$$

$$\tilde{m}_M \leq 7\Big(\frac{m_{SUSY}}{100GeV}\Big)^{\frac{7}{2}} GeV, \quad \chi \simeq \tilde{H} \tag{40}$$

for the limiting cases that the lightest neutralino is a pure Bino $\tilde{B}$, as suggested by the SUSY solution of the dark matter problem [Jun96], or a pure Higgsino. Actual values for $\tilde{m}_M$ for other choices of the neutralino composition should lie in between these two values.

$\lambda^{(\prime)}_{ijk}\lambda^{(\prime)}_{i^\prime kj}$	Our Bounds	Previous Bounds
$m_{ee} < 0.36$ eV		
$\lambda^{\prime}_{133}\lambda^{\prime}_{133}$	$5.0 \cdot 10^{-8}$	$4.9 \cdot 10^{-7}$
$\lambda^{\prime}_{132}\lambda^{\prime}_{123}$	$1.0 \cdot 10^{-6}$	$1.6 \cdot 10^{-2}$
$\lambda^{\prime}_{122}\lambda^{\prime}_{122}$	$3.0 \cdot 10^{-5}$	$4.0 \cdot 10^{-4}$
$\lambda_{133}\lambda_{133}$	$9.0 \cdot 10^{-7}$	$9.0 \cdot 10^{-6}$
$\lambda_{132}\lambda_{123}$	$2.0 \cdot 10^{-5}$	$2.0 \cdot 10^{-3}$
$\lambda_{122}\lambda_{122}$	$2.0 \cdot 10^{-4}$	$1.6 \cdot 10^{-3}$

Table 2. Correlation among neutrino mass bounds from neutrinoless double beta decay and upper limits on RPV couplings. We have used m_d=9 MeV, m_s= 170 MeV, m_b=4.4 GeV [PDG98]. For λ-products, $m_{\tilde{d}}$ should be read as $m_{\tilde{e}}$. The relevant scalars are always assumed to have a common mass of 100 GeV.

Another way to deduce a limit on the 'Majorana' sneutrino mass $\tilde{m}_M$ is to start from the experimental neutrino mass limit, since the sneutrino contributes to the Majorana neutrino mass m^{ν}_M at the 1–loop level proportional to $\tilde{m}^2_M$ [Hir98b]. Starting from the mass limit determined for the electron neutrino by $0\nu\beta\beta$ decay this leads to

$$\tilde{m}_{M_{(e)}} \leq 14 MeV \tag{41}$$

This result is somewhat dependent on neutralino masses and mixings. A non–vanishing 'Majorana' sneutrino mass would result in new processes at future colliders, like sneutrino–antisneutrino oscillations. Reactions at the Next Linear Collider (NLC) like the SUSY analog to inverse neutrinoless double beta decay $e^-e^- \to \chi^-\chi^-$ (where χ^- denote charginos) or single sneutrino production, e.g. by $e^-\gamma \to \tilde{\nu}_e\chi^-$ could give information on the Majorana sneutrino mass, also. This is discussed by [Hir97a, Hir98b, Hir98a]. A conclusion is that future accelerators can give information on second and third generation sneutrino Majorana masses, but for first generation sneutrinos cannot compete with $0\nu\beta\beta$–decay.

Compositeness Evaluation of the $0\nu\beta\beta$ half–life limit assuming exchange of excited Majorana neutrinos ν^* yields for the mass of the excited neutrino a lower bound of [Pan97a, Tak97, Pan99].

$$m_N \geq 3.4 m_W \tag{42}$$

for a coupling of order O(1) and $\Lambda_c \simeq m_N$. Here, m_W is the W–boson mass. Fig. 24 shows that this result is more stringent than the result

Fig. 3
obtained by LEPII..

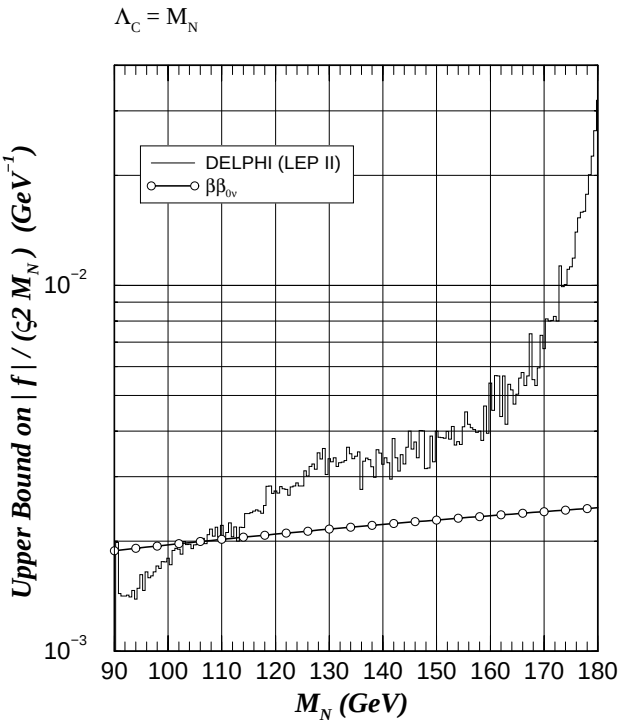

Figure 24. Comparison between the $0\nu\beta\beta$ (Heidelberg-Moscow experiment) and the LEPII upper bound on the quantity $|f|(\sqrt{2}M_N)$ as a function of the heavy neutrino mass M_N, with the choice $\Lambda_C = M_N$. Regions above the curves are excluded (from [Pan99]).

Leptoquarks Assuming that either scalar or vector leptoquarks contribute to $0\nu\beta\beta$ decay, the following constraints on the effective LQ parameters (see subsection 1.3.1) can be derived [Hir96b]:

$$\epsilon_I \leq 1.0 \times 10^{-9} \left(\frac{M_I}{100\text{GeV}} \right)^2, \tag{43}$$

$$\alpha_I^{(L)} \leq 1.3 \times 10^{-10} \left(\frac{M_I}{100\text{GeV}} \right)^2, \tag{44}$$

$$\alpha_I^{(R)} \leq 2.8 \times 10^{-8} \left(\frac{M_I}{100\text{GeV}} \right)^2 . \tag{45}$$

Since the LQ mass matrices appearing in $0\nu\beta\beta$ decay are (4×4) matrices [Hir96b], it is difficult to solve their diagonalization in full generality algebraically. However, if one assumes that only one LQ-Higgs coupling is present at a time, the (mathematical) problem is simplified greatly and one can deduce from, for example, eq. 1.41 that either the LQ-Higgs coupling must be smaller than $\sim 10^{-(4-5)}$ or there can not be any LQ with e.g. couplings of electromagnetic strength with masses below $\sim 250 GeV$. These bounds from $\beta\beta$ decay are of interest in connection with recently discussed evidence for new physics from HERA [Hew97, Bab97a, Kal97, Cho97]. Assuming that actually leptoquarks have been produced at HERA, double beta decay (the Heidelberg–Moscow experiment) would allow to fix the leptoquark–Higgs coupling to a few 10^{-6} [Hir97b]. It may be noted, that after the first consideration of leptoquark–Higgs coupling in [Hir96b] recently Babu et al. [Bab97b] noted that taking into account leptoquark–Higgs coupling reduces the leptoquark mass lower bound deduced by TEVATRON – making it more consistent with the value of 200 GeV required by HERA.

Special Relativity and Equivalence Principle

Violation of Lorentz invariance (VLI): The bound obtained from the Heidelberg–Moscow experiment is

$$\delta v < 2 \times 10^{-16} \quad \text{for} \quad \theta_v = \theta_m = 0 \tag{46}$$

where $\delta v = v_1 - v_2$ is the measure of VLI in the neutrino sector. θ_v and θ_m denote the velocity mixing angle and the weak mixing angle, respectively. In Fig. 25 (from [Kla98f]) the bound implied by double beta decay is presented for the entire range of $sin^2(2\theta_v)$, and compared with bounds obtained from neutrino oscillation experiments (see [Hal96]).

Violation of equivalence principle (VEP): Assuming only violation of the weak equivalence principle, there does not exist any bound on the amount of VEP. It is this region of the parameter space which is most restrictively bounded by neutrinoless double beta decay. In a linearized theory the gravitational part of the Lagrangian to first order in a weak gravitational field $g_{\mu\nu} = \eta_{\mu\nu} + h_{\mu\nu}$ ($h_{\mu\nu} = 2\frac{\phi}{c^2}\text{d}iag(1,1,1,1)$) can be written as $\mathcal{L} = -\frac{1}{2}(1+g_i)h_{\mu\nu}T^{\mu\nu}$, where $T^{\mu\nu}$ is the stress-energy in the gravitational eigenbasis. In the presence of VEP the g_i may differ. We obtain [Kla98f] the following bound from the Heidelberg–Moscow experiment, for $\theta_v = \theta_m = 0$:

$$\begin{aligned} \phi\delta g &< 2 \times 10^{-16} \text{ (for } \bar{m} < 13\text{eV)} \\ \phi\delta g &< 1 \times 10^{-18} \text{ (for } \bar{m} < 0.08\text{eV)}. \end{aligned} \tag{47}$$

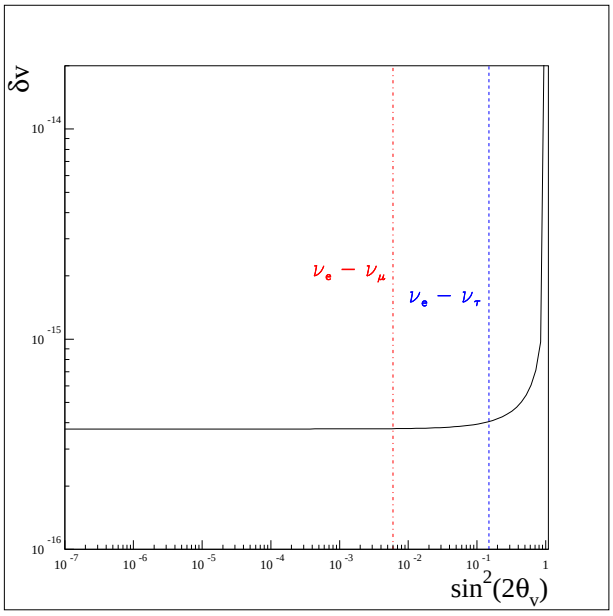

Figure 25. Double beta decay bound (solid line) on violation of Lorentz invariance in the neutrino sector, excluding the region to the upper left. Shown is a double logarithmic plot in the δv–$\sin^2(2\theta)$ parameter space. The bound becomes most stringent for the small mixing region, which has not been constrained from any other experiments. For comparison the bounds obtained from neutrino oscillation experiments (from [Hal96]) in the $\nu_e - \nu_\tau$ (dashed lines) and in the $\nu_e - \nu_\mu$ (dashed-dotted lines) channel, excluding the region to the right, are shown (from [Kla98f]).

Here $\bar{g} = \frac{g_1+g_2}{2}$ can be considered as the standard gravitational coupling, for which the equivalence principle applies. $\delta g = g_1 - g_2$. The bound on the VEP thus, unlike the one for VLI, will depend on the choice for the Newtonian potential ϕ.

Half–life of $2\nu\beta\beta$ decay The Heidelberg–Moscow experiment produced for the first time a high statistics $2\nu\beta\beta$ spectrum ($\gg$ 20000 counts, to be compared with the 40 counts on which the first detector observation of $2\nu\beta\beta$ decay by [Ell87] (for the decay of ^{82}Se) had to rely). The deduced half–life is [HM2000]

$$T^{2\nu}_{1/2} = (1.55 \pm 0.01(stat.)^{+0.03}_{-0.02}(norm.)^{+0.16}_{-0.13}(syst.)) \cdot 10^{21} y \qquad (48)$$

This result brings $\beta\beta$ research for the first time into the region of 'normal' nuclear spectroscopy and allows for the first time statistically reliable investigation of Majoron–accompanied decay modes.

Majoron–accompanied decay From simultaneous fits of the 2ν spectrum and one selected Majoron mode, experimental limits for the half–lives of the decay modes of the newly introduced Majoron models [Bur96] are given for the first time [Päs96, HM96].

The small matrix elements and phase spaces for these modes [Päs96, Hir96c] already determined that these modes by far cannot be seen in experiments of the present sensivity if we assume typical values for the neutrino–Majoron coupling constants around $\langle g \rangle = 10^{-4}$.

1.3.3 The GENIUS Potential for Double Beta Decay

Neutrino mass matrix and neutrino oscillations GENIUS will allow a large step in sensitivity for probing the neutrino mass. It will allow to probe the effective neutrino Majorana mass down to $10^{-(2-3)}$ eV, and thus surpass the existing experiments being sensitive on the mass eigenstate by a factor of 50-500. GENIUS will test the structure of the neutrino mass matrix and thereby also neutrino oscillation parameters * superior in sensitivity to many present dedicated terrestrial neutrino oscillation experiments and will provide complementary informations to recent proposals for the future in this field. Already in the first stage GENIUS will test degenerate or inverted neutrino mass scenarios, discussed in the literature as possible solutions of current hints to finite neutrino masses (see [Kla2000, Giu99, Cza99, Vis99]). If the 10^{-3} eV level is reached, GENIUS will allow to test the large angle and for degenerate models even the small angle MSW solution of the solar neutrino problem. It will also allow to test the hypothesis of a shadow world underlying introduction of a sterile neutrino [Moh97b]. The Figures

* The double beta observable, the effective neutrino mass (eq. 10), can be expressed in terms of the usual neutrino oscillation parameters, once an assumption on the ratio of m_1/m_2 is made. E.g., in the simplest two–generation case

$$\langle m_\nu \rangle = |c_{12}^2 m_1 + s_{12}^2 m_2 e^{2i\beta}|, \tag{49}$$

assuming CP conservation, i.e. $e^{2i\beta} = \eta = \pm 1$, and $c_{12}^2 m_1 << \eta s_{12}^2 m_2$,

$$\Delta m_{12}^2 \simeq m_2^2 = \frac{4\langle m_\nu \rangle^2}{(1 - \sqrt{1 - sin^2 2\theta})^2} \tag{50}$$

A little bit more general, keeping corrections of the order (m_1/m_2) one obtains

$$m_2 = \frac{\langle m_\nu \rangle}{|(\frac{m_1}{m_2}) + \frac{1}{2}(1 - \sqrt{1 - sin^2 2\theta})(\pm 1 - (\frac{m_1}{m_2}))|}. \tag{51}$$

For the general case see [Kla97c].

26, 27, 28, 29 show some examples of this potential (for more details see [Kla97c, Kla98a, Kla98b, Kla98c, Kla99a]. Fig. 26 compares the potential of GENIUS with the sensitivity of CHORUS/NOMAD and with the proposed future experiments NAUSIKAA-CERN and NAUSIKAA-FNAL – now renamed to TOSCA and COSMOS, looking for $\nu_e \leftrightarrow \nu_\tau$ oscillations, for different assumptions on m_1/m_2.

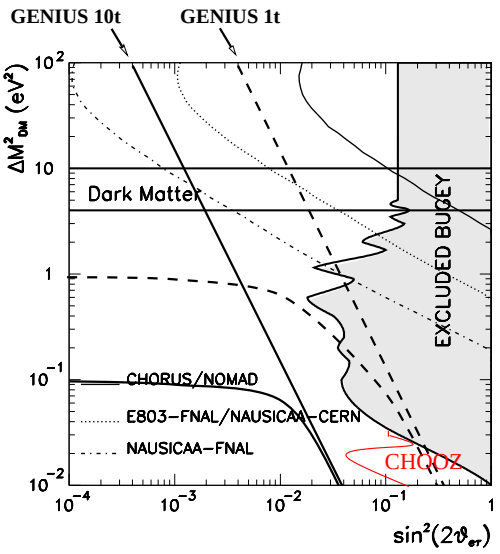

Figure 26. Current limits and future experimental sensitivity on $\nu_e - \nu_\tau$ oscillations. The shaded area is currently excluded from reactor experiments. The thin line is the estimated sensitivity of the CHORUS/NOMAD experiments. The dotted and dash-dotted thin lines are sensitivity limits of proposed accelerator experiments, NAUSICAA and E803-FNAL [Gon95]. The thick lines show the sensitivity of GENIUS (broken line: 1 t, full line: 10 t), for two examples of mass ratios. The straight lines are for the strongly hierarchical case (R=0), while the lines bending to the left assume R=0.01. (from [Kla97c])

Already in the worst case for double beta decay of $m_1/m_2 = 0$ GENIUS 1 ton is more sensitive than CHORUS and NOMAD. For quasi–degenerate models, for example $R = 0.01$ already, GENIUS 1 ton would be more sensitive than the planned future experiments TOSCA and COSMOS.

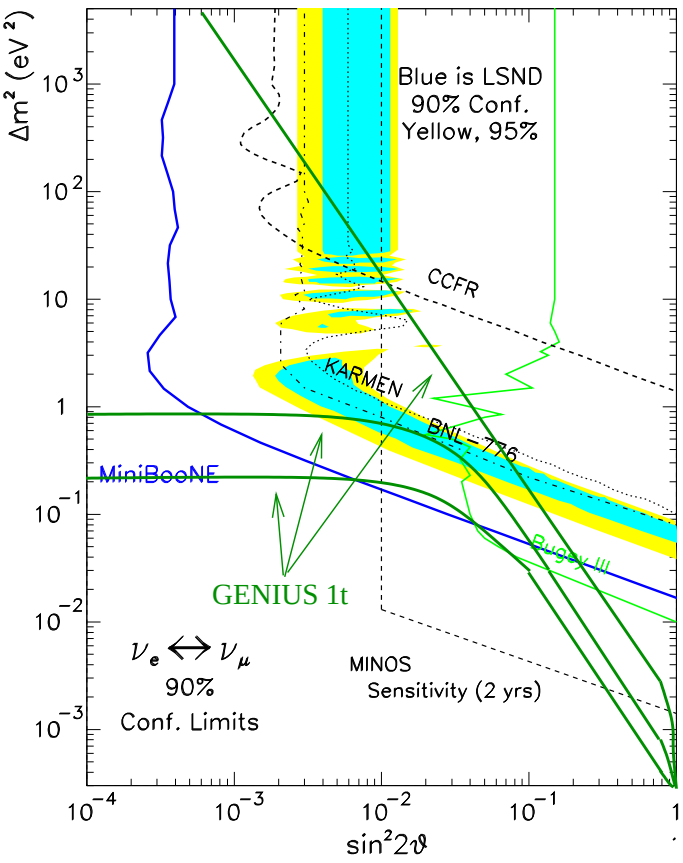

Figure 27. LSND compared to the sensitivity of GENIUS 1t for $\eta^{CP} = +1$ and three ratios R_{12}, from top to bottom $R_{12} = 0, 0.01, 0.02$ (from [Kla97c])

Fig. 27 shows the potential of GENIUS for checking the LSND indication for neutrino oscillations (original figure from [Lou98]). Under the assumption $m_1/m_2 \geq 0.02$ and $\eta = 1$, GENIUS 1 ton will be sufficient to find $0\nu\beta\beta$ decay if the LSND result is to be explained in terms of $\nu_e \leftrightarrow \nu_\mu$ oscillations. This sensitivity is comparable to – and for small and large mixing angles better than – the one of the dedicated project MINIBOONE and might be of particular interest also since the upgraded KARMEN will not completely cover [Dre97] the full allowed LSND range. Fig. 28 shows the situation for ν_e - ν_μ oscillations in reactor and accelerator experiments (assuming $\sin^2\theta_{13} = 0$). The original figure is taken from [Gel95]. The GENIUS 10 ton sensitivity is superior to the one obtained by CHOOZ and could compete with the long baseline project MINOS, even in the worst

case of $m_{\nu_e} << m_{\nu_\mu}$. In the quasi-degenerate models GENIUS would be much more sensitive - see Fig. 27.

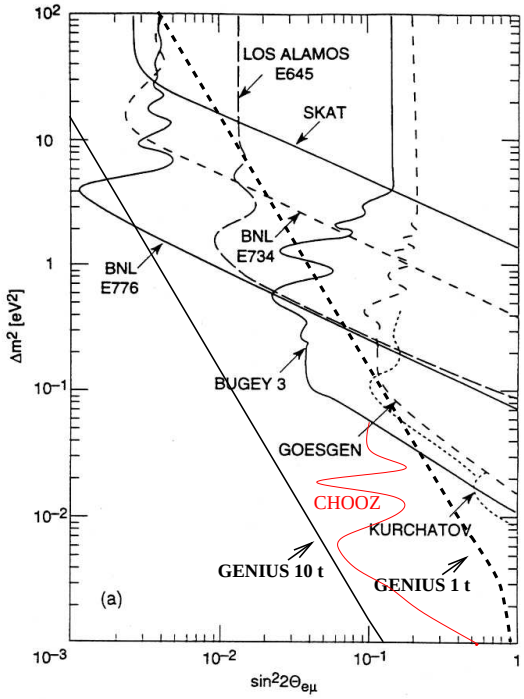

Figure 28. Current limits on $\nu_e - \nu_\mu$ oscillations. Various existing experimental limits from reactor and accelerator experiments are indicated, as summarized in ref. [Gel95]. In addition, the figure shows the expected sensitivities for GENIUS with 1 ton (thick broken line) and GENIUS with 10 tons (thick, full line) (from [Kla97c])

Fig. 29 shows a summary of currently known constraints on neutrino oscillation parameters (original taken from [Hat94]), but including the $0\nu\beta\beta$ decay sensitivities of GENIUS 1 ton and GENIUS 10 tons, for different assumptions on m_1/m_2 (for $\eta^{CP} = +1$, for $\eta^{CP} = -1$ see [Kla97c]). It is seen that already GENIUS 1 ton tests all degenerate or quasi–degenerate ($m_1/m_2 \geq\sim 0.01$) neutrino mass models in any range where neutrinos are interesting for cosmology, and also the atmospheric neutrino problem, if it is due to $\nu_e \leftrightarrow \nu_\mu$ oscillations. GENIUS in its 10 ton version would directly test the large angle solution of the solar neutrino problem and in case of almost degenerate neutrino masses, also the small angle solution.

After this overview we discuss the potential of GENIUS for the various neutrino mass scenarios in some detail, putting some emphasis on the relations to the solar and atmospheric neutrino oscillation experiments and on the complementarity of recent and future projects in these fields including the investigation of cosmological parameters like by the future satellite experiments MAP and PLANCK.

In a three neutrino framework the atmospheric neutrino data are assumed to be described by $\nu_\mu - \nu_\tau$ oscillations [Smi99] with:

$$\Delta m^2_{atm} = (1-10)\ 10^{-3}\mathrm{eV}^2\ , \quad \sin^2 2\theta_{atm} = 0.8-1, \tag{52}$$

as the leading mode. Also small contributions of other modes are not excluded.

For solar neutrinos different possibilities are considered [Smi99] which in general lead to different expectations for the double beta decay:

1. Small mixing MSW solution with

$$\Delta m^2_{\odot} = (0.4-1)\cdot 10^{-5}\mathrm{eV}^2\ , \quad \sin^2 2\theta_{\odot} = (0.3-1.2)\cdot 10^{-2} \tag{53}$$

2. Large mixing MSW solution with

$$\Delta m^2_{\odot} = (0.1-3)\cdot 10^{-4}\mathrm{eV}^2\ , \quad \sin^2 2\theta_{\odot} = (0.7-1) \tag{54}$$

3. Vacuum oscillation solutions

$$\Delta m^2_{\odot} = (0.6-6)\cdot 10^{-10}\mathrm{eV}^2\ , \quad \sin^2 2\theta_{\odot} = (0.6-1) \tag{55}$$

The so-called MSW low solution gives a worse fit to the data and will not be considered in the following (see however subsection 1.4).

Expressing eq. 9 in terms of oscillation parameters we get

$$\langle m\rangle = |U_{e1}|^2 m_0 + e^{i\phi_{21}}|U_{e2}|^2\sqrt{\Delta m^2_{21}+m_0^2} + e^{i\phi_{31}}|U_{e3}|^2\sqrt{\Delta m^2_{31}+m_0^2}\ , \tag{56}$$

where ϕ_{ij} are the relative phases of masses m_i and m_j. Assuming m_1 to be the lightest state we have absorbed m_1^2 in the definition of m_0^2, $m_0^2 \rightarrow m_0^2 + m_1^2$ so that now $m_0 \geq 0$.

The crucial assumption in order to link neutrino oscillations and the double beta observable eq. 56 concerns the grade of degeneracy in the

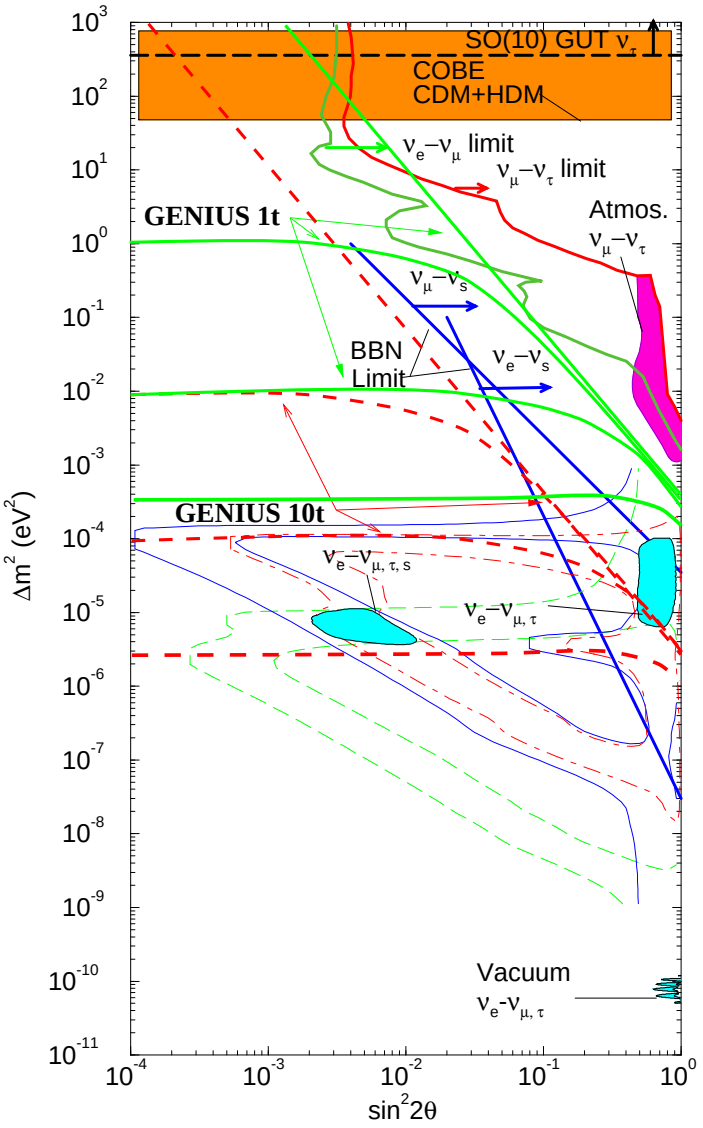
SO(10) GUT ν_τ
COBE
CDM+HDM
ν_e–ν_μ limit
ν_μ–ν_τ limit
GENIUS 1t
Atmos.
ν_μ–ν_τ
ν_μ–ν_s
BBN
Limit
ν_e–ν_s
GENIUS 10t
ν_e–ν_μ, τ, s
ν_e–ν_μ, τ
Vacuum
ν_e-ν_μ, τ
Δm² (eV²)
sin²2θ

Figure 29. Summary of currently known constraints on neutrino oscillation parameters. The (background) figure without the $0\nu\beta\beta$ decay constraints can be obtained from http://dept.physics.upenn.edu/~www/neutrino/solar.html. Shown are the vacuum and MSW solutions (for two generations of neutrinos) for the solar neutrino problem, the parameter range which would solve the atmospheric neutrino problem and various reactor and accelerator limits on neutrino oscillations. In addition, the mass range in which neutrinos are good hot dark matter candidates is indicated, as well as limits on neutrino oscillations into sterile states from considerations of big bang nucleosynthesis. Finally the thick lines indicate the sensitivity of GENIUS (full lines 1 ton, broken lines 10 ton) to neutrino oscillation parameters for three values of neutrino mass ratios $R = 0, 0.01$ and 0.1 (from top to bottom). For GENIUS 10 ton also the contour line for $R = 0.5$ is shown. The region beyond the lines would be excluded. While already the 1 ton GENIUS would be sufficient to constrain degenerate and quasi-degenerate neutrino mass models, the 10 ton version of GENIUS could cover a significant new part of the parameter space, including the large angle MSW solution to the solar neutrino problem, even in the worst case of $R = 0$. For $R \geq 0.5$ it would even probe the small angle MSW solution (see [Kla98g, Kla98e]).

neutrino mass spectrum, which may be described by the value of m_0. Three possibilities are determined by the relative values of m_0^2, Δm_{21}^2 and Δm_{31}^2:

- neutrino schemes with strong hierarchy: $m_0^2 \ll \Delta m_{21}^2 \ll \Delta m_{31}^2$,
- with partial degeneracy: $\Delta m_{21}^2 \ll m_0^2 \ll \Delta m_{31}^2$,
- and with complete degeneracy: $\Delta m_{21}^2 \ll \Delta m_{31}^2 \ll m_0^2$.

1.3.4 Schemes with mass hierarchy In the hierarchical case,

$$m_0^2 \ll \Delta m_{21}^2 \ll \Delta m_{31}^2 \ , \tag{57}$$

the absolute values of two heavy neutrinos are completely determined by the mass squared differences (that is, by the oscillation parameters):

$$m_3^2 = \Delta m_{31}^2 = \Delta m_{atm}^2, \quad m_2^2 = \Delta m_{21}^2 = \Delta m_{\odot}^2, \quad m_1^2 = m_0^2, \tag{58}$$

and the only freedom is the choice of the value of m_1. In this scheme there is no explanation of the LSND result, and the contribution to the Hot Dark Matter component of the universe is small: $\Omega_\nu < 0.01$. Different solutions of the solar neutrino problem lead to different implications for

the effective neutrino mass. It is useful to discuss the contributions of the mass eigenstates separately. They are shown in figs. 30-32.

In the *single maximal (large) mixing scheme* ν_μ and ν_τ are mixed strongly in ν_2 and ν_3. The electron flavor is weakly mixed: it is mainly in ν_1 with small admixtures in the heavy states. The solar neutrino data are explained by $\nu_e \to \nu_2$ resonance conversion inside the Sun.

For double beta decay searches this scheme is a kind of worst–case scenario. Due to the hierarchy of masses and the small admixture of m_μ in m_1 $\langle m \rangle$ is dominated by $m_3 \sim \Delta m_{13}$:

$$\langle m \rangle^{(3)} \simeq U_{e3}^2 m_3, \tag{59}$$

which is severely constrained by the CHOOZ experiment (see fig. 30). In terms of oscillation parameters the effective neutrino mass can be written as

$$\langle m \rangle \simeq \frac{1}{2}\sqrt{\Delta m_{atm}^2} \cdot \left(1 - \sqrt{1 - \sin^2 2\theta}\right). \tag{60}$$

The contribution from the second mass (first term) is $< 10^{-5}$ eV. As follows from fig. 30 in the range of Δm^2 relevant for the solution of the atmospheric neutrino problem $\langle m \rangle$ can reach $\langle m \rangle \approx \langle m \rangle^{(3)} = (3-4) \cdot 10^{-3}$ eV and in the best fit range: $\langle m \rangle \approx 2 \cdot 10^{-3}$ eV. Thus the 10 ton GENIUS experiment could access the unexcluded region of $\langle m \rangle$, while the observation of neutrinoless double beta decay induced by the neutrino mass mechanism with $\langle m \rangle > 6 \cdot 10^{-3}$eV, the final sensitivity of the 1 ton version, would rule out the single maximal scenario with maximal mass hierarchy.

Bi-large mixing: The previous scheme can be modified in such a way that solar neutrino data are explained by large angle MSW conversion. The contribution from the third state is the same as in eq. 60.

However now the contribution from the second level can be significant: both mixing parameter and the mass are now larger. The contribution from the second state equals

$$\langle m \rangle^{(2)} = m_2 |U_{e2}^2| = \sqrt{\Delta m_\odot^2} \sin^2 \theta_\odot \sim (0.8 - 6) \cdot 10^{-3}\text{eV}. \tag{61}$$

Providing a sensitivity of $\langle m \rangle = 0.001$ eV GENIUS could cover the main part of the large mixing angle MSW solution of the solar neutrino deficit and could be complementary to the search of day-night effects (see fig. 31).

Contributions of the first state: For a non-vanishing m_0 a further contribution for both schemes is implied by an offset over the oscillation pattern. This contribution arising from m_1 is shown in fig. 32. The total effective neutrino mass can easily be determined from figs. 30 - 32 by adding the single contributions.

This is true as long as $m_1^2 \ll \Delta m_{12}^2 \simeq m_2^2$. As can be seen from fig. 32 this additional contribution ($< \langle m \rangle^{(1)} + 2m_0$) easily may reach 10^{-2}

eV without leaving the hierarchical pattern, shifting the effective neutrino mass to observable values for the 1 ton version of GENIUS. However, also cancellation of the contributions may appear. In any case neutrino oscillations are not sensitive on this quantity, pushing GENIUS into some key position for testing the mass of the first state.

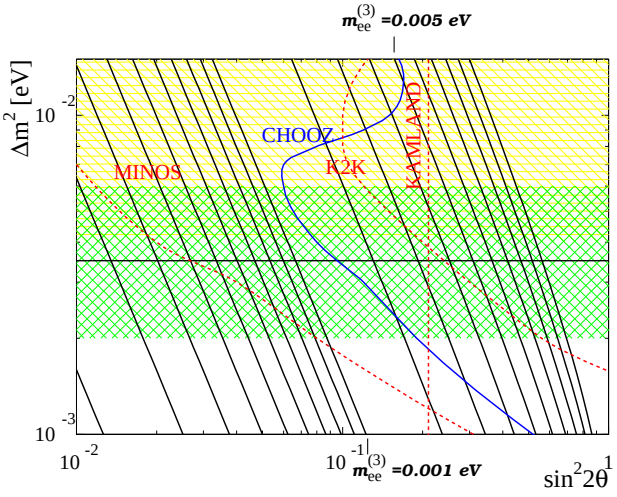

Figure 30. Iso-mass ($\langle m \rangle$) lines in the single maximal mixing scheme with hierarchical mass pattern. From the upper right downward $\langle m \rangle$ = 0.01, 0.009, 0.008, 0.007, 0.006, 0.005, 0.004, 0.003, 0.002, 0.001, 0.0009, 0.0008, 0.0007, 0.0006, 0.0005, 0.0004, 0.0003 eV. Also shown are the regions favored by the atmospheric neutrino data of Super–Kamiokande with current bestfit and Kamiokande (lower and upper shaded areas respectively according [Kaj99]) and the borders of regions excluded by CHOOZ and BUGEY (solid lines) as well as the expected final sensitivity of CHOOZ (according to [Apo99]) and KAMLAND (dashed) as well as of MINOS and K2K (dash-dotted) (according to [Zub98]). For less hierarchical scenarios additional contributions from the first state arise (see fig. 32). (from [Kla2000])

Schemes with partial degeneracy In the partially degenerate case,

$$\Delta m_{21}^2 \ll m_0^2 \ll \Delta m_{31}^2 \ , \tag{62}$$

the two light neutrinos have close masses determined by m_0 and the heaviest mass is determined by the oscillation parameter:

$$m_1^2 \approx m_2^2 \approx m_0^2 \ , \quad m_3^2 \approx \Delta m_{31}^2 = \sqrt{\Delta m_{atm}^2} \ . \tag{63}$$

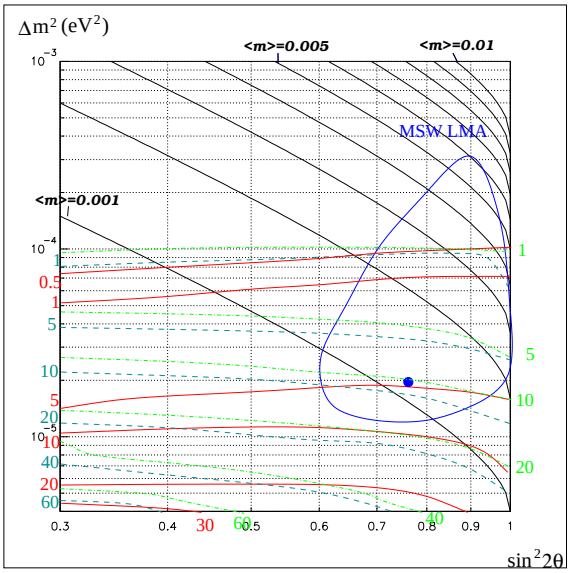

Figure 31. The iso-mass $\langle m\rangle^{(2)}$ lines, determining the contribution of the second state in the $\Delta m^2_{12} - \sin^2 2\theta_{12}$ plane for the hierarchical scheme with the LMA MSW solution. From the upper right downward: $\langle m\rangle^{(2)} = 0.01$, 0.009, 0.008, 0.007, 0.006, 0.005, 0.004, 0.003, 0.002, 0.001 eV. Also shown is the MSW LMA 90 % C.L. allowed region from the combined rate analysis of Homestake, Gallex, Sage and Super-K with the BP98 SSM and the Super–Kamiokande Day-Night variation [Fuk99] with the point showing the bestfit (rates only) according to [Bah98a]. The solid, dashed and dash-dotted lines correspond to contours of constant day-night assymmetry $A_{n-d} = Q_n - Q_d/Q_n + Q_d$ of average rates Q in Super-Kamiokande, SNO and ICARUS respectively, according to [Bah97]. KAMLAND should observe a disappearance signal and the 10 ton version of GENIUS should see double beta decay in this model. (from [Kla2000])

The expression for the effective neutrino mass can be written as

$$\langle m\rangle = m_0(\sin^2\theta_\odot + e^{i\phi_{21}}\cos^2\theta_\odot) + e^{i\phi_{31}}\sqrt{\Delta m^2_{atm}}\sin^2\theta_{atm}, \qquad (64)$$

where θ_{atm} determines the admixture of the ν_e in ν_3. For the small mixing MSW solution of the solar neutrino problem we get

$$\langle m\rangle \approx m_0 + e^{i\phi_{31}}\sqrt{\Delta m^2_{atm}}\sin^2\theta_{atm}. \qquad (65)$$

For the *large mixing angle MSW solution* cancellation of contributions from the lightest states may occur, so that even for relatively large m_0 the con-

tribution from the third neutrino state gives the main contribution, which is severely constrained by CHOOZ (see fig. 30).

The partially degenerate spectrum with

$$\Delta m^2_{21} \ll \Delta m^2_{31} = m^2_0 \ . \tag{66}$$

leads to a scheme with inverse mass hierarchy:

$$m^2_1 \approx m^2_2 \approx m^2_0 \ = \Delta m^2_{atm}, \quad m^2_3 \ll m^2_0. \tag{67}$$

The effective Majorana mass can be written as

$$\langle m \rangle \approx \sqrt{\Delta m^2_{atm}}(\sin^2\theta_\odot + e^{i\phi_{21}}\cos^2\theta_\odot) \ , \tag{68}$$

where we have neglected the small contribution from the third state: $m_3 U^2_{e3}$ ($U^2_{e3} < 5 \cdot 10^{-2}$). The two heavier eigenstates contribute to the hot dark matter (HDM)

$$\Omega_\nu = \frac{2m_1}{91.5eV} h^{-2} \tag{69}$$

Assuming the *vacuum oscillation solution* (for inverse hierarchy no level–crossing in the sun and thus no MSW effect appears), both addition yielding $\langle m \rangle \simeq 0.03 - 0.1$ eV as well as compensation of the contributions from the two heavy states can occur. In the case of the bi-maximal scheme the compensation is complete. Again, additional contributions from the lightest state, here m_3 may be possible. In Fig. 33 the sensitivity in the $m_0 - \sin^2 2\theta$ plane is shown together with the favored regions of the "Just-so" vacuum solution. Allowing for CP violation here just implies the cancellation to be less effective. All values for ϕ_{12}, ϕ_{13} imply a behavior of the mass eigenstates settled between the extreme values of 0 and π. As can be seen, GENIUS may provide sensitive informations about the mixing and the grade of cancellation among the states, being complementary to determinations of the sum of the neutrino mass eigenstates due to studies of the power spectra of the cosmic microwave background or galaxies by MAP and Planck or the SDSS (Sloan Digital Sky Survey) [Eis98].

Schemes with complete degeneracy In degenerate schemes the common mass is much larger than the mass splittings:

$$\Delta m^2_{21} \ll \Delta m^2_{31} \ll m^2_0. \tag{70}$$

In this case the effective neutrino mass is

$$\langle m \rangle = (|U_{e1}|^2 + |U_{e2}|^2 e^{i\phi_{21}} + |U_{e3}|^2 e^{i\phi_{31}}) m_0, \tag{71}$$

which is determined by mixing angles and relative phases of the mass terms.

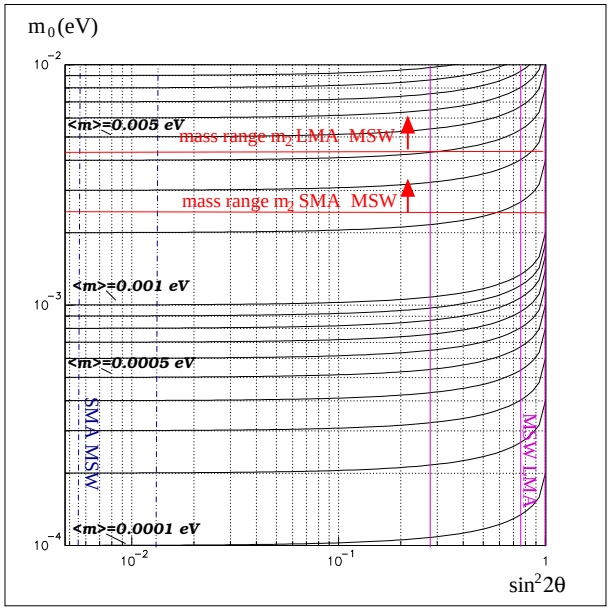

Figure 32. Contribution of the first state in hierarchical models with $m_1 > 0$. Shown is $\langle m \rangle$ in the $m_0 - sin^2(2\theta_{12})$ plane, together with the favored regions for LMA MSW (solid) and SMA MSW (dash-dot-dot), the SMA extends further to smaller mixing, where $\langle m \rangle = m_0 = const.$ The horizontal solid lines indicate the region above which the assumption $m_1^2 \ll \Delta m^2 = m_2^2$ is not valid anymore (Super-K bestfit for MSW LMA and SMA). Vacuum oscillations are not included here, since for this case the model will be partially degenerate before any significant contribution to $\langle m \rangle$ arises. It is easy to see that sizable contributions from the first state could lead to observable double beta rates even in hierarchical models. (from [Kla2000])

In the case of the small mixing MSW solution ($U_{e1}^2 \gg U_{e2}^2, U_{e3}^2$) no substantial cancellation appears and $\langle m \rangle \approx m_0$. The same expression can be obtained for any solution of the solar neutrino problem if the CP violating phases are zero: $\phi_{12} = \phi_{13} = 0$ or $\phi_{12} = 0$,$U_{e3}^2 \simeq 0$. Double beta decay and neutrino oscillations decouple. The effective neutrino mass can be restricted by cosmological observations. The contribution of neutrinos to the HDM in the universe is

$$\Omega_\nu = \frac{3m_0}{91.5eV} h^{-2} \tag{72}$$

(see Fig. 33). In bimaximal schemes $\langle m \rangle$ is exactly vanishing. However, comparing with the quark sector, this case seems to be rather unnatural.

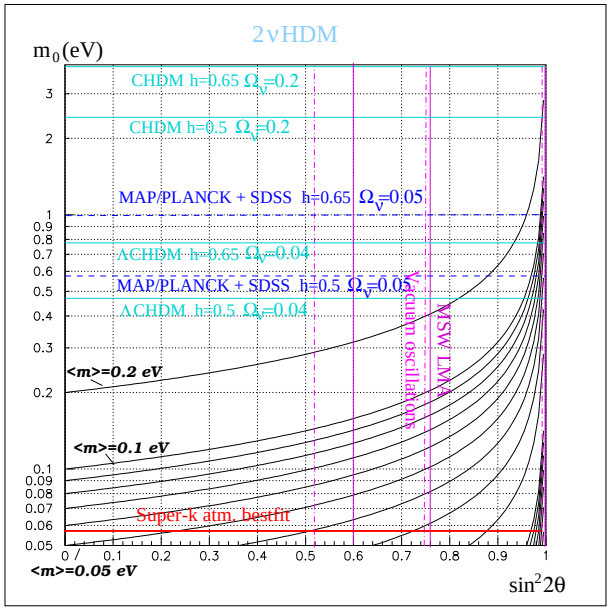

Figure 33. Plotted are iso-mass lines in the $m_0 - sin^2(2\theta)$ plane for the case of cancellation between degenerate states m_1 and m_2 in partially degenerate scenarios with two neutrinos contributing to the hot dark matter. Mass splitting is neglected, since $m_1 - m_2 \ll m_0$ and $m_3 - m_1$ changes the cosmological considerations less than 10 %. Shown are the bestfits for CHDM (according to [Gaw98]), and ΛCHDM (according to [Pri98]) for different values of the Hubble constant. Also shown is the sensitivity of MAP/Planck combined with SDSS according to [Eis98]. The regions of the MSW LMA and vac. osc. have been taken from [Bah98a]. Also shown is the bestfit for atmospheric neutrinos, which gives a lower limit for m_0 in inverse hierarchical models. Combined with the neutrino oscillation results and the precision determinations of cosmological parameters GENIUS will allow to give precise informations about mixing and the absolute mass scale in partially degenerate scenarios. Assuming, e.g. a worst case $m_0 = 0.06$ eV just above the atmospheric neutrino bestfit, the MSW LMSA or vacuum solution would imply $\langle m \rangle = 0.03$ eV (from [Kla2000]).

For $U_{e3}^2 \simeq 0$ and $\phi_{12} = \pi$ in eq. 56 the double beta observable becomes

$$\langle m \rangle \simeq m_0 \sqrt{1 - \sin^2 2\theta}. \tag{73}$$

As in fig. 33 in fig. 34 the sensitivity in the $m_0 - \sin^2 2\theta$ plane is shown together with the favored regions of the solar MSW large mixing angle solution as well as the "Just-so" vacuum solution. Again GENIUS pro-

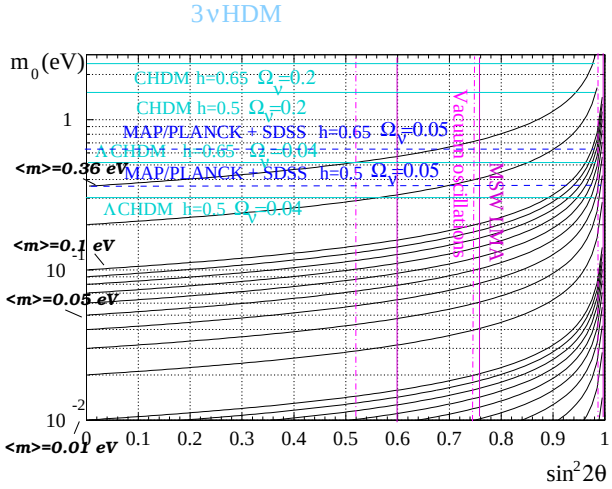

Figure 34. As figure 33 for totally degenerate scenarios, that means three neutrinos are contributing to the hot dark matter. Combined with the neutrino oscillation results and the precision determinations of cosmological parameters GENIUS will allow to give precise informations about mixing and the absolute mass scale in degenerate scenarios. E.g. assuming an overall scale of 0.3 eV corresponding to the ΛCHDM models with $\Omega = 0.04$ and $h = 0.5$, the bestfit of either the MSW or the vacuum solution would imply $\langle m \rangle = 0.15$ eV (from [Kla2000]).

vides a tool of unique sensitivity for determining mixings and the grade of cancellation among the states.

LSND and four neutrino scenarios Additional neutrino states being singlets under the usual SU(2) have been discussed [Smi99] in order to account for the LSND anomaly with

$$\Delta m^2_{LSND} \simeq 1eV^2. \tag{74}$$

The viable schemes contain two light states responsible for the solution of the solar neutrino problem and two heavy states in the range relevant for structure formation in the universe and for oscillations of atmospheric neutrinos (see also the discussion in [Giu99]). ν_μ and ν_τ are strongly mixed in two heavy mass eigenstates ν_2 and ν_3 with

$$\sqrt{m_3^2 - m_2^2} \equiv \sqrt{\Delta m^2_{ATM}} \ll m_3 \approx m_{HDM}, \tag{75}$$

so that $\nu_\mu \leftrightarrow \nu_\tau$ oscillations solve the atmospheric neutrino problem. ν_e and ν_s are weakly mixed in the two lightest mass states. Resonance conversion

$\nu_e \to \nu_s$ solves the solar neutrino problem. As has been pointed out in [Giu99] the inverse scheme requires strong cancellation in the heavy states to fit the present bound from the Heidelberg–Moscow experiment. This requires large mixing of ν_s and ν_e, which is excluded by BBN bounds on the number of neutrino species. Since this issue is still rather controversial (see [Giu99] and references therein) it may be interesting to study the situation of a weakened BBN bound. In this case the inverse hierarchical scheme is still unexcluded in combination with the MSW LMA or vacuum solution and [Bil99]

$$7 \cdot 10^{-2} eV < \langle m \rangle < 1.4 eV. \tag{76}$$

In fig. 35 $\langle m \rangle$ is plotted as a function of Δm^2 for the case of the LMA MSW solution.

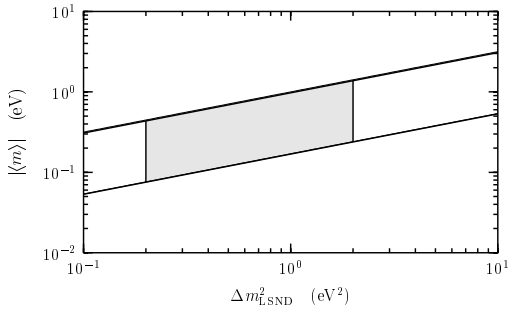

Figure 35. Four neutrinos in the scheme with direct mass hierarchy: The shaded area shows the possible value of the effective Majorana mass $\langle m \rangle$ in the range of Δm^2_{LSND} for the case of the MSW LMA solution of the solar neutrino problem. This case can be easily checked by the 1 ton version of GENIUS (from [Bil99]).

Turning to the hierarchical scheme the contribution to m_{ee} from the pair of heavy mass states can be written as

$$m_{ee}^{(23)} = U_{e2}^2 m_2 + U_{e3}^2 m_3 \approx (|U_{e2}|^2 + |U_{e3}|^2 e^{i\phi}) m_3 \ . \tag{77}$$

The masses $m_3 \approx m_2$ can be relevant for cosmology, their value determines the splitting between pairs of the heavy and the light states and can induce the oscillations observed by LSND:

$$m_3 = \sqrt{\Delta m^2_{LSND}} = \frac{1}{2} m_{HDM} \ . \tag{78}$$

Therefore,

$$\langle m\rangle^{(23)} = (|U_{e2}|^2 + |U_{e3}|^2 e^{i\phi})\sqrt{\Delta m^2_{LSND}}. \quad (79)$$

Taking the bound from Bugey into account this is leading to

$$7 \cdot 10^{-4} < \langle m\rangle^{(23)} < 2 \cdot 10^{-2}, \quad (80)$$

which may yield a positive signal in GENIUS [Giu99]. The contribution of the light states corresponds to the situation in hierarchical schemes discussed above. It may become significant in the case of strong cancellation in the heavy states.

Summary In summary, GENIUS can play an important role in reconstructing the neutrino mass spectrum. In strongly hierarchical schemes the magnitude of the double beta observable depends crucially on the assumed solution for the solar neutrino problem. While with assuming the MSW SMA or vacuum oscillations the observation of $0\nu\beta\beta$ with $\langle m\rangle > 6 \cdot 10^{-3}$ would rule out the scheme, in scenarios with MSW LMA GENIUS (10 tons) should observe a positive signal for the main part of the MSW LMA solution, being complementary to the search for day-night effects in present and future solar neutrino experiments such as Superkamiokande, SNO or ICARUS. In any case GENIUS may provide a unique possibility to determine the mass of the lightest state. Even more stringent restrictions may be obtained in partially or completely degenerate schemes, motivated by giving sizable contributions to the hot dark matter in the universe. In such scenarios already the present half life limit of the Heidelberg–Moscow experiment requires strong cancellation between the mass eigenstates. GENIUS could help to determine the mixing in such schemes with extreme accuracy, providing informations being complementary to precision tests of cosmological parameters by MAP and Planck. In four neutrino scenarios GENIUS has good perspectives for testing the LSND signal. For further recent discussions of the potential of GENIUS for probing neutrino masses we refer, e.g., to [Kla2000, Giu99, Cza99, Vis99, Bil99].

1.3.3.2 GENIUS and super–heavy left–handed neutrinos: Fig. 36 (from [Bel98]) compares the sensitivity of GENIUS for heavy left-handed neutrinos (as function of U^2_{ei}, for which the present LEP limit is $U^2_{ei} \leq 5 \cdot 10^{-3}$ [Nar95]) with the discovery limit for $e^-e^- \to W^-W^-$ at Next Linear Colliders. The observable in $0\nu\beta\beta$ decay is

$$\langle m_\nu^{-1}\rangle_H = \sum_i {}'' U^2_{ei} \frac{1}{M_i}. \quad (81)$$

Also shown are the present limits from the Heidelberg–Moscow experiment (denoted by $0\nu\beta\beta$) assuming different matrix elements. It is obvious that $0\nu\beta\beta$ is more sensitive than any reasonable future Linear Collider.

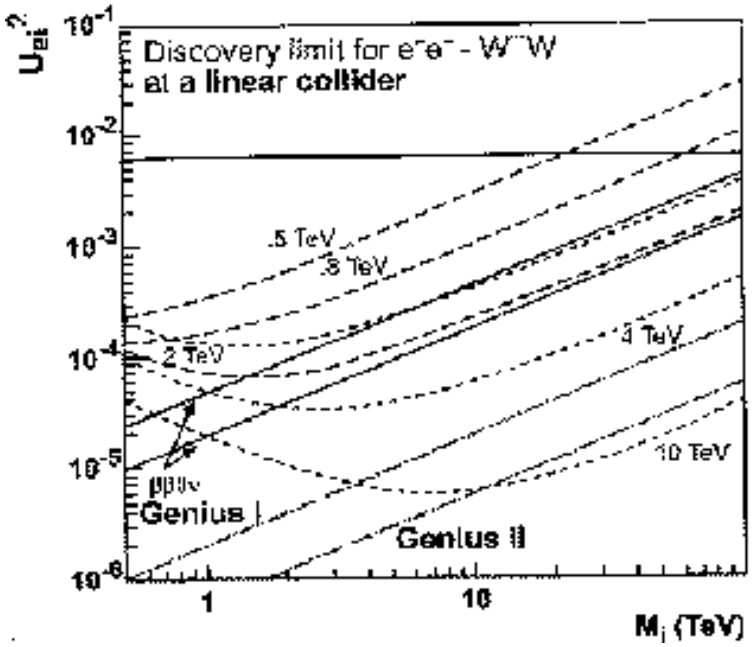

Figure 36. Discovery limit for $e^-e^- \to W^-W^-$ at a linear collider as function of the mass M_i of a heavy left–handed neutrino, and of U_{ei}^2 for $\sqrt{s}$ between 500 GeV and 10 TeV. In all cases the parameter space above the line corresponds to observable events. Also shown are the limits set by the Heidelberg–Moscow $0\nu\beta\beta$ experiment as well as the prospective limits from GENIUS. The areas above the $0\nu\beta\beta$ contour lines are excluded. The horizontal line denotes the limit on neutrino mixing, U_{ei}^2, from LEP. Here the parameter space above the line is excluded. (from [Bel98]).

1.3.3.3 GENIUS and left–right symmetry: If GENIUS is able to reach down to $\langle m_\nu \rangle \leq 0.01$ eV, it would at the same time be sensitive to right-handed W-boson masses up to $m_{W_R} \geq 8$ TeV (for a heavy right-handed neutrino mass of 1 TeV) or $m_{W_R} \geq 5.3$ TeV (at $\langle m_N \rangle = m_{W_R}$) [Kla97c]. Such a limit would be comparable to the one expected for LHC, see for example [Riz96], which quotes a final sensitivity of something like $5 - 6$ TeV. Note, however that in order to obtain such a limit the experiments at LHC need to accumulate about $100 fb^{-1}$ of statistics. A 10 ton version of GENIUS could even reach a sensitivity of $m_{W_R} \geq 18$ TeV (for a heavy right-handed neutrino mass of 1 TeV) or $m_{W_R} \geq 10.1$ TeV (at $\langle m_N \rangle = m_{W_R}$).

This means that already GENIUS 1 ton could be sufficient to definitely test recent supersymmetric left–right symmetric models having the nice

features of solving the strong CP problem without the need for an axion and having automatic R–parity conservation [Kuc95, Moh96a].

1.3.3.4 GENIUS and R_p–violating SUSY: The improvement on the R–parity breaking Yukawa coupling $\lambda^{'}_{111}$ (see subsection 1.3.1) is shown in Fig. 37. The full line to the right is the expected sensitivity of the LHC – in the limit of large statistics. The three dashed–dotted lines denote (from top to bottom) the current constraint from the Heidelberg–Moscow experiment and the sensitivity of GENIUS 1 ton and GENIUS 10 tons, all for the conservative case of a gluino mass of 1 TeV. If squarks would be heavier than 1 TeV, LHC could not compete with GENIUS. However, for typical squark masses below 1 TeV, LHC could probe smaller couplings. However, one should keep in mind, that LHC can probe squark masses up to 1 TeV only with several years of data taking.

The potential of GENIUS on R-parity breaking coupling products derived from the neutrino mass bounds is shown in tab. 3 [Bha99]. GENIUS in the 1(10) ton version would provide a further improvement by 1(2) orders of magnitude compared to the Heidelberg–Moscow experiment.

$\lambda^{(')}_{ijk}\lambda^{(')}_{i'kj}$	Our Bounds	Previous Bounds
$m_{ee} < 0.01(0.001)$ eV	[GENIUS 1(10)t]	
$\lambda^{'}_{133}\lambda^{'}_{133}$	$1.5 \cdot 10^{-9(-10)}$	$4.9 \cdot 10^{-7}$
$\lambda^{'}_{132}\lambda^{'}_{123}$	$3.7 \cdot 10^{-8(-9)}$	$1.6 \cdot 10^{-2}$
$\lambda^{'}_{122}\lambda^{'}_{122}$	$9.2 \cdot 10^{-7(-8)}$	$4.0 \cdot 10^{-4}$
$\lambda_{133}\lambda_{133}$	$2.6 \cdot 10^{-8(-9)}$	$9.0 \cdot 10^{-6}$
$\lambda_{132}\lambda_{123}$	$4.3 \cdot 10^{-7(-8)}$	$2.0 \cdot 10^{-3}$
$\lambda_{122}\lambda_{122}$	$7.1 \cdot 10^{-6(-7)}$	$1.6 \cdot 10^{-3}$

Table 3. Correlation among neutrino mass bounds from GENIUS and upper limits on RPV couplings. We have used m_d=9 MeV, m_s= 170 MeV, m_b=4.4 GeV [PDG98]. For λ-products, $m_{\tilde{d}}$ should be read as $m_{\tilde{e}}$. The relevant scalars are always assumed to have a common mass of 100 GeV.

1.3.3.5 GENIUS and R_p–conserving SUSY: Since the limits on a 'Majorana–like' sneutrino mass $\tilde{m}_M$ scale with $(T_{1/2})^{1/4}$, GENIUS 1 ton (or 10 tons) would test 'Majorana' sneutrino masses lower by factors of about 7(20), compared with present constraints [Hir97a, Hir98b, Hir97b].

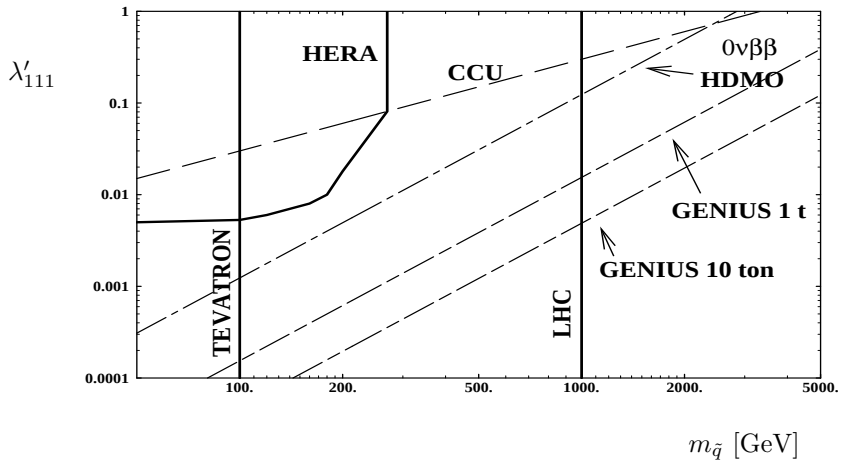

Figure 37. Comparison of sensitivities of existing and future experiments on $R\!\!\!/_p$SUSY models in the plane $\lambda'_{111} - m_{\tilde{q}}$. Note the double logarithmic scale! Shown are the areas currently excluded by the experiments at the TEVATRON, the limit from charged-current universality, denoted by CCU, and the limit from absence of $0\nu\beta\beta$ decay from the Heidelberg-Moscow collaboration ($0\nu\beta\beta$ HDMO). In addition, the estimated sensitivity of HERA and the LHC is compared to the one expected for GENIUS in the 1 ton and the 10 ton version (from [Kla97c]).

1.3.3.6 GENIUS and Leptoquarks: Limits on the lepton–number violating parameters as defined previously improve as $\sqrt{T_{1/2}}$. This means that for leptoquarks in the range of 200 GeV LQ–Higgs couplings down to (a few) 10^{-8} could be explored. In other words, if leptoquarks interact with the standard model Higgs boson with a coupling of the order $\mathcal{O}(1)$, either $0\nu\beta\beta$ must be found, or LQs must be heavier than (several) 10 TeV.

1.3.3.7 GENIUS and composite neutrinos GENIUS in the 1(10) ton version would improve the limit on the excited Majorana neutrino mass deduced from the Heidelberg–Moscow experiment (eq. 32) to

$$m_N \geq 1.1(2.3) \quad TeV \tag{82}$$

A recent detailed study [Pan99] shows that while the HEIDELBERG–MOSCOW experiment already exceeds the sensitivity of LEPII in probing compositeness, GENIUS will reach the sensitivity of LHC. With the $0\nu\beta\beta$

half life against decay by exchange of a composite Majorana neutrino given by [Pan99]

$$T_{1/2}^{-1} = \left(\frac{f}{\Lambda_c}\right)^4 \frac{m_A^8}{M_N^2} |\mathcal{M}_{FI}|^2 \frac{G_{01}}{m_e^2} \tag{83}$$

where M_N is the composite neutrino Majorana mass, and f denotes the coupling with the electron. Fig. 38 shows the situations of GENIUS and LHC.

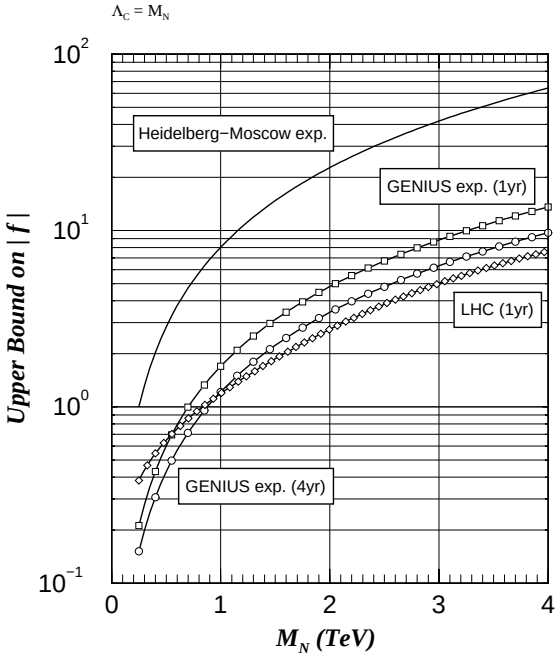

Figure 38. Sensitivity of LHC and GENIUS to compositeness parameters (assuming $\Lambda_C = M_N$). Regions above the curves are excluded. The LHC bound is weaker than the GENIUS bound for $M_N < 550(1000)$ GeV. (from [Pan99])

1.3.3.8 GENIUS, special relativity and equivalence principle in the neutrino sector The already now strongest limits given by the Heidelberg–Moscow experiment discussed in subsection 1.3.2 would be improved by 1–2 orders of magnitude. It should be stressed again, that while neutrino oscillation bounds constrain the region of large mixing of the weak and gravitational

eigenstates, these bounds from double beta decay apply even in the case of no mixing and thus probe a totally unconstrained region in the parameter space.

1.4. The Solar Neutrino Potential of GENIUS

1.4.1. Introduction The study of neutrinos coming from the Sun is a very active area of research. Results from five solar neutrino experiments are now available. These experiments measure the solar neutrino flux with different energy thresholds and using very different detection techniques. All of them, the Chlorine experiment at Homestake [Cle98], the radiochemical Gallium experiments, GALLEX [GAL99] and SAGE [SAG99], the water Cerenkov detectors Kamiokande [KAM89] and Super-Kamiokande [SK98], measure a deficit of the neutrino flux compared to the predictions of the standard solar model (SSM) [Bah98]. Recently it has been stated out that it is imposible to construct a solar model which would reconcile all the data [Min99]. Moreover, a global analysis of the data of all the experiments do not leave any room for the ^{7}Be neutrinos [Bah98b]. On the other hand the predictions of the SSM have been confirmed by helioseismology [Bas97] to a high precision. An explanation of the results of solar neutrino experiments seems to require new physics beyond the standard model of electroweak interaction.

If neutrinos have non-zero masses and if they mix in analogy to the quark sector, then conversions between different neutrino flavours become possible. Flavour conversions can occur in different physical scenarios, depending on certain parameters on neutrino masses and mixing angles. One oscillation scenario makes use of the MSW-mechanism [MSW85], where the solar ν_e transform into other neutrino flavours or into sterile neutrinos as they pass through a thin resonance region near the solar core. The other scenario assumes that the neutrinos oscillate in the vacuum between the Sun and the Earth [Gla87], which means that the oscillation length 'just so' matches the Earth-Sun distance.

1.4.2. The solar neutrino spectrum The Sun acquires its energy by nuclear reactions taking place in the core, mainly via the so-called pp-chain (see Fig. 39).

The neutrino spectrum predicted by the SSM for the pp-chain is shown in Fig. 40. The dominant part of the flux is emitted at energies below 1 MeV.

The pp neutrinos, emitted in the reaction $\mathrm{p+p} \rightarrow \mathrm{D+e^+}+\nu_e$, have a continuous energy spectrum with the endpoint at 420 keV. Their flux is most accurately predicted in the SSM, since it is strongly restricted by the solar luminosity and by helioseismological measurements. The other main

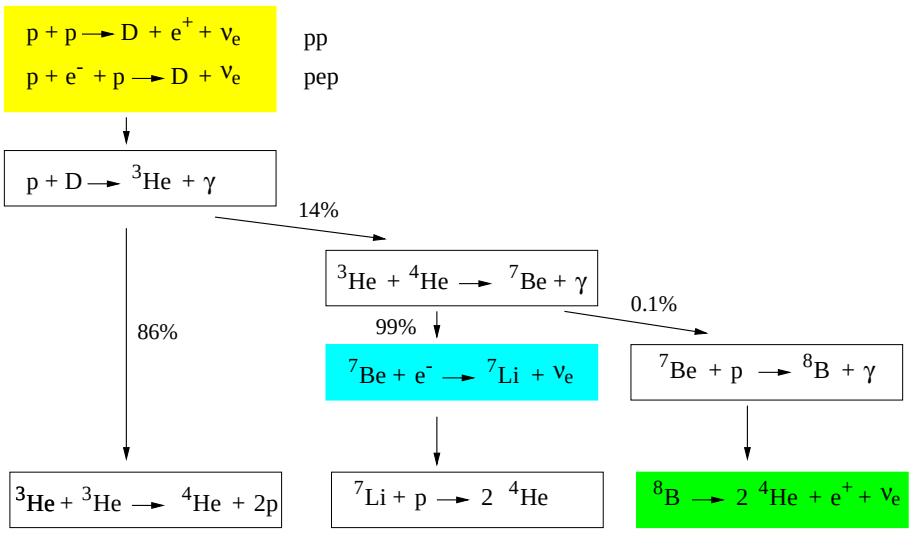

Figure 39. Nuclear reactions in the pp-chain in the Sun.

features of the solar neutrino spectrum are a strong monoenergetic line at 861 keV, from the reaction ^{7}Be+ e$^-\rightarrow$ ^{7}Li+γ+ν_e, the ^{7}Be neutrinos, and a continuous spectrum of neutrinos extending up to 15 MeV, due to the reaction ^{8}B$\rightarrow$2α+e$^+$+ν_e, the ^{8}B neutrinos. Table 4 gives the solar neutrino fluxes in the SSM with their respective uncertainties (from [Bah98c]).

1.4.3. Present status of the solar neutrino experiments The solar neutrino problem has been known for two decades, since the Homestake experiment reported its first result. At that time, however, it was not clear if the difference between the chlorine measurement and the standard solar model prediction was due to experimental systematics or the uncertainties in the SSM or if it was a sign of new physics. Meanwhile, the observed discrepancy was confirmed by other four solar neutrino experiments (see Fig. 41, from [Bah96]). Model independent analysis performed by many authors (see [Min99] and references therein) suggest that the solar neutrino problem can only be solved if some additional assumptions are made in the standard electroweak theory. The most generic assumption is to give neutrinos a mass, which leads to neutrino oscillations in vacuum or matter.

Oscillations between two neutrino species are characterized by two parameters: Δm^2, the difference of the squared mass eigenstates, and θ, the mixing angle between the mass eigenstates.

The Ga experiments, sensitive to the low-energy pp and ^{7}Be neutrinos, combined with the Homestake and Super-Kamiokande experiments, which

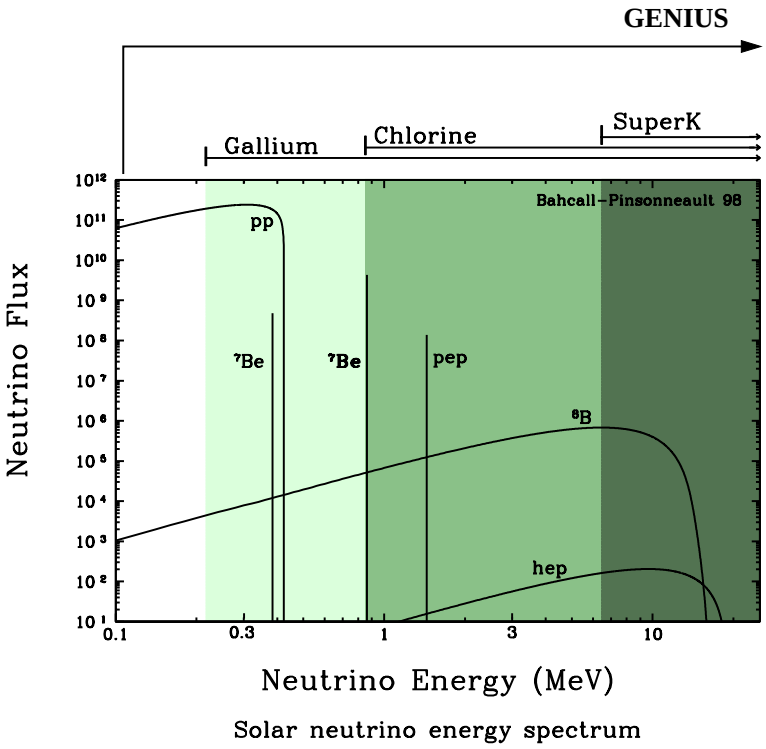

Figure 40. Predicted solar neutrino spectrum in the SSM (from [Bah91]).

are sensitive to the high-energy ^{8}B neutrinos, strongly restrict the allowed range of Δm^2 and θ for all oscillation scenarios. There exist four parameter areas compatible with the results of all existing solar neutrino experiments: the large mixing angle solution (LMA), the small mixing angle solution (SMA), the low mass solution (LOW) and the vacuum oscillation solution with strong mixing (see Fig. 42 for the MSW-solutions). Up to date, there is no clear evidence for one of the above solutions. To clarify the situation, there is great demand for additional solar neutrino experiments, especially at energies below 1 MeV.

Borexino [BOR91] is now being built up especially to measure the flux of ^{7}Be neutrinos in real time. It will use 300 tons of organic scintillator (100 tons of fiducial volume) to detect recoil electrons from elastic neutrino-electron scattering. Since the scintillator has no directional information and the signal is characterized only by the scintillation light produced by the recoil electron, very stringent constraints on the radiopurity of the scintilator and on the activity of all detector materials are imposed.

Source	Flux (10^{10} cm^{-2}s^{-1})
pp	5.94 ± 0.01
pep	$1.39\times10^{-2}\pm 0.01$
^{7}Be	$4.80\times10^{-1}\pm 0.09$
^{8}B	$5.15\times10^{-4}\pm 0.19$

Table 4. Solar Standard Model predictions of the neutrino fluxes, from [Bah98c]

So far, there exist three proposals to measure the pp-flux in real time, HERON [Lan87], HELLAZ [Arz94] and LENS [Rag97].

The HERON project will use ^{4}He in its superfluid state (at 20 mK) as the target medium. The detection reaction is elastic neutrino-electron scattering, the electron recoil energy is converted into low-energy elementary excitations of the helium, rotons, which can be detected. For a fiducial volume of seven tons, the total SSM predicted event rate is 14 per day (8 events per day from the pp neutrinos). HERON would measure only the energy distribution of recoiling electrons, without a direct determination of the neutrino energy.

In the HELLAZ project a large TPC (2000 m^3) filled with gaseous helium at high pressure (5 atm.) and low temperature (77 K) will serve as a target. It is planned to measure both the kinetic energy and the scattering angle of recoil electrons from elastic neutrino-electron scattering and thus to determine the solar neutrino energy. The kinetic energy of recoil electrons is measured by counting the individual electrons in a ionisation cloud generated by the energy loss of the recoil electron due to ionisation in the helium gas. The expected event rate for 2×10^{30} target electrons is 7 per day and 4 per day for pp neutrinos and ^{7}Be neutrinos, respectively.

LENSE would be a complementary approach to the above detectors using flavour independent elastic scattering from electrons. The method of neutrino detection is neutrino capture in ^{82}Se, ^{160}Gd or ^{176}Yb. The neutrino captures occur to excited states of the final nuclides, providing a strong signature against radioactive background. The thresholds for neutrino capture are 173 keV for^{82}Se, 244 keV for ^{160}Gd and 301 keV for ^{176}Yb. Three different techniques for implementation as a solar neutrino detector are explored at present [LEN99]: liquid scintillator loaded with Yb or Gd, scintillating crystals of silicates of Gd (GSO) and time projection chambers with a gaseous compound of isotopic ^{82}Se.

All of these projects are still in a stage of research and development, they have not yet shown full feasibility for implementation as a solar neutrino detector.

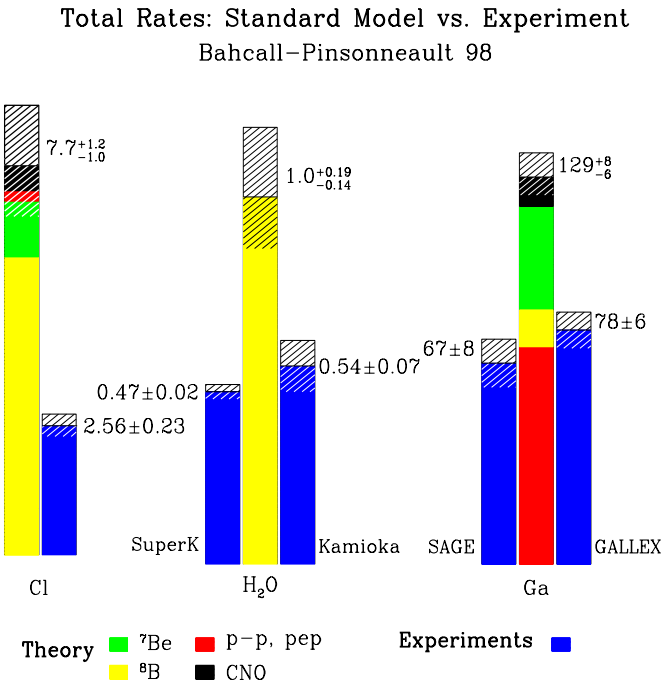

Figure 41. Comparison of the total rates predicted in the SSM and the observed rates in the present solar neutrino experiments, from [Bah96].

1.4.4. Time signatures of solar neutrinos Due to the eccentricity of the Earth orbit, seasonal variations in the flux of solar neutrinos are expected. The number of neutrinos of all flavours reaching the Earth is larger when the Earth is closer to the Sun than when it is farther away and should vary with $1/R^2$, where R is the Eart-Sun distance, $R=R_0(1-\epsilon\cos(2\pi t/\text{year}))$. R_0= 1AU and ϵ=0.017. The neutrino flux thus shows a seasonal variation of about 7% from maximum to minimum. This variation can in principle be used by a real time solar neutrino experiment to extract the neutrino signal independently of background (if the background is stable in time) and is limited only by statistics.

Beyond the so-called 'normal' seasonal variation, an anomalous seasonal variation is predicted for the ^{7}Be neutrino flux in case of the vacuum oscillation solution, since their oscillation length in this case is comparable to the seasonal variation of the Earth-Sun distance due to the eccentricity of the Earth orbit. The flux variations in this case are much larger than

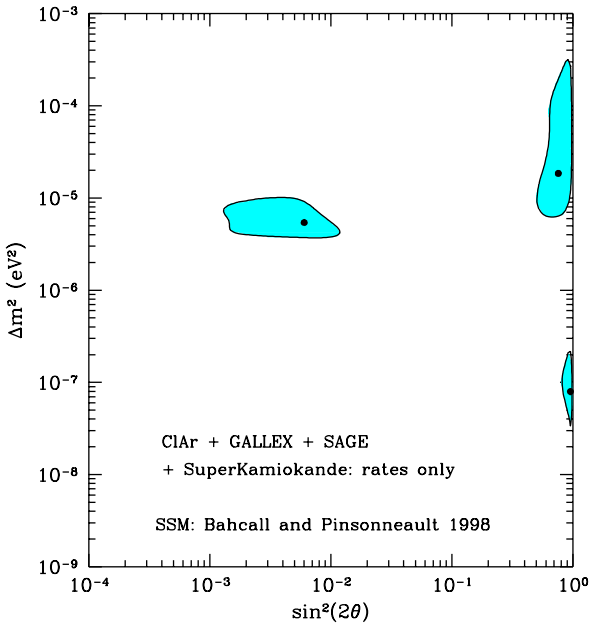

Figure 42. The allowed regions (99% C.L.) in Δm^2 — $\sin^2 2\theta$ parameter space for the MSW solution, from [Bah98a].

for the normal seasonal variation, they could serve as a unique signature of vacuum oscillations [Gla87].

If neutrinos oscillate via the MSW-effect, then a regeneration of electron-neutrinos while passings through the Earth is predicted [Bah89]. The so-called day/night-effect is neutrino energy dependent, its detection would be a strong evidence for the MSW-effect. In Fig. 43 (from [Bah97]) the ν_e survival probabilities for the MSW solutions computed for the day-time and night-time are shown. At low energies only the LOW solution shows significant differences between the day- and night-time survival probability. Therefore this solution could be tested by a real-time detector of low energy solar neutrinos, in particular by measuring the pp and ^{7}Be neutrino flux.

1.4.5. GENIUS as a solar neutrino detector The goal of the GENIUS project as a dark matter detector is to achieve the background level of

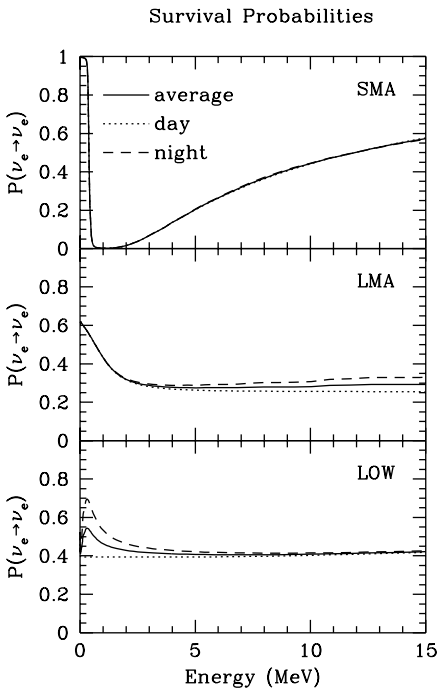

Figure 43. Survival probabilities for an electron neutrino created in the Sun for the three MSW solutions, from [Bah97]. SMA, LMA, LOW stand for the small mixing angle, the large mixing angle and the low Δm^2 MSW-solutions.

10^{-3} events/kg y keV in the energy region below 100 keV. Such a low background in combination with a target mass of at least 1 ton of natural (or enriched) Ge opens the possibility to measure the solar pp- and ^{7}Be-neutrino flux in real time with a very low energy threshold.

1.4.6. Signal Detection The detection reaction is the elastic scattering process $\nu + e^- \rightarrow \nu + e^-$. The maximum electron recoil energy is 261 keV for the pp-neutrinos and 665 keV for the ^{7}Be-neutrinos [Bah89]. The energy of the recoiling electrons is detected through ionisation in high purity Ge detectors. GENIUS in its 1 ton version would consist of an array of about 400 HPGe detectors, 2.5 kg each. Thus, the sensitive volume would be naturally divided into 400 cells which helps in background discrimination, since a neutrino interaction is taking place in a single cell.

Case	Events/day 11-665 keV (1 ton)	Events/day 11-665 keV (10 tons)
SSM	2.4	24
Full $\nu_e \rightarrow \nu_\mu$ conversion	0.62	6.2

Table 5. Neutrino signal rates in GENIUS for 1 ton (10 tons) of Germanium.

1.4.7. Signal Rates The dominant part of the signal in GENIUS is produced by pp-neutrinos (66 %) and the ^{7}Be-neutrinos (33%).

A target mass of 1 ton (10 tons) of natural or enriched Ge corresponds to about 3×10^{29} (3×10^{30}) electrons.

With the cross section for elastic neutrino-electron scattering [Bah89]:

$\sigma_{\nu_e} = 11.6 \times 10^{-46}\mathrm{cm}^2$ pp
$\sigma_{\nu_e} = 59.3 \times 10^{-46}\mathrm{cm}^2$ ^{7}Be

and the neutrino fluxes [Bah98c]:

$\phi_{pp} = 5.94 \times 10^{10}\ \mathrm{cm}^{-2}\mathrm{s}^{-1}$
$\phi_{^7Be} = 0.48 \times 10^{10}\ \mathrm{cm}^{-2}\mathrm{s}^{-1}$

the expected number of events calculated in the standard solar model (BP98 [Bah98]) can be estimated:

R_{pp} = 69 SNU = 1.8 events/day (18 events/day for 10 tons)
$R_{^7Be}$ = 28.5 SNU = 0.6 events/day (6 events/day for 10 tons),

The event rates for full $\nu_e \rightarrow \nu_\mu$ conversion are 0.48 events/day for pp-neutrinos and 0.14 events/day for ^{7}Be-neutrinos for 1 ton of Ge and ten times higher for 10 tons (see also Table 5)

1.4.8. Background requirements GENIUS is conceived such that the external background from the natural radioactivity of the environment and from muon interactions is reduced to a minimum, the main background contributions coming from the liquid nitrogen shielding and the Ge detectors themselves. To measure the low-energy solar neutrino flux, a nitrogen shielding of 13 m in diameter is required. Regarding the radiopurity of liquid nitrogen, the values reached at present by the Borexino collaboration for their liquid scintillator would be sufficient. Much attention has to be paid to the cosmogenic activation of the Ge crystals at the Earth surface.

Energy region	Events/day
11 - 260 keV	1.4
11 - 665 keV	1.8

Table 6. Expected background events in the GENIUS experiment (1 ton of Germanium).

In case of one day exposure, five years of deactivation below ground are required. The optimal solution would be to produce the detectors in an underground facillity.

Table 6 shows the expected background events in the energy region 11-260 keV and 11-665 keV.

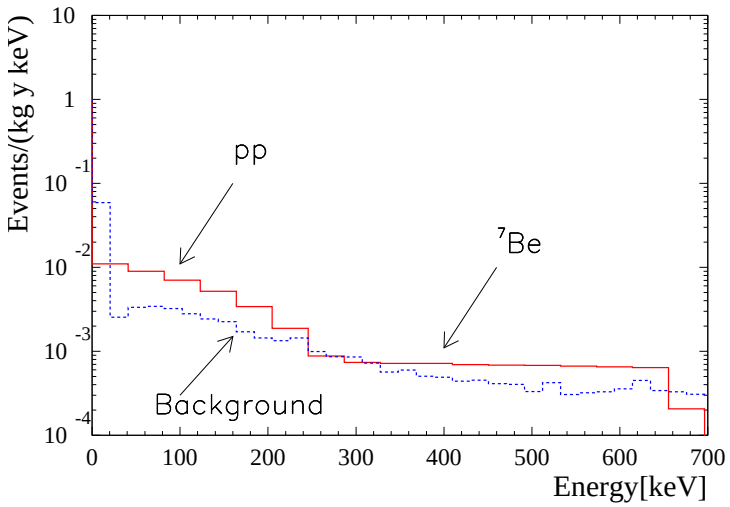

Figure 44. Simulated spectra of the low energy neutrino signal (in the SSM) and the total background in GENIUS (1 ton of natural germanium).

Fig. 44 shows the simulated spectrum of the low-energy neutrino signal in GENIUS, together with the total expected background.

If the signal to background ratio S/B will be greater than 1, than the pp- and ^{7}Be-neutrino flux can be measured by spectroscopic techniques alone. If S/B < 1, one can make use of a solar signature in order to derive the flux.

The eccentricity of the Earth's orbit induces a seasonal variation of about 7% from maximum to minimum. Even if the number of background

events is not known, the background event rate and the signal event rate can be extracted independently by fitting the event rate to the seasonal variation. The only assumption is that the background is stable in time and that enough statistics is available.

In case of a day/night - variation of the solar neutrino flux, GENIUS would be sensitive to the LOW MSW solution of the solar neutrino problem (compare Fig. 43).

GENIUS could be the *first detector to detect the solar pp neutrinos in real time*. Although this imposes very strong purity restrictions for all the detector components, with a liquid nitrogen shielding of 13 m in diameter and production of the Germanium detectors below ground, it should be feasible to achieve such a low background level. The advantages are the well understood detection technique (ionization in a HPGe detector), the excellent energy resolution (1 keV at 300 keV), low energy threshold (about 11 keV) and the measurement of the recoiling electrons in real time.

The good energy resolution for detecting the recoiling electrons would allow for the first time to measure the 1.3 keV predicted shift of the average energy of the beryllium neutrino line. This shift is a direct measure of the central temperature of the Sun [Bah93].

2. The GENIUS experiment

2.1. Design, detection technique, threshold

GENIUS will operate an array of 40 or 300 'naked' Ge crystals (natural Ge for WIMP-detection and measurement of the pp-flux, enriched ^{76}Ge for double beta decay searches) in a cylindrical vessel filled with liquid nitrogen. The basic idea of the GENIUS setup relies on the fact that most of the contributions of measured spectra in conventional low level detectors result from the cryostat system and the shielding material. If these can be eliminated reasonably, the sensitivity of the experiment increases accordingly (linearly in the case of Dark Matter and solar Neutrino search). It is therefore essential to keep away radioactive materials and sources as far as possible from the detector itself. In case of the GENIUS project this will be accomplished by the use of liquid nitrogen as a cooling medium and as the shielding material against natural radioactivity of the environment at once. Liquid nitrogen has the advantage that it can be processed to a very high purity through fractional distillation. In this way practically all radioactive impurities in the material near the detectors, which are known to produce the main part of the radioactive background, are eliminated.

2.1.1. Detector Size Due to its rather low density (0.8 g/cm^3), the nitrogen shielding has to be several meters in diameter. The dimensions of the vessel depend on the gamma- and n-flux in the Gran Sasso Laboratory and on the intrinsic radiopurity of the steel vessel. The required background conditions imply a tank size of 12m diameter and height (13 m for solar neutrino detection), if no other shielding is used in addition to the nitrogen (see Chapter 3.1). The tank size could be reduced to some limited extent against the γ-radiation and neutron flux from outside the tank, by replacing part of the outer nitrogen by other shielding material, e.g. lead (2m of nitrogen could be replaced by a layer of 10.8 cm Pb). The minimal diameter of the nitrogen tank would physically be determined by the contamination of the vessel and the shielding material and the distance between the lead and the tank wall from the crystals. It has been calculated that a nitrogen tank with $\sim$ 8m in diameter would be the minimum for this purpose. This gives some flexibility to adapt the setup to the different sizes of the halls in the Gran Sasso. Of course the cost of the project would be increased in a non-negligible way by such a lead layer (10.8 cm correspond to $\sim$1000 tons). We have also considered other alternative setups (see, e.g. [Kla98i]). We see, however, no other reasonable way to accomplish the goal of reducing the background to the required level than to use a tank of the above dimensions. These considerations show also that an intermediate size test setup (as discussed in chapter 3.1) as a first step of the full setup seems unreasonable.

Figure 54 shows the design of the experiment, which could be located, e.g., in the Gran Sasso Underground Laboratory, or in the WIPP laboratory.

2.1.2. Detection Technique The proposed detection technique for GENIUS is ionization in a Germanium detector. The detectors would be coaxial HPGe crystals of p-type, weighting about 2.5 kg each. For p-type crystals, the outer contact is n^+ and the surface dead layer has a thickness of several hundred micrometers. This prevents the detection of β-particles and gamma rays of low energy from outside the crystals. The optimal working temperature is 77 K. Besides the energy signal, the pulse shape of the interactions can be recorded in view of background discrimination.

The energy resolution of GENIUS would be about 0.3%, the energy threshold about 11 keV.

2.2. Signals and signatures

2.2.1. Dark Matter The signal for a dark matter WIMP with mass between 20 GeV and 1 TeV is expected in the energy region below 100 keV. The event rates for the neutralino as the lightest supersymmetric particle range in most SUSY models from 10^{-2} to 10^2 events/kg y keV. The low-energy spectrum in GENIUS is dominated by the $2\nu\beta\beta$ signal from the decay

of ^{76}Ge. For natural Germanium (7.8% ^{76}Ge) an event rate of 3×10^{-2} events/kg y keV from $2\nu\beta\beta$ decay is expected. Therefore, the $2\nu\beta\beta$- signal has to be subtracted. Another possibility is to make use of the predicted seasonal modulation of the WIMP flux. Due to the motion of the Sun in the galactic halo and the Earth motion around the Sun, a flux variation of 7% between two extremes is expected [Fre88] .

2.2.2. Neutrinoless double beta decay The expected signature for the $0\nu\beta\beta$ decay of ^{76}Ge is a peak at the energy of 2038.56±0.32 keV [Hyk91]. The event rate for 1 ton of enriched ^{76}Ge and an effective Majorana neutrino mass of 0.01 eV is 0.3 events/yr. Due to the good energy resolution of Ge detectors (typically better than 0.3 %), the $0\nu\beta\beta$ signal is not affected by the $2\nu\beta\beta$ spectrum.

2.2.3. Solar neutrinos The reaction used to detect solar neutrinos is the elastic neutrino electron scattering: $\nu + e^- \rightarrow \nu + e^-$. The maximum electron recoil energy is 261 keV for the pp-neutrinos and 665 keV for the ^{7}Be-neutrinos [Bah89]. The detection rates for the pp and ^{7}Be-fluxes, calculated for the SSM [Bah98], are $R_{pp} \simeq 70$ SNU and $R_{^7Be} \simeq 26$ SNU (1 SNU = 10^{-36}/(s target atom)). For one ton of natural (or enriched) Ge (corresponding to 3×10^{29} electrons), the total rates are $R_{pp} \simeq 1.8$ events/day and $R_{^7Be} \simeq 0.65$ events/day, assuming the detection of all electrons. This is about ten times higher than the rates in present radiochemical Gallium (GALLE and SAGE) experiments. The event rates for full $\nu_e \rightarrow \nu_\mu$ conversion are 0.48 events/day for pp-neutrinos and 0.14 events/day for ^{7}Be-neutrinos. GENIUS can measure only the energy distribution of the recoiling electrons, whereas the energy of the incoming neutrinos is not directly determined. However, due to the excellent energy resolution of the detectors and the difference in the elastic scattering cross section of electron and muon neutrinos, a comparison of the energy spectrum of recoiling electrons with the theoretical prediction of the SSM can be made. Due to its relatively high counting rate, GENIUS would be able to test the LOW MSW flavour conversion solution [Bah97] via the day-night modulation of the neutrino flux and the vacuum-oscillation solution via the seasonal flux variation.

2.3. Technical study of detector operation

To demonstrate the feasibility of operating Ge detectors in liquid nitrogen, instead of in a vacuum–tight cryostat system [Kno98], a first experiment has been successfully performed in the low level laboratory in Heidelberg with one naked p–type Ge crystal immersed in a 50 l dewar [Kla98c]. Already in this attempt we could not see any deterioration in the detector performance relative to our conventionally operated detectors.

Figure 45. The three–crystal holder-system with germanium crystals mounted shortly before cooling. Some crystal-to-FET cables can be seen.

In a second phase the goal was to look for possible interferences between two or more naked Ge crystals, to test different cable lengths between FETs and crystals and to design and test a preliminary holder system of high molecular polyethylene. We performed a technical study operating three germanium detectors on a common plastic holder system inside liquid nitrogen [Bau98]. All crystals were of p–type and weighted about 300 g each.

A picture of the three–crystal holder–system can be seen in figure 45. Two thin polyethylene plates (1 cm thick) are used to fix the contacts to the crystals. The FETs are placed close to the liquid nitrogen surface but kept inside. Cables having three different lengths (2, 4 and 6 m) connect the three crystals to their FETs.

The main purpose of the experiment was to test the behaviour of the crystals in the low energy region: energy resolution, energy threshold, crosstalk between the detectors and possible signs of microphonic events caused by nitrogen boiling. The general performance of the crystals is as stable as already seen with a single detector inside liquid nitrogen. We couldn't observe any cross talk using only p–type detectors (same polarity for the HV-bias), since cross talk signals have the wrong polarity and are filtered by the amplifier.

Figure 46 shows a background spectrum and figure 47 a ^{133}Ba calibration spectrum of one of the naked Ge detectors in liquid nitrogen. The cable length between detector and FET was 6 m (winded up in loops). We achieved an energy resolution of 1.0 keV at 300 keV and a threshold of 2

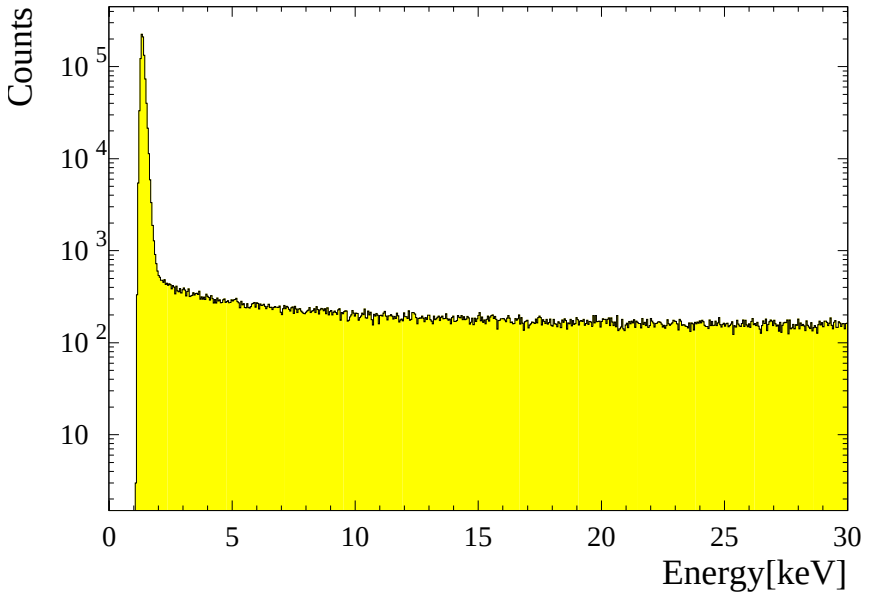

Figure 46. Background spectrum of a naked, unshielded Ge crystal in liquid nitrogen. Note the low energy threshold of 2 keV of the detector.

keV. No microphonic events due to nitrogen boiling beyond 2 keV could be detected. We conclude that the performance of the Ge detectors is as good (or even better) as for conventionally operated crystals, even with 6 m cable lengths between crystal and FET.

A third phase was dedicated to the optimization of the holder system design (material minimization). In figure 48 a Ge crystal suspended on kevlar wires can be seen. The inner contact is fixed with a stainless steel spring, the outer contact with a thin stainless steel wire. Only 3 g of material in total (kevlar plus steel wires) were used. Figure 49 and 50 show a background and a ^{133}Ba calibration spectrum of a 400 g crystal in liquid nitrogen. An energy energy resolution of 1.2 keV at 300 keV and a threshold of 2.5 keV were achieved.

Currently we are measuring the radiopurity of kevlar and at the same time we are testing other possible materials for the holder system.

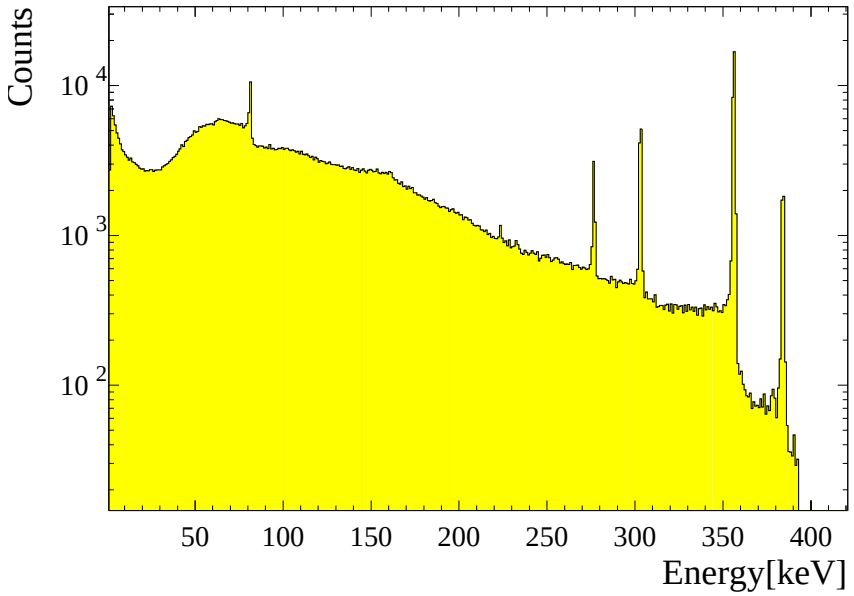

Figure 47. Calibration ^{133}Ba spectrum of a naked Ge crystal in liquid nitrogen. The energy resolution is 1 keV at 300 keV.

3. Background simulations

To study the expected background in the GENIUS experiment, we performed detailed Monte Carlo simulations and calculations of all the relevant background sources [Bau98]. The sources of background can be divided into external and internal ones. External background is generated by events originating from outside the liquid shielding, such as photons and neutrons from the Gran Sasso rock, muon interactions and muon induced activities. Internal background arises from residual impurities in the liquid nitrogen, in the steel vessels, in the crystal holder system, in the Ge crystals themselves and from activation of both liquid nitrogen and Ge crystals at the Earths surface.

For the simulation of muon showers, the external photon flux and the radioactive decay chains we used the GEANT3.21 package [GEA93] extended for nuclear decays [Mue93]. This version had already successfully been tested in establishing a quantitative background model for the Heidelberg–Moscow experiment [HM97].

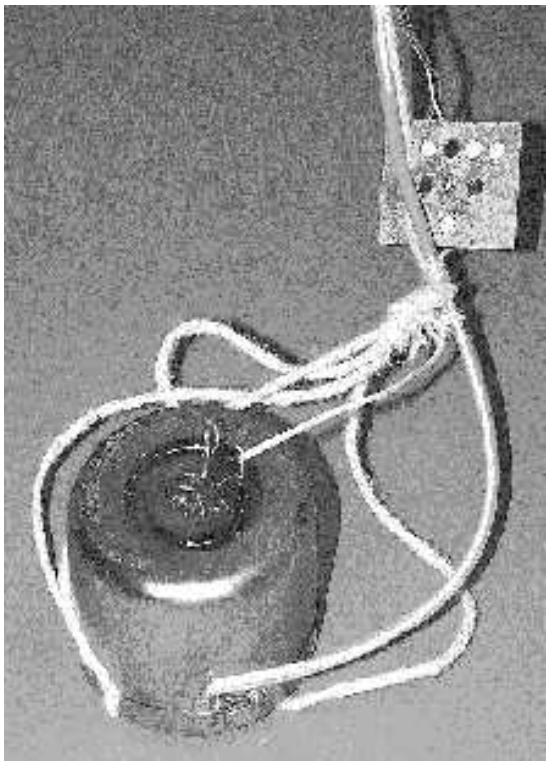

Figure 48. A naked Ge crystal suspended on kevlar wires. Only 3 g of material in total (kevlar and electrical contacts) were used.

We used the following detector geometry to perform the simulations. The nitrogen shielding is given by a cylindrical geometry of variable diameter and height, with the crystals positioned in its center. The vessel is surrounded by a 2 m thick polyethylene-foam isolation, which is held by two 2 mm thick steel layers (constructional data from Messer–Griesheim). The simulated setup consists of natural Ge detectors integrated into a holder system of high molecular polyethylene.

3.1. Photon flux from the surroundings

We simulated the influence of the photon flux with energies between 0 – 3 MeV measured in hall C of the Gran Sasso laboratory [Arp92]. This measurement is in good agreement with photon flux calculations by the Borexino Collaboration [BOR91]. The main contributions are given in table 7.

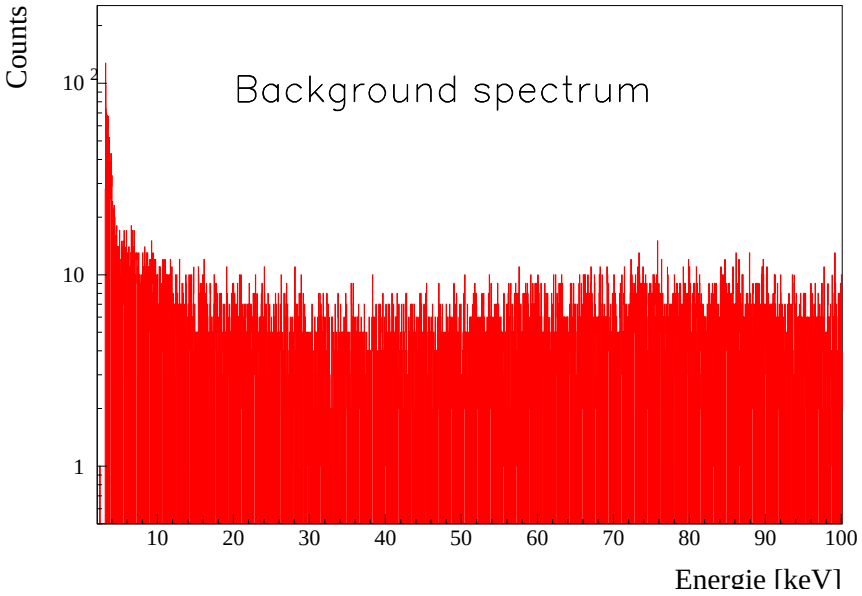

Figure 49. Background spectrum of a naked, unshielded 400g Ge crystal in liquid nitrogen. The energy threshold is 2.5 keV.

3.1.1. Intermediate size detector (4×4 m) The dimensions of the cylindrical tank are dictated by the photon flux measured in the Gran Sasso laboratory and the radiopurity of the tank walls (made of stainless steel).

Isotope	Energy [keV]	Flux [$m^{-2}d^{-1}$]
^{40}K	1460	3.8×10^{7}
^{214}Pb	295.2	0.8×10^{7}
^{214}Pb	352	1.8×10^{7}
^{214}Bi	609.3	2.9×10^{7}
^{214}Bi	1120.3	1.4×10^{7}
^{214}Bi	1764.5	1.7×10^{7}
^{208}Tl	2614.5	1.35×10^{7}

Table 7. Simulated components of the gamma ray flux from natural radioactivity in the Gran Sasso Laboratory (from [Arp92]).

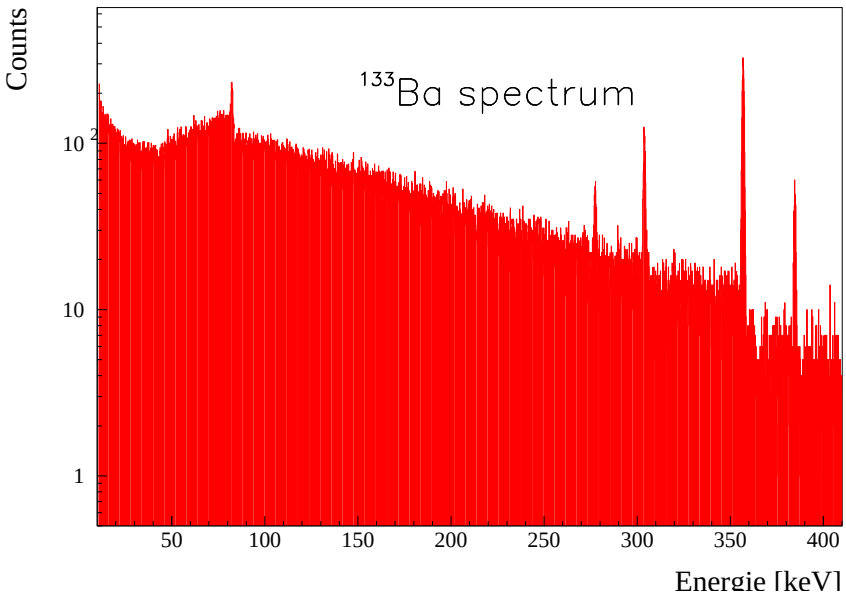

Figure 50. Calibration ^{133}Ba spectrum of a 400g naked Ge crystal in liquid nitrogen. The energy resolution is 1 keV at 300 keV.

With a diameter and a height of 4 m for the liquid shielding, the contribution from the surrounding gammas is about 70 counts/(kg y keV) in the energy region 11 – 100 keV. This is almost 4 orders of magnitude higher than the goal of 10^{-2} events/(kg y keV) of the GENIUS experiment. An alternative would be to use an additional outer water shielding. In this case however, the limitations of the tank dimensions are given by the radiopurity of the steel walls. Assuming an U/Th contamination of 5×10^{-9} g/g for the steel, as measured by the BOREXINO collaboration, a count rate of about 1.5 counts/(kg y keV) from this component is achieved. This again is too high by more than 2 orders of magnitude. For the assumed steel radiopurity of 5×10^{-9} g/g, the minimal allowed tank dimensions are $\sim 8\times8$ m (maximal allowed countrate due to this component was assumed to be 0.3×10^{-3} counts/(kg y keV) in the energy region between 11 keV and 100 keV) or, the other way round, for a tank size of 4×4 m, an unrealistic contamination level of the order of 10^{-11} g/g for the steel is required. It has been suggested to set up an intermediate size detector in order to prove the predictions of the concept in a first step, i.e. to prove that no unexpected background components appear, which would dramatically decrease the sensitivity with respect to the predictions. However, we see no

sense in such an intermediate step, since its costs would be only negligibly smaller than that of the full setup - increasing the total costs of the project by about a factor of two.

This means a test of the proposed setup by a smaller tank as a first step seems unreasonable.

3.1.2. Full size detector For GENIUS as a dark matter and neutrinoless double beta decay detector, a 12×12 m tank is suggested. The obtained count rate from the external gammas in the energy region 11 – 100 keV is 4×10^{-3} counts/(kg y keV). However, to measure the solar pp- and ^{7}Be neutrino flux, a tank size of 13×13 m is needed (with a count rate from external gammas of 9×10^{-4} counts/(kg y keV) below 260 keV).

3.2. Neutron flux from the surroundings

We simulated the measured neutron flux [Bel89] in the Gran Sasso laboratory. The 2 m polyethylene foam isolation (ρ = 0.03 g cm^{-3}) around the nitrogen tank reduces the neutron flux for energies below 1 keV by more than 5 orders of magnitude. Only about 3% of neutrons with energies between 1 keV and 2.5 MeV will pass the polyethylene isolation, whereas for energies between 2.5 and 15 MeV the overall flux is reduced by about 40%. The neutron flux reaching the tank can be reduced by another two orders of magnitude by doping the polyethylene foam isolation with about 1.4 t of boron. The flux of the ^{7}Li deexcitation gamma rays from the reaction n + ^{10}B→ α + ^{7}Li*, with an energy of 0.48 MeV, would be too low to reach the inner part of the liquid shielding. After the first meter of liquid nitrogen the total neutron flux is reduced by another 4–5 orders of magnitude, therefore we simulated the neutron capture reactions randomly distributed in the first meter of the nitrogen shielding.

With the conservative assumption that all neutrons reaching the nitrogen are thermalized and captured by the reactions ^{14}N(n,p)^{14}C* and ^{14}N(n,γ)^{15}N*, a total of 4.4×10^{7} neutron capture reactions per year have to be taken into account. The relevant contribution to the background comes from the deexcitation of the ^{14}C* and ^{15}N* nuclei. The contribution of the β–decay of ^{14}C nuclei in the liquid nitrogen is negligible, since only low energy electrons ($E_{\beta max}$ = 156 keV) are emitted and the decay probability is very low due to the long half life (10^{-4} per year).

Using the assumptions of a 12×12m tank and a 2m isolation around it, the mean count rate in the low–energy region due to neutron capture reactions would be about 4×10^{-4} counts/(kg y keV).

3.3. Activities induced by muons

The muon flux in the Gran Sasso laboratory was measured to be ϕ_μ=2.3×10^{-4} m^{-2}s^{-1} with a mean energy of $\bar{E}_\mu$=200 GeV [Arp92].

We simulated the effect of muon-induced showers in the liquid nitrogen. With the aid of a muon veto in form of scintillators or gas counters on top of the tank, the total induced background can be drastically reduced. Here we assumed a veto efficiency of 96% as measured in a more shallow laboratory [Heu91]. The count rate due to muon induced showers in the low–energy region is about 2×10^{-3} counts/(kg y keV). This can be further improved using the anticoincidence power of the Ge detectors among each other. For example, for 300 Ge detectors (1 ton), the count rate reduces to 7.2×10^{-6} counts/(kg y keV) in the energy region below 260 keV.

Besides muon showers, we have to consider muon-induced nuclear disintegration and interactions due to secondary neutrons generated in the above reactions.

3.3.1. Neutrons generated by cosmic muons The muon-induced production of neutrons can be approximated by A$_n$ ∼ 3.2×10^{-4} (g^{-1} cm^2), due to the $< E >^{0.75}$ dependence of the number of neutrons on the mean muon energy [Agl89]. With the geometry of the tank h = 12 m, r = 6 m, the density of nitrogen ρ = 0.808 g/cm^3 and the cited flux, a mean production rate of $\phi_{n\mu}$ = 2.5×10^5 neutrons/year in the whole vessel is obtained. Table 8 gives the neutron-induced reactions in the liquid nitrogen for neutron energies < 20 MeV (based on all reactions found in [McL88]).

Reaction	$T_{1/2}$ of the product	Decay energy
^{14}N(n,p)^{14}C	$T_{1/2}$=5.7×10^{3}y	E_{β^-}=0.16 MeV
^{14}N(n,γ)^{15}N	stable	
^{14}N(n,2n)^{13}N	$T_{1/2}$= 9.96 m	E_{β^+}=1.2 MeV
^{14}N(n,α)^{11}B	stable	
^{14}N(n,t)^{12}C	stable	
^{14}N(n,2α)^{7}Li	stable	

Table 8. Neutron interactions in the liquid nitrogen for neutron energies < 20 MeV.

All of the produced nuclides are stable or short-lived with the exception of ^{14}C and ^{13}N. The contribution of gammas from the excited ^{14}C* nucleus corresponds to 10^{-3} counts/(kg y keV) between 0 – 100 keV. The contribution from the β^-– particles with E_{max} = 156 keV is negligible due to the low decay probability of ^{14}C. The production rate of ^{13}N is 1×10^6 atoms per year in the whole tank. From 10^6 simulated positrons with E_{max}

= 1.2 MeV (β^+-decay), corresponding to an exposure of about 1 year, only one event could be observed in the detectors. Therefore, the contribution of ^{13}N to the background will be negligible.

In the Germanium material, 2.3×10^2 neutrons/(y ton) due to muon interactions are produced. For the low energy region the most significant reaction is the ^{70}Ge(n,γ)^{71}Ge capture reaction. ^{71}Ge decays through EC (100%) with $T_{1/2}$ = 11.43 d and Q_{EC} = 229.4 keV [Fir96] and can not be discriminated by the anticoincidence method. The simulation of this decay yields 5×10^{-4} counts/(kg y keV) in the energy region below 260 keV.

3.3.2. Negative muon capture A negative muon stopped in the liquid shielding can be captured by a nitrogen nucleus, leading to one of the reactions that are listed in table 9. Estimations of the number of stopping muons in the nitrogen tank [Ber82, Gai90, Loh85] lead to 86 stopped muons per day (for a 12×12 m tank). The rates of decaying and captured muons are shown in table 10.

Reaction	$T_{1/2}$	Decay energy	Rate [y^{-1}]
^{14}N(μ,ν_μ)^{14}C	$T_{1/2}=5.7\times10^4$y	E_{β^-}=0.16 MeV	584
^{14}N(μ,$\nu_\mu\alpha$)^{10}Be	$T_{1/2}=1.6\times10^{10}$y	E_{β^-}=0.6 MeV	29
^{14}N(μ,ν_μp)^{13}B	$T_{1/2}$=17.33ms	E_{β^-}=13.4 MeV	116
^{14}N(μ,ν_μn)^{13}C	stable		3798
^{14}N(μ,$\nu_\mu\alpha$n)^{9}Be	stable		17
^{14}N(μ,$\nu_\mu\alpha$p)^{9}Li	$T_{1/2}$=178ms	E_{β^-}=13.6 MeV	0.6
^{14}N(μ,ν_μ2n)^{12}C	stable		1168
^{14}N(μ,ν_μ3n)^{11}C	$T_{1/2}$=20.38m	E_{β^-}=13.4 MeV	292
^{14}N(μ,ν_μ4n)^{10}C	$T_{1/2}$=19.3s	E_{β^+}=1.9 MeV	117

Table 9. Spallation reactions from muon capture.

Muon flux	124 h^{-1}	
Stopped muons	86 d^{-1}	
Decaying muons	μ^+	μ^-
	50 d^{-1}	20 d^{-1}
Captured muons	μ^+	μ^-
	0	16 d^{-1}

Table 10. Muon flux, stopped, captured and decaying muons in the nitrogen shielding of the Genius detector (for a 12×12 m tank).

The derived production rates [Cha71] for the various isotopes are listed in table 9. Only the isotopes ^{14}C, ^{10}Be, ^{11}C and ^{10}C can not be discriminated by muon anticoincidence, since their individual lifetime is too long. ^{14}C and ^{10}Be will not be seen in our detector due to their very low decay probabilities (10^{-4} and 10^{-10} per year) and low production rates. The contribution of ^{10}C and ^{11}C, with a production rate of 117 atoms/year and 292 atoms/year, respectively, in the whole nitrogen tank, will be negligible. The gamma rays from the excited nuclei produced in all the reactions can be discriminated by anticoincidence with the muon shielding on the top of the tank.

3.3.3. Inelastic muon scattering Another way of producing radioactive isotopes in the liquid shielding are electromagnetic nuclear reactions of muons through inelastic scattering off nitrogen nuclei: $\mu + \mathrm{N} \rightarrow \mu' + \mathrm{X}^*$. The only resulting isotopes with half lifes $>$ 1s are ^{14}N(γ,n)^{13}N, with $\mathrm{T}_{1/2}$=9.96 m and ^{14}N(γ,tn)^{10}C, with $\mathrm{T}_{1/2}$=19.3 s. The production rate per day for one isotope can be written as [OCo88]: $\mathrm{R(d^{-1})}= 6\times10^{-2}\phi_\mu(\mathrm{d^{-1}m^{-2}})\mathrm{N}_T(\mathrm{kt})\sigma_\mu(\mu\mathrm{b})/\mathrm{A}$, where ϕ_μ is the flux of muons on the detector, N_T is the number of target nuclei, σ_μ the reaction cross section and A the atomic weight of the target nucleus. For our detector this yields $\mathrm{R(y^{-1})}= 45\times\sigma_\mu(\mu\mathrm{b})$. With typical reaction cross sections of a few hundred μb [OCo88, Nap73], we obtain a production rate of (5–10)$\times10^3$ atoms per year. A simulation of an activation time of ten years for both isotopes yields negligible count rates in comparison to contributions from other background components.

3.4. Intrinsic impurities in the nitrogen shielding, Ge crystals, holder system and steel vessel

The assumed impurity levels for the liquid nitrogen are listed in table 11. For the ^{238}U and ^{232}Th decay chains they have been measured by the Borexino collaboration [Ali98] for their liquid scintillator. Due to the very high cleaning efficiency of fractional distillation, it is conservative to assume that these requirements will also be fulfilled for liquid nitrogen. The ^{238}U and ^{232}Th decay chains were simulated under the assumption that the chains are in secular equilibrium. The count rate due to ^{238}U, ^{232}Th and ^{40}K contaminations of the liquid nitrogen is about 1.2×10^{-3} in the energy region below 100 keV.

New measurements of the ^{222}Rn contamination of freshly produced liquid nitrogen yield 325 μBq/m^3 [Rau99]. After about a month it is reduced to about 3 μBq/m^3 ($\mathrm{T}_{1/2}$ = 3.8 days). Such a level could be maintained if the evaporated nitrogen is always replaced by Rn–pure nitrogen, previously stored in an underground facility or if a nitrogen cleaning system is used. It is planned to install a nitrogen recycling device (through condensation)

Source	Radionuclide	Purity
Nitrogen	^{238}U	3.5×10^{-16}g/g
	^{232}Th	4.4×10^{-16}g/g
	^{40}K	1×10^{-15}g/g
Steel vessel	U/Th	5×10^{-9}g/g

Table 11. Assumed contamination levels for the liquid nitrogen and steel vessel.

inside the tank. This would reduce the Rn contamination to a negligible level. Surface emanations are reduced to a negligible level for cooled surfaces in direct contact with the liquid nitrogen.

The mean count rate from the contamination of ^{222}Rn in the region below 100 keV is 3×10^{-4} counts/(kg y keV) assuming an activity of 3 μBq/m^3 in the liquid nitrogen.

For the intrinsic impurity concentration in Ge crystals we can give only upper limits from measurements with the detectors of the Heidelberg–Moscow experiment. We see a clear α–peak in two of the enriched detectors at 5.305 MeV, and an indication for the same peak in two other detectors. It originates from the decay of ^{210}Po (which decays with 99% through an α–decay to ^{206}Pb) and is a sign for a ^{210}Pb contamination of the detectors. However, it is very unlikely that the contamination is located inside the Ge-crystals, most probably it is located on the crystals surface at the inner contact.

Using three Ge detectors, we derive an upper limit at 90% CL (after 19 kg y counting statistics) of 1.8×10^{-15}g/g for ^{238}U and 5.7×10^{-15}g/g for ^{232}Th. Assuming these impurity concentrations throughout the whole Ge detector volumes, our simulations yield a count rate of about 10^{-2} counts/(kg y keV) for both ^{238}U and ^{232}Th decay chains. It is however secure to assume that these upper limits are very conservative and that the true contamination of HPGe is much lower. Special attention will have to be paid in order to avoid surface contaminations of the crystals.

An important factor in the background spectrum is the effect of the holder-system. For the simulation we assumed the possibility to obtain a polyethylene with an impurity concentration of 10^{-13}g/g for the U/Th decay chains (this is a factor of 100 worse than the values reached at present for the organic liquid-scintillator by the Borexino collaboration [Ali98]). Encouraging are the results already achieved by the SNO experiment [Sno97], which developed an acrylic with current limits on ^{232}Th and ^{238}U contamination of 10^{-12}g/g. Since it is not yet sure that such a low contamination level will be reached for polyethylene, we are currently

testing also other materials.

Assuming the above impurity level with the simulated geometry (130 g of material per detector) a count rate of $\sim 8\times10^{-4}$ counts/(kg y keV) in the energy region below 100 keV from this component is reached. This result will be further improved by using the new developed holder design with a minimized amount of material. In case of using about 10 g of material per detector, a contamination level of 10^{-12}g/g for the holder system material would suffice.

For the steel vessel an impurity concentration of 5×10^{-9} g/g for U/Th was assumed (as measured in [BOR91]). The contribution in the energy region 0 – 100 keV is 1.5×10^{-5} counts/(kg y keV). Assuming an equal contamination for the polyethylene foam isolation as for steel, the contribution of both materials to the background is negligible (for a 12×12 m tank).

3.5. Cosmic activation of the germanium crystals

We have estimated the cosmogenic production rates of radioisotopes in the germanium crystals with the Σ programme [Boc94a]. The programme was developed to calculate cosmogenic activations of natural germanium, enriched germanium and copper. It was demonstrated that it can reproduce the measured cosmogenic activity in the Heidelberg–Moscow experiment [HM97] within about a factor of two [Mai96].

Assuming a production plus transportation time of 10 days at sea level for the natural Ge detectors (with the exception of ^{68}Ge, where the saturation activity is assumed), and a deactivation time of three years, we obtain the radioisotope concentrations listed in table 12. All other produced radionuclides have much smaller activities due to their shorter half lifes. The required short production time has been guaranteed by detector production companies.

The count rate below 11 keV is dominated by X–rays from the decays of ^{68}Ge, ^{49}V, ^{55}Fe and ^{65}Zn (see table 12). Due to their strong contribution, the energy threshold of GENIUS would be at 11 keV, which is still acceptable (as can be seen from figure 5).

Between 11 keV and 70 keV the contribution from ^{63}Ni dominates due to the low Q–value (66.95 keV) of the β^-–decay.

^{68}Ge plays a special role. Since it can not be extracted by zone melting like all other, non–germanium isotopes, the starting activity would be in equilibrium with the production rate. After 3 years of deactivation below ground, the activity is about 100 μBq/kg. With a half–life of 288 d it will dominate the other background components (with about 4×10^{-2} events/kg y keV below 100 keV). However, with such a background level one already would be able to test a significant part of the SUSY predicted parameter

Isotope	Decay mode, $T_{1/2}$	Energy [keV]	A μBq/ kg
^{49}V	EC, 330 d	no γ, E (K_α ^{49}Ti)=4.5	0.17
^{54}Mn	EC, 312.2 d	E_γ=1377.1 E (K_α ^{54}Cr)=5.99	0.20
^{55}Fe	EC, 2.73 a	no γ, E (K_α ^{55}Mn)=5.9	0.31
^{57}Co	EC, 271.3 d	136.5 (99.82%)E (K_α ^{57}Fe)=7.1	0.18
^{60}Co	β^-, 5.27 a	318 (99.88%), $E_{\gamma 1,2}$=1173.24, 1332.5	0.18
^{63}Ni	β^-, 100.1 a	E_{β^-}= 66.95 no γ	0.01
^{65}Zn	EC, 244.3 d	E_γ=1115.55 (50.6%),E (K_α ^{65}Cu)=8.9	1.14
^{68}Ge	EC, 288 d	E (K_α ^{68}Ga)=10.37, Q_{EC}(^{68}Ga)= 2921	101.4

Table 12. Cosmogenic produced isotopes in the Ge crystals for an exposure time at sea level of 10 days and for 3 years deactivation time (for ^{68}Ge an initial saturation activity was assumed).

space for neutralinos (see Fig. 5). After 5 years of deactivation the activity reduces to 14.7μBq/kg (5.3×10^{-3} events/kg y keV below 100 keV). At this point one can in addition reduce the contribution of ^{68}Ga by applying a time analysis method. ^{68}Ge decays through EC (100%) to the ground state of ^{68}Ga. The resulting line at 10.37 keV (88% K-capture) would be observed in GENIUS with an energy resolution of about 1 keV. Thus one could use an event with an energy of 10.37 keV as a trigger for subsequent events in the same detector during a few half-lives of ^{68}Ga ($T_{1/2}$ = 68.1 m), removing up to 88% of the ^{68}Ga caused events. With about 2.5 events per day and detector one would loose only 30% of the measuring time.

Another solution could be to process the germanium ore directly in an underground facility or to use high purity germanium which has already been stored for several years in an underground laboratory.

Figure 51 shows the sum and the single contributions from the different isotopes.

The sum of all contributions from the cosmogenic activation of the Ge crystals is 5.2×10^{-2} counts/(kg y keV) between 11 – 100 keV, for an activation time of 10 days at the Earths surface and a deactivation time of three years. Under the mentioned conditions, after 5 years of deactivation the background would be reduced to less than 1×10^{-2} counts/(kg y keV), allowing for the sensitivity for dark matter shown in Fig. 5. Since the cosmogenic activation of the Ge crystals will be the dominant background component in the low-energy region, special attention to short crystal exposure times at sea level is essential. The best solution would be to produce

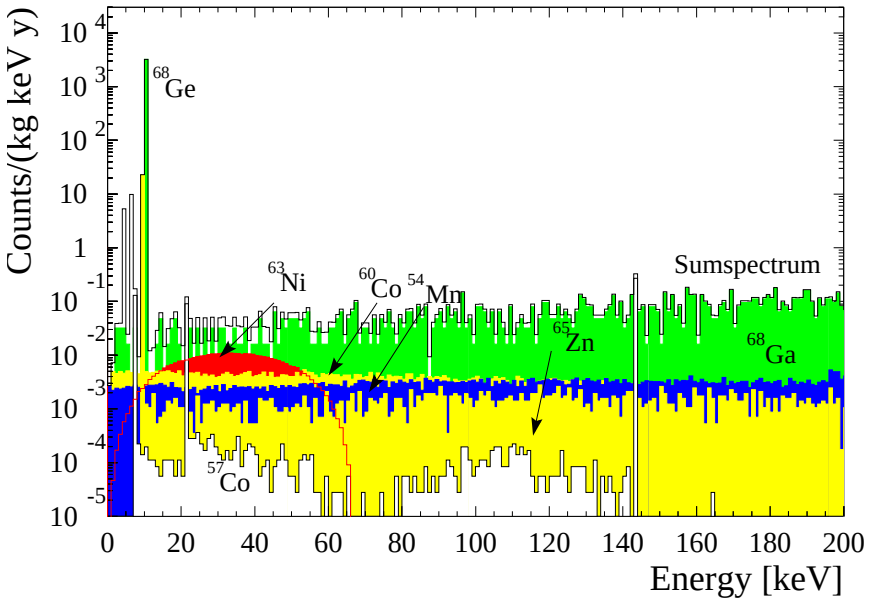

Figure 51. Background originating from cosmic activation of the Ge crystals at sea level with 10 days exposure and 3 years deactivation. For ^{68}Ge an initial saturation activity was assumed.

the detectors below ground and to apply strong shielding during the transportation.

The two–neutrino accompanied double beta decay of ^{76}Ge is not negligible in spite of the low abundance (7.8%) of this isotope in natural germanium. The contribution to the background after three years of measurement is shown in figure 52 . Due to the already high statistics reached in the Heidelberg–Moscow experiment [HM97], the half life and spectral form of the decay are well known and a subtraction of this part raises no difficulties. The statistical error of the subtraction is not shown in fig. 5.

The cosmogenic activation of the Ge crystals in the Gran Sasso laboratory is negligible in comparison to the assumed activation scenario at sea level.

3.6. Cosmic activation of the nitrogen at sea level

An estimation of the production rates of long–lived isotopes in the nitrogen at sea level reveals the importance of ^{7}Be, ^{10}Be, ^{14}C and ^{3}H. The neutron

flux at sea level is 8.2×10^{-3}cm^{-2}s^{-1} for neutron energies between 80 MeV and 300 MeV [All83]. Since we did not find measurements of the cross sections of neutron- induced spallation reactions in nitrogen, we assumed that at high neutron energies (10^2–10^4 MeV) the cross sections are similar to the proton-induced ones. For the reaction ^{14}N(n,tαn)^{7}Be the cross section is (9.0±2.1) mb at E_p = 450 MeV, (9.3±2.1) mb at E_p = 3000 MeV by [Rey81] and (13.3±1.3) mb at E_p = 1600 MeV by [Mic95]. For the reaction ^{14}N(n,αp)^{10}Be the cross sections are (1.5±0.4) mb at E_p = 450 MeV, (2.6±0.6) mb at E_p = 3000 MeV [Rey81] and (1.75±0.11) mb at E_p = 1600 MeV [Mic95].

Taking 10 mb for the ^{7}Be channel we obtain a production rate of 3.3×10^9d^{-1} in the whole tank. This corresponds with a realistic 10 days sea level exposure after production by fractional distillation to 4×10^8 decays per day. The simulation of this activity yields a count rate of about 10 events/(kg y keV) in the energy region between 0 – 100 keV. This is three orders of magnitude higher than the required level. However, a large fraction of ^{7}Be will removed from the liquid nitrogen at the cleaning process for Rn and in addition by underground storage ($T_{1/2}$=53.3 d) the contribution of ^{7}Be will be reduced to less than 10^{-2} events/(kg y keV).

For ^{10}Be, with σ= 2 mb, the production rate is 6.6×10^8d^{-1}, which is negligible due to the long half life of $T_{1/2}=1.6\times10^6$ y.

Tritium in nitrogen can be produced in the following reactions: ^{14}N(n,t)^{12}C, ^{14}N(n,t2α)^{4}He, ^{14}N(n,tαn)^{7}Be and ^{14}N(n,tn)^{11}C. The cross section for the production by ^{14}N(n,t)^{12}C was measured to be 40 mb [Kin70]. For a rough estimation, we assumed the same cross sections for the other reactions as for the production of ^{7}Be to be 10 mb. The total production rate of tritium corresponds to 2.3×10^{10}d^{-1}. With $T_{1/2}$=12.33 y, the activity after 10 days exposure at sea level would be 3.5×10^7d^{-1}. We simulated 10^{10} decays randomly distributed in the nitrogen tank. No events were detected mainly due to the absorption in the dead layer of the p–type Ge detectors.

The muon flux at sea level is 1.6×10^7m^{-2}d^{-1}. The only long–lived isotopes which are produced by inelastic muon scattering are ^{13}N and ^{10}C, with a production rate of about 3.7×10^7 atoms/days (taking σ = 500 μb for both reactions). However, ^{13}N and ^{10}C are of no relevance due to the short half lifes of 9.96 m and 19.3 s, respectively.

The isotopes produced through negative muon capture with half lifes > 1s are ^{14}C, ^{10}Be, ^{11}C and ^{10}C (see also table 9). Again, the number of ^{11}C and ^{10}C isotopes are soon reduced to a negligible level due to their short half lifes. The production rate for the whole tank for ^{14}C is 8×10^6d^{-1} and 4×10^5d^{-1} for ^{10}Be, which have to be added to the production rates by neutron capture or spallation reactions.

For the production of ^{14}C due to the ^{14}N(n,p)^{14}C capture reaction, three neutron sources at sea level are relevant. The flux of secondary cosmic ray neutrons with energies between a few keV and 20 MeV is about 2×10^{-2}cm^{-2}s^{-1}[All83]. These neutrons penetrate the wall of the transportation tank and are captured in the liquid nitrogen. For a tank surface of 678 m^2, about 1.3×10^5 s^{-1} neutrons are expected. The second component are neutrons produced in fast neutron spallation reactions in the liquid nitrogen. The production rate of these neutrons is 2×10^4 s^{-1} in the nitrogen tank [Lal88]. The third component are neutrons produced in muon reactions, which correspond to 0.85×10^3 s^{-1} [Lal88]. Thus the total flux at sea level is about 1.5×10^4 s^{-1}. Assuming that every neutron is captured in the nitrogen, yielding a ^{14}C nucleus, the production rate of ^{14}C is about 1.3×10^{10}d^{-1}. For a production and transportation time of ten days, the simulation yields less than 10^{-4} counts/(kg keV y) in the relevant energy region. Through the purification of the nitrogen this contribution will be further reduced.

3.7. Sum spectrum from simulations

In table 13 the components discussed so far are listed and summed up. Not included in the table are the contributions from the intrinsic impurities in the Ge crystals and from the ^{7}Be activation of the liquid nitrogen during its transportation at sea level. For the Ge–crystals we have only very conservative upper values for their true contamination, which is expected to be much lower (see Subsection 3.2.1). Regarding the ^{7}Be contamination of liquid nitrogen, the cleaning efficiency of the liquid nitrogen should already be high enough in order to reduce this contribution to a negligible level. Furthermore it is planned to use a recycling device for the evaporated nitrogen, thus the activation with ^{7}Be will be reduced further by storage ($T_{1/2}$ =53 d).

Assuming a background as stated above, we will achieve a mean count rate in the interesting region for dark matter search of about 6.1×10^{-2} events/(kg y keV). This means a further reduction of background in comparison to our best measurement (about 20 counts/(kg y keV) below 100 keV [HM98]) by more than two orders of magnitude. This count rate will further improve after another 2 years of running time (decay of ^{68}Ge), to reach a level of 1×10^{-2} events/(kg y keV). These results have been confirmed by an independent simulation for the GENIUS project by the Kiev group [Zde98].

In figure 52 the spectra of individual contributions and the summed-up total background spectrum are shown. As mentioned before, the low-energy spectrum is dominated by events originating from the cosmogenic activation of the Ge crystals at the Earths surface. Production of the detectors underground would significantly reduce this contribution.

Source	Component	[counts/(kg y keV)] 11–100 keV
Nitrogen	^{238}U	7×10^{-4}
intrinsic	^{232}Th	4×10^{-4}
	^{40}K	1×10^{-4}
	^{222}Rn	3×10^{-4}
N activation	^{14}C	1×10^{-4}
Steel vessel	U/Th	1.5×10^{-5}
Holder system	U/Th	8×10^{-4}
Surrounding	Gammas	4×10^{-3}
	Neutrons	4×10^{-4}
	Muon shower	2×10^{-3}
	$\mu \rightarrow$ n	1×10^{-3}
	$\mu \rightarrow$ capture	$<<1\times10^{-4}$
Cosmogenic	^{54}Mn	3×10^{-3}
activities	^{57}Co	1×10^{-4}
in the crystals	^{60}Co	4×10^{-3}
	^{63}Ni	6×10^{-3}
	^{65}Zn	1.5×10^{-3}
	^{68}Ge	3.7×10^{-2}
Total		6.1×10^{-2}

Table 13. Summation of background components in the region 11 keV–100 keV.

4. The GENIUS Facility: Technical Design

4.1. General description

The GENIUS detector will consist of two concentric stainless steel tanks with the Ge crystals positioned in the centre. The inner tank will contain liquid nitrogen as working medium for the Ge crystals and as shielding from the Gran Sasso rock backgrounds. The outer vessel will contain the isolation material, which will be doped with Boron as shielding against the neutron background. The Ge crystals will be placed on a holder system made of teflon, which can house up to six layers of 40 crystals each (see Fig. 53). On the top of the tank there will be a clean room with a lock chamber, a room for the elecronics and the data acquisition system and a muon veto shield.

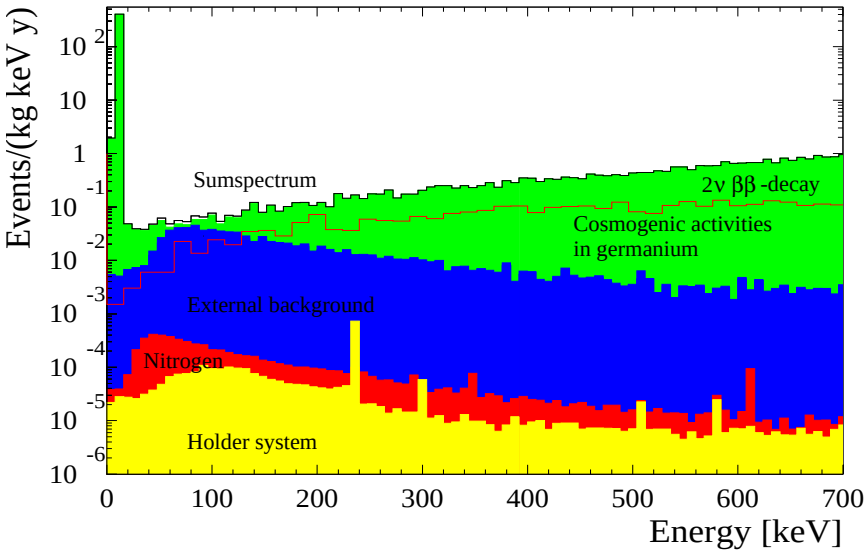

Figure 52. Simulated spectra of the dominant background sources for a nitrogen tank of 12 m diameter. Shown are the contributions from the tank walls, the detector holder system, from neutron capture in the nitrogen, from natural radioactivity and from the ^{222}Rn contamination of the nitrogen. The solid line represents the sum spectrum of all the simulated components (note the different channel binning compared to figure 51).

4.2. Technical Data

Capacity of the inner vessel = 1400000 l liquid nitrogen ≃ 95% of geom. vol.

Outer vessel:
Dimension: ⌀× H ≃ 14.4 m × 19 m
Roof type: round roof
Floor type: flat floor
Maximum allowed pressure: 10 mbar/ -2 mbar
Working pressure: 5 mbar
Design temperature: 77 K for the floor and 60% for the outer mantel, 293 K for the rest cylinder and roof

Inner vessel:
Dimension: ⌀× H ≃ 12 m × 13.6 m

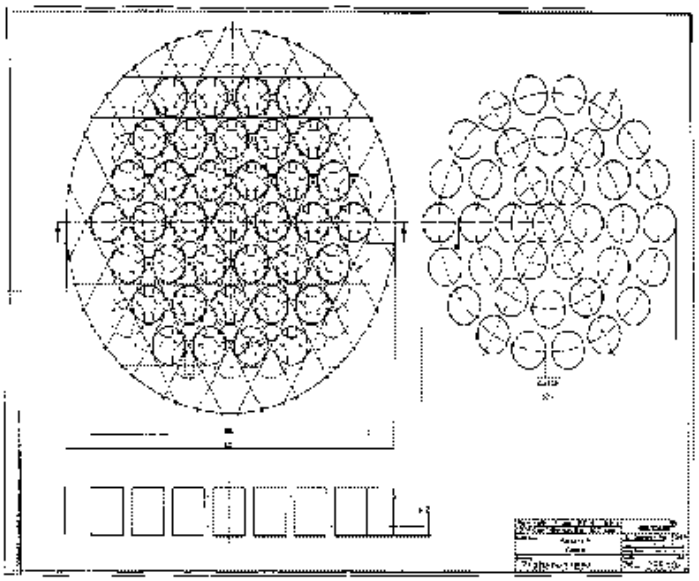

Figure 53. Schematic view of possible configurations for the holder system of the Ge crystals.

Roof type: round roof
Floor type: flat floor
Maximum allowed pressure: 100 mbar/ -2 mbar
Working pressure: 50 mbar
Design temperature: 77 K
Maximum waste gas through heat flow in: 0.27% / day of the max. content

4.3. Design

The standing, flat floor tank is made of an inner and an outer vessel in concentrical geometry. The inner vessel is storing the liquid nitrogen, the outer vessel the isolating material. A removement of the isolating material is possible. The fundament is shielded by polystyrol. The isolation will be flushed with gaseous nitrogen, thus preventing the immersion of humidity. The vessels are gas tight welded. Both inner and outer vessel are equipped with security devices against over and under pressure.

Figure 54 displays a schematic view of the GENIUS tank (the tank is lowered 4 m into the earth).

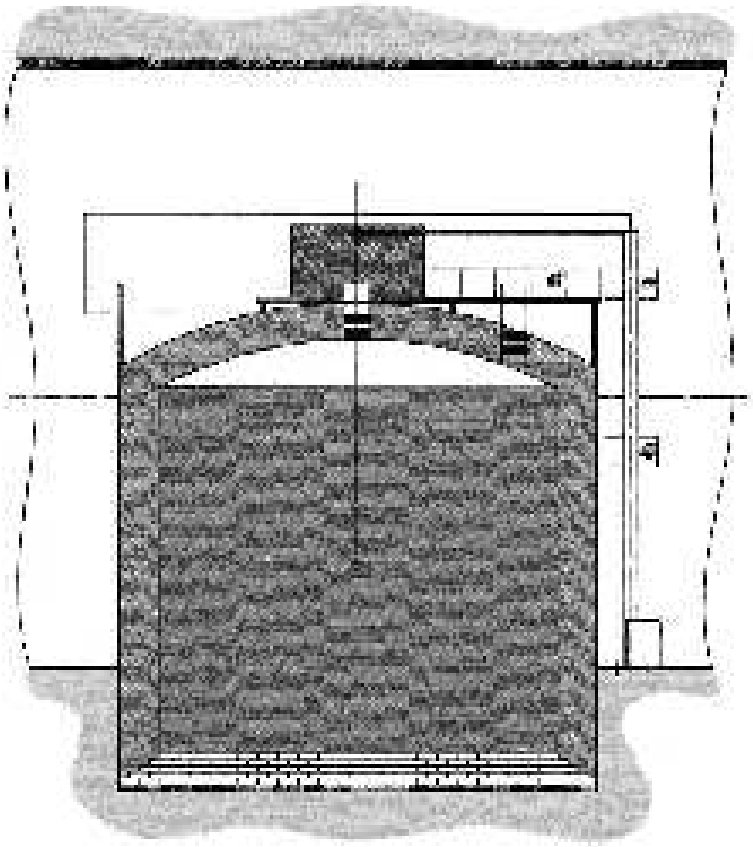

Figure 54. Design of the GENIUS tank. The tank is lowered 4m into the earth.

4.4. Time schedule of the GENIUS experiment

This schedule is valid under the assumptions, that the requested space is provided in the Gran Sasso Laboratory in near future and that detector production will start in the year 2000. It has been verified with potential producers, that technically and logistically the production of the required super-low level natural and enriched Ge detectors can be performed within the given time periods.

References

[Adh98] R. Adhikari, G. Rajasekaran, hep-ph/9812361vs3, Dec1998

Phase I: Dark Matter Search

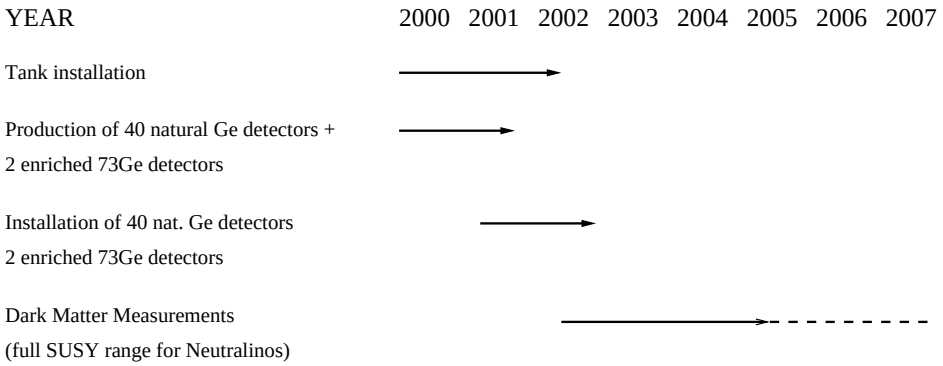

Phase II: Double Beta Decay Search

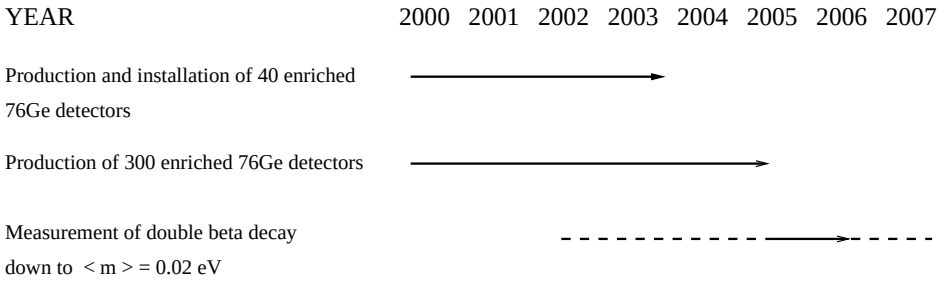

[Agl89] M. Aglietta et al., Il Nuovo Cimento C **12** (1989) 467

[Ake97] D.S. Akerib et al. (CDMS collab.), preprint astro-ph/9712343

[Ake98] D. S. Akerib et al., CDMS Collaboration, Nucl. Phys. B **70** (Proc. Suppl) (1998) 64

[Ale94] A. Alessandrello et al., Phys. Lett **B 335** (1994) 519

[Alc97] C. Alcock et al., ApJ **486** (1997) 697

[Ali98] G. Alimonti *et al.*, Borexino collaboration, Astr. Part. Phys. **8** (1998) 141 and Phys. Lett. B **422** (1998) 349.

[All83] O.C. Allkofer, P.K. Grieder, Cosmic Rays on Earth, Fachinformations-zentrum Karlsruhe, 1983

[Als89] M. Alston-Garnjost et al., Phys. Rev Lett. **71** (1993) 831

[Alt97] G. Altarelli, J. Ellis, G.F. Guidice, S. Lola, M.L. Mangano, preprint hep-ph/9703276

[Apo99] M. Apollonio et al. (CHOOZ collab.), hep-ex/9907037

[Ath96] C. Athanassopoulos *et al.*, LSND collab., Phys. Rev. **C 54** (1996) 2685, Phys. Rev. Lett. **77** (1996) 3082

[HdMo] Heidelberg–Moscow Collaboration, M. Günther et al., Phys. Rev. D **55** (1997) 54 and L. Baudis et al., Phys. Lett. **B 407** (1997) 219

[Arp92] C. Arpesella, Nucl. Phys. (Proc. Suppl.) **A 28** (1992) 420–424

[Arz94] F. Arzarello *et al.*, LPC/94-28 (CERN-LAA/94-19), J. Seguinot *et al.*, LPC/95-08 (CERN-LAA/95-11), J. Seguinot *et al.*, LPC/96-31 (CERN-LAA/96-05).

[Bab95] K.S. Babu, R.N. Mohapatra, Phys. Rev. Lett. **75** (1995) 2276

[Bab97a] K.S. Babu et al., preprint hep-ph/9703299 (March 1997)

[Bab97b] K.S. Babu *et al.*, preprint hep-ph/9705414v2 (1997)

[Bae97] H. Baer. M. Bhrlik, hep-ph/9706509

[Bah89] J.N. Bahcall, *Neutrino Astrophysics*, Cambridge University Press 1989

[Bah91] J.N. Bahcall, Phys. Rev. D **44** (1991) 1644

[Bah93] J.N. Bahcall, Phys. Rev. Lett. **71** (1993) 2369

[Bah95] J.N. Bahcall, M. Kamionkowski and A. Sirlin, Phys. Rev. D **51** (1995) 6146-6158

[Bah96] J.N. Bahcall, Astrophys. Journ. **467** (1996) 475

[Bah97] J.N. Bahcall and P.I. Krastev, Phys. Rev. C **56** (1997) 2839.

[Bah98] J.N. Bahcall, S. Basu and M. Pinsonneault, Phys. Lett. B **433** (1998) 1.

[Bah98a] J.N. Bahcall, P.I. Krastev, A.Yu. Smirnov, Phys. Rev. **D 58** (1998) 096016

[Bah98b] J.N. Bahcall, Nucl. Phys. **A 631** (1998) 29

[Bah98c] J.N. Bahcall, Phys. Lett. **B 433** (1998) 1

[Bam95a] P. Bamert, C.P. Burgess, R.N. Mohapatra, Nucl. Phys. **B 438** (1995) 3

[Bam95b] P. Bamert, C.P. Burgess, R.N. Mohapatra, Nucl. Phys. **B 449** (1995) 25

[Bar89] V. Barger, G.F. Guidice, T. Han. Phys.Rev. **D 40** (1989) 2987

[Bar93] S.D. Barthelmy *et al.*, AIP Conf. Proc. **280** (1993) 1166

[Bar94] S. D. Barthelmy et al., Astrophys. J. **427** (1994) 519

[Bar97] A.S. Barabash, Proc. NEUTRINO 96, Helsinki, June 1996, World Scientific, Singapore (1997), p. 374

[Bar98] G. Barenboim, F. Scheck, hep-ph/9808327

[Bas97] S. Basu *et al.*, Mon. Not. R. Astron. Soc. **292** (1997) 234.

[Bau97] L. Baudis, J. Hellmig, H.V. Klapdor–Kleingrothaus, A. Müller, F. Petry, Y. Ramachers, H. Strecker, Nucl. Inst. Meth. **A 385** (1997) 265

[Bau98] L. Baudis, G. Heusser, B. Majorovits, Y. Ramachers, H. Strecker, H.V. Klapdor–Kleingrothaus, hep-ex/9811040 and Nucl. Instr. Meth. **A 426** (1999) 425

[Bau99a] L. Baudis et al. (Heidelberg–Moscow collab.), hep-ex/9902014 and Phys. Rev. Lett. 83 (1999) 41-44.

[Bau99b] L. Baudis, H.V. Klapdor–Kleingrothaus, Eur. Phys. J. **A 5** (1999) 441 and hep-ex/9906044

[Bed94] V. Bednyakov, H.V. Klapdor–Kleingrothaus, S.G. Kovalenko, Phys. Lett. **B 329** (1994) 5 and Phys. Rev. **D 50** (1994) 7128

[Bed97a] V. Bednyakov, H.V. Klapdor–Kleingrothaus, S.G. Kovalenko, Phys. Rev. **D 55** (1997) 503

[Bed97b] V. Bednyakov, H.V. Klapdor–Kleingrothaus, S.G. Kovalenko, Y. Ramachers, Z. Phys. **A 357** (1997) 339

[Bed97c] V. Bednyakov, V.B. Brudanin, S.G. Kovalenko, Ts. D. Vylov, Mod. Phys. Lett. **A 12** (1997) 233

[Bed98] V. Bednyakov, A. Faessler, S. Kovalenko, hep-ph/9808224v2, Phys. Lett. **B 442** (1998) 203

[Bel96] G. Belanger, F. Boudjema, D.London, H. Nadeau, Phys. Rev. **D 53** (1996) 6292

[Bel98] G. Belanger, Proc. Int. Conf. on Lepton and Baryon Number Violation in Part. Phys. and Cosmology, Trento, Italy, april 20–25, 1998, editors: H.V. Klapdor-Kleingrothaus and I. Krivosheina (IoP, Bristol, 1999), p. 605.

[Bel89] P. Belli et al., Nuovo Cim., **101A** (1989) 959

[Ber82] L. Bergamasco et al., Il Nuovo Cimento A **67** (1982) 255

[Ber95] Z. Berezhiani, R.N. Mohapatra, Phys. Rev. **D 52** (1995) 6607

[Ber97a] R. Bernabei *et al.*, Phys. Lett. **B 389** (1997) 757

[Ber97b] R. Bernabei *et al.*, ROM2F/97/33; P. Belli at TAUP, Gran Sasso, Sept. 7 (1997)

[Ber98] R. Bernabei et al., Nucl. Phys. B **70** (Proc. Suppl) (1998) 79

[Ber98a] R. Bernabei et al., ROM2F/98/34, August (1998)

[Bha97] G. Bhattacharyya, in [Kla98], p. 194.

[Bha99] G. Bhattacharyya,H.V. Klapdor-Kleingrothaus, H. Päs, submitted to Phys. Lett. B.

[Bib99] K. van Bibber et al., Phys. Rev. Lett. **80** (1998) 2043

[Bil99] S.M. Bilenky *et al.*, Phys. Lett. **B 465** (1999) 193 and hep-ph/9907234

[Boc94] J. Bockholt, H.V. Klapdor–Kleingrothaus, Nucl. Phys. **B** (Proc. Suppl.) **35** (1994) 403

[Boc94a] J. Bockholt, PhD Thesis, University of Heidelberg 1994

[BOR91] Borexino Collaboration, Proposal for a real time detector for low energy solar neutrinos, Dept. of Physics of the University of Milano (1991).

[Bot97] A. Bottino *et al.*, Phys. Lett. **B 423** (1998) 109 and hep-ph/9709292

[Bot98] A. Bottino *et al.*, Phys. Rev. **D 59** (1999) 095003 and hep-ph/9808456

[Buc87] W. Buchmüller, R. Rückl and D. Wyler, Phys.Lett. **B 191** (1987) 442.

[Bue96] M. Bühler et al., NIM **A 370** (1996) 237

[Bur93] C.P. Burgess, J.M. Cline, Phys. Lett. **B 298** (1993) 141; Phys. Rev. **D 49** (1994) 5925

[Bur96] C.P.Burgess, in [Kla96a] p. 110

[Bur99] A. Burkert, in [DARK98] p. 375

[Bur99a] S. Burles, K.M. Nollet, J.N. Truram, M.S. Turner Phys. Rev. Lett. **82** (1999) 4176 and astro-ph/9901157

[But93] M. N. Butler *et al.*, Phys. Rev. **D47**, 2615 (1993); A. Halprin and C. N. Leung, Phys. Rev. Lett. **67**, 1833 (1991); J. Pantaleone, A. Halprin, and C. N. Leung, Phys. Rev. **D47**, R4199 (1993); K. Iida, H. Minakata and O. Yasuda, Mod. Phys. Lett. **A8** (1993) 1037.

[But93a] J. Butterworth, H. Dreiner, Nucl. Phys. **B397** (1993) 3 and H. Dreiner, P. Morawitz, Nucl. Phys. **B428** (1994) 31

[Cal93] D.O. Caldwell, R.N. Mohapatra, Phys. Rev. **D 48** (1993) 3259

[Car93] C.D. Carone, Phys. Lett. **B 308** (1993) 85

[Cha71] S. Charalambus, Nucl. Phys. **A 166** (1971) 145

[Cho97] D. Choudhury, S. Raychaudhuri, Phys. Lett. **B 401** (1997) 54 and preprint hep-ph/9702392

[Cli97] D. Cline, in: Proceedings of the *International Workshop Dark Matter in Astro– and Particle Physics* (DARK96), Eds. H.V. Klapdor–Kleingrothaus, Y. Ramachers, World Scientific 1997, p. 479

[Cle98] B.T. Cleveland et al., Astrophy. J. **496** (1998) 505

[Col97] S. Coleman and S.L. Glashow, Phys. Lett. **B 405**, 249 (1997).

[Cza99] M. Czakon, J. Gluza, M. Zralek, Phys. Lett. **B 465** (1999) 211 and hep-ph/9906381

[Dan95] F. A. Danevich et al., Phys. Lett. **B 344** (1995) 72

[DARK98] Proc. of the Second Int. Conference on Dark Matter in Astro– and Particle Physics (DARK98) July 1998, Heidelberg, Eds. H.V. Klapdor–Kleingrothaus and L. Baudis, (IOP , Bristol& Philadelphia, 1999).

[Dim87] S. Dimopoulos, L. Hall, Phys. Lett. **B207** (1987) 210; R. Godbole, P. Roy, X. Tata, Nucl. Phys. **B 401** (1993) 67.

[Dod96] S. Dodelson, E.I. Gates, M.S. Turner, Science **247** (1996) 69

[Doi85] M. Doi, T. Kotani, E.Takasugi, Progr. Theor. Phys. Suppl. **83** (1985) 1

[Doi93] M. Doi, T. Kotani, Progr. Theor. Phys. **89** (1993) 139

[Dre97] G. Drexlin, Proc. Internat. School on Neutrino Physics, Erice, Italy, Sept. 1997, Prog. Part. Nucl. Phys **40** (1998)

[Dre98] For recent studies, see M. Drees, S. Pakvasa, X. Tata and T. ter Veldhuis, Phys. Rev. **D 57** (1998) 5335 ; S. Rakshit, G. Bhattacharyya, A. Raychaudhuri, Phys. Rev. **D 59** (1999) 091701; R. Adhikari, G. Omanovic, Phys. Rev. **D 59** (1999) 073003; O. Kong, Mod. Phys. Lett. **A 14** (1999) 903; E.J. Chun, S.K. Kang, C.W. Kim, U.W. Lee, Nucl. Phys. **B 544** (1999) 89; K. Choi, K. Hwang, E.J. Chun, Phys. Rev. **D 60** (1999) 031301 and hep-ph/9811363; A. Joshipura, S. Vempati, Phys. Rev. **D 60** (1999) 111303 and hep-ph/9903435.

[Eis98] D.J. Eisenstein, W. Hu, M. Tegmark astro-ph/9807130, Submitted to ApJ.

[Ell87] S.R. Elliot, A.A. Hahn, M.K. Moe, Phys. Rev. Lett. **59** (1987) 1649

[Ell92] S. R. Elliott et al., Phys. Rev. **C 46** (1992) 1535

[ERO98] EROS collaboration, Astron. Astrophys. **332** (1998) 1

[Evr98] A. E. Evrard, Talk at the Second International Conference on Dark Matter in Astro- and Particle Physics, Heidelberg, 20–25 July 1998.

[Fal94] T. Falk, A. Olive, M. Srednicki, Phys. Lett. **B339** (1994) 248

[Fel98] G. J. Feldman and R. D. Cousins, Phys. Rev. **D57** (1998) 3873

[Fir96] R.B. Firestone *et al.*, *Table of Isotopes*, 8th Edition, J. Wiley & Sons, 1996.

[Fre88] K. Freese, J. Frieman, A. Gould, Phys. Rev. **D 37**, (1988) 3388

[Fre99] K. Freese, in [DARK98] p. 397

[Fri88] J.Friemann, H.Haber, K.Freese, Phys. Lett. **B 200** (1988) 115; J. Bahcall, S. Petcov, S. Toshev and J.W.F. Valle, Phys.Lett. **B 181** (1986) 369; Z. Berezhiani and M. Vysotsky, Phys. Lett. **B 199** (1988) 281.

[Fri95] H. Fritzsch and Zhi-zhong Xing, preprint hep-ph/9509389, Phys. Lett. **B 372** (1996) 265

[Fuc99] B. Fuchs, in [DARK98] p. 387.

[Fuk98a] Y. Fukuda et al. (SuperKamiokande Collaboration) Phys. Lett. **B 433** (1998) 9

[Fuk98b] Y. Fukuda et al. (SuperKamiokande Collaboration) Phys. Rev. Lett. **81** (1998) 1562

[Fuk99] Y. Fukuda *et al.*, Phys. Rev. Lett. **82** (1999) 1810

[Gai90] Th. Gaisser, Cosmic Rays and Particle Physics, Cambridge University Press, 1990.

[Gai98] R.J. Gaitskell et al., in [Kla98] p. 781

[GAL99] GALLEX collaboration, W. Hampel et al., Phys. Lett. **B 447** (1999) 127

[Gas89a] M. Gasperini, Phys. Rev. **D38** (1988) 2635; *ibid.* **D39** (1989) 3606.

[Gas89b] M. Gasperini, Phys. Rev. Lett. **62** (1989) 1945.

[Gaw98] E. Gawiser, J. Silk, Science **280** (1998) 1405-1411

[GEA93] GEANT3.21 Detector description and simulation tool, Geneva 1993

[Geo81] H.M. Georgi, S.L.Glashow and S. Nussinov, Nuc. Phys. **B 193** (1981) 297

[Giu99] C. Giunti, Phys. Rev. **D 61** (2000) 036002 and hep-ph/9906275 (June 1999)

[Gla87] S.L. Glashow and L.M. Krauss, Phys. Lett. **B 190** (1987) 199

[Gla97] S.L. Glashow, A. Halprin, P.I. Krastev, C.N. Leung, and J. Panteleone, Phys. Rev. **D 56**, 2433 (1997).

[Gon95] M. Gonzalez–Garcia, hep-ph/9510419, Int. Workshop on 'Elementary Part. Phys., Present and Future', Valencia, Spain, 5-9 june (1995)

[Goo61] M.L. Good, Phys. Rev. **121** (1961) 311; O. Nachtmann, Acta Physica Austriaca, Supp. VI *Particle Physics* ed. P. Urban, (1969) p. 485; S.H. Aronson, G.J. Bock, H-Y Cheng and E. Fishbach, **48** (1982) 1306; Phys. Rev. **D28** (1983) 495; I.R. Kenyon, Phys. Lett. **B237** (1990) 274; R.J. Hughes, Phys. Rev. **D46** (1992) R2283;

[Gro90] K. Grotz, H.V. Klapdor, 'The Weak Interaction in Nuclear, Particle and Astrophysics' (Adam Hilger: Bristol, Philadelphia) 1990

[Gri99] K. Griest, in [DARK98], p. 418.

[H196] H1 Collab., S. Aid et al., Phys. Lett. **B 369** (1996) 173

[Hab93] H. E. Haber, in Proc. on Recent Advances in the Superworld, Houston, April 14-16 (1993), hep-ph/9308209

[Hag90] C. Hagmann et al., Phys. Rev. **D 42** (1990) 1297

[Hal84] L. Hall, M. Suzuki, Nuclear Physics **B 231** (1984) 419

[Hal91] A. Halprin and C.N. Leung, Phys. Rev. Lett. **67** (1991) 1833; Nucl. Phys. **B28A** (Proc. Supp.) (1992) 139; J. N. Bahcall, P. I. Krastev, and C. N. Leung, Phys. Rev. **D 52** (1995) 1770; R.B. Mann and U. Sarkar, Phys. Rev. Lett **76** (1996) 865;

[Hal96] A. Halprin, C.N. Leung, J. Pantalone, Phys.Rev. **D 53** (1996) 5365

[Ham98] T. Hambye, R.B. Mann and U. Sarkar, Phys. Lett. **B 421**, 105 (1998); Phys. Rev. **D 58** (1998) 025003.

[Hat94] N. Hata, P. Langacker, Phys. Rev. **D 50** (1994) 632

[Hel97] J. Hellmig, H.V. Klapdor–Kleingrothaus, Z. Phys. **A 359** (1997) 351

[Heu91] G. Heusser, Nucl. Instr. and Meth. in Phys. Res. **B 58** (1991) 79

[Heu95] G. Heusser, Ann. Rev. Nucl. Part. Sci. **45**, (1995) 543

[Hew97] J.L. Hewett, T.G. Rizzo, preprint hep-ph/9703337v3 (May1997) and Phys. Rev. **D 56** (1997) 5709-5724.

[Hir95a] M. Hirsch, H.V. Klapdor–Kleingrothaus, S.G. Kovalenko, Phys. Rev. Lett. **75** (1995) 17

[Hir95b] M. Hirsch, H.V. Klapdor–Kleingrothaus, S. Kovalenko, Phys. Lett. **B 352** (1995) 1

[Hir96a] M. Hirsch, H.V. Klapdor–Kleingrothaus, S.G. Kovalenko, Phys. Lett. **B 372** (1996) 181, Erratum: Phys. Lett. **B381** (1996) 488

[Hir96b] M. Hirsch, H.V. Klapdor–Kleingrothaus, S.G. Kovalenko, Phys. Lett. **B 378** (1996) 17 and Phys. Rev. **D 54** (1996) R4207

[Hir96c] M. Hirsch, H. V. Klapdor–Kleingrothaus, S. G. Kovalenko, H. Päs, Phys. Lett. **B 372** (1996) 8

[Hir96d] M. Hirsch, H.V. Klapdor–Kleingrothaus, S. Kovalenko, Phys. Rev. **D 53** (1996) 1329

[Hir96e] M. Hirsch, H.V. Klapdor–Kleingrothaus, in [Kla96a] p. 91, M. Hirsch, H.V. Klapdor–Kleingrothaus, O. Panella, Phys. Lett. **B 374** (1996) 7

[Hir97a] M. Hirsch, H.V. Klapdor–Kleingrothaus, S.G. Kovalenko, Phys. Lett. **B 398** (1997) 311 and **B 403** (1997) 291

[Hir97b] M. Hirsch, H.V. Klapdor–Kleingrothaus, S. Kovalenko, in [Kla98] p. 237

[Hir97c] M. Hirsch, H.V. Klapdor–Kleingrothaus, Proc. Int. Workshop on Dark Matter in Astro– and Particle Physics (DARK96), Heidelberg, Sept. 1996, Eds. H.V. Klapdor–Kleingrothaus and Y. Ramachers (World Scientific, Singapore) 1997, p. 640

[Hir98a] M. Hirsch, H.V. Klapdor–Kleingrothaus, St. Kolb, S.G. Kovalenko, Phys. Rev. **D 57** (1998) 2020

[Hir98b] M. Hirsch, H.V. Klapdor–Kleingrothaus, S.G. Kovalenko, Phys. Rev. **D 57** (1998) 1947

[HM94] HEIDELBERG–MOSCOW collab., Phys. Lett. **B 336** (1994) 141

[HM95] HEIDELBERG–MOSCOW collab., Phys. Lett. **B 356** (1995) 450

[HM96] HEIDELBERG–MOSCOW collab., Phys. Rev. **D 54** (1996) 3641,

[HM97] HEIDELBERG–MOSCOW collab., Phys. Rev. **D 55** (1997) 54 and Phys. Lett. **B 407** (1997) 219

[HM98] HEIDELBERG–MOSCOW collab., L. Baudis et al., Phys. Rev. **D 59** (1998) 022001-1

[HM2000] HEIDELBERG–MOSCOW collab., preprint, 2000.

[Hug60] V.W. Hughes, H.G. Robinson, and V. Beltran-Lopez, Phys. Rev. Lett. **4** (1960) 342; R.W.P. Drever, Philos. Mag. **6** (1961) 683; D. Newman, G.W. Ford, A. Rich and E. Sweetman, Phys. Rev. Lett. **40** (1978) 1355; A. Brillet and J.L. Hall, Phys. Rev. Lett. **42** (1979) 549; J.D. Prestage, J.J. Bollinger, W.M. Itano, and D.J. Wineland, Phys. Rev. Lett. **54** (1985) 2387; S.K. Lamoureaux, J.P. Jacobs, B.R. Heckel, R.J. Raab, and E.N. Fortson, Phys. Rev. Lett. **57** (1986) 3125.

[Hyk91] J.G. Hykawy *et al.*, Phys. Rev. Lett **67** (1991) 1708.

[Ioa94] A. Ioanissyan, J.W.F. Valle, Phys. Lett **B 322** (1994) 93

[Joer94] V. Jörgens et al., Nucl. Phys. (Proc. Suppl.) **B 35** (1994) 378

[Jun96] G. Jungmann, M. Kamionkowski, K. Griest, Phys. Rep. **267** (1996) 195

[Kaj99] T. Kajita, in Proc. Beyond'99, 'Beyond the Desert', 'Accelerator and Non-accelerator and Space Approaches', Tegernsee, Germany, june 6-12, 1999, ed. H.V. Klapdor–Kleingrothaus and I.V. Krivosheina, IoP, Bristol (2000)

[Kal97] J. Kalinowski et al., Z. Phys. **C 74** (1997) 595 and preprint hep-ph/9703288v2 (March 1997)

[KAM89] KAMIOKANDE II collaboration, K.S. Hirata et al., Phys. Rev. Lett. **63** (1989) 16

[Kam99] M. Kamionkowski, in [DARK98], p. 461.

[Kan97] G. Kane, in [Kla98] p. 151

[Kin70] G.P. Kincaid, E. R. Ibert jun., Nature **226** (1970) 139

[Kla87] H.V. Klapdor–Kleingrothaus, MPI–H 1987, proposal.

[Kla91] H.V. Klapdor–Kleingrothaus, Proc. Int. Symposium on γ-Ray Astrophysics, Paris 1990, AIP Conf. Proc. **232** (1991) 464

[Kla92] H.V. Klapdor–Kleingrothaus, K. Zuber, Phys. Bl. **48** (1992) 1017

[Kla94] H.V. Klapdor–Kleingrothaus, Progr. Part. Nucl. Phys. **32** (1994)261

[Kla95] H. V. Klapdor–Kleingrothaus, A. Staudt, Non–Accelerator Particle Physics, IOP Publ., Bristol, Philadelphia, 1995; and Teilchenphysik ohne Beschleuniger, Teubner Verlag, Stuttgart, 1995

[Kla96a] H.V. Klapdor–Kleingrothaus and S. Stoica (Eds.), Proc. *Int. Workshop on Double Beta Decay and Related Topics*, Trento, 24.4.–5.5.95, World Scientific Singapore

[Kla96b] H.V. Klapdor–Kleingrothaus, in Proc. *Int. Workshop on Double Beta Decay and Related Topics*, Trento, 24.4.–5.5.95, World Scientific Singapore 1996, Ed.: H.V. Klapdor–Kleingrothaus and S. Stoica p. 3

[Kla97a] H.V. Klapdor–Kleingrothaus, Invited talk at NEUTRINO 96, Helsinki, June 1996, World Scientific Singapore 1997, p. 317

[Kla97b] H.V. Klapdor–Kleingrothaus, M.I. Kudravtsev, V.G. Stolpovski, S.I. Svertilov, V.F. Melnikov, I. Krivosheina, J. Moscow. Phys. Soc. **7** (1997) 41

[Kla97c] H.V. Klapdor–Kleingrothaus, M. Hirsch, Z. Phys. **A 359** (1997) 361

[Kla97d] H.V. Klapdor–Kleingrothaus, Y. Ramachers, in: Proc. Int. Workshop on Dark Matter in Astro– and Particle Physics (DARK96) Sept. 1996, Eds. H.V. Klapdor–Kleingrothaus and Y. Ramachers, Heidelberg, (World Scientific Singapore) 1997, p. 459

[Kla98] H.V. Klapdor–Kleingrothaus and H. Päs (Eds.), Beyond the Desert – Accelerator- and Non–Accelerator Approaches, Tegernsee, Germany, june 8-14, 1997, IOP, Bristol, 1998

[Kla98a] H.V. Klapdor–Kleingrothaus, in [Kla98], p. 485.

[Kla98b] H.V. Klapdor–Kleingrothaus, Int. J. Mod. Phys. **A 13** (1998) 3953-3992

[Kla98c] H.V. Klapdor–Kleingrothaus, J. Hellmig, M. Hirsch, J. Phys. **G 24** (1998) 483-516

[Kla98d] H.V. Klapdor–Kleingrothaus, Y. Ramachers, Eur. Phys. J. **A 3** (1998) 85

[Kla98e] H.V. Klapdor–Kleingrothaus, H. Päs; in: Proc. of the 6th Symp. on Particles, Strings and Cosmology (PASCOS'98), Boston/USA, 1998

[Kla98f] H.V. Klapdor–Kleingrothaus, H. Päs, U. Sarkar, Eur. Phys. J. **A 5** (1999) 3, and hep-ph/9809396

[Kla98g] H.V. Klapdor–Kleingrothaus, Proc. NEUTRINO'98 ed. Y. Suzuki and Y. Totsuka, (Takayama,Japan,June 1998) World Scientific, Singapore (1999) p. 357

[Kla98h] H.V. Klapdor–Kleingrothaus et al., Adv. Space Res. **21** (1998) 347

[Kla98i] H.V. Klapdor–Kleingrothaus , Y. Zdesenko, Eur. Phys. J. **A 3** (1998) 107

[Kla99a] H.V. Klapdor–Kleingrothaus, Proc. LEPTON and BARYON NUMBER VIOLATION in Particle Physics, Astrophysics and Cosmology, Trento, Italy, 20-25 April 1998, eds. H.V.Klapdor-Kleingrothaus and I.V.Krivosheina, IOP, (1999) 251

[Kla2000] H.V. Klapdor–Kleingrothaus, H. Päs, A.Yu. Smirnov, hep-pf/0003219

[Kol94] E. W. Kolb and M. S. Turner, *The Early Universe* (Addison-Wesley, Reading MA, 1994).

[Kol99] E. W. Kolb in [DARK98] p. 592

[Kol97] S. Kolb, M. Hirsch, H.V. Klapdor–Kleingrothaus, Phys. Rev. **D 56** (1997) 4161

[Kno98] G. F. Knoll, Radiation Detection and Measurement, 2. ed., Wiley, 1989

[Kuc95] R. Kuchimanchi, R.N. Mohapatra, Phys. Rev. Lett. **75** (1995) 3939

[Kum96] K. Kume (ELEGANT collaboration), in [Kla96a] p. 490

[Kus99] A. Kusenko in [DARK98] p. 626

[Kuz90] V. Kuzmin, V. Rubakov, M. Shaposhnikov, Phys. Lett. **B 185** (1985) 36; M. Fukugita, T. Yanagida, Phys. Rev. **D 42** (1990) 1285; G. Gelmini, T. Yanagida, Phys. Lett. **B 294** (1992) 53; B. Campbell *et al.*, Phys. Lett. **B 256** (91) 457

[Lal88] D. Lal, Ann. Rev. Earth Planet. Sci. **16** (1988) 355–388

[Lan88] P. Langacker, in 'Neutrinos' (Springer: Heidelberg, New York), 1988, ed. H.V. Klapdor, p. 71

[Lan87] R.E. Lanou *et al.*, Phys. Rev. Lett **58** (1997) 2498, S.R. Bandler *et al.*, Phys. Rev. Lett. **74** (1995) 3169.

[Lee94] D.G. Lee, R.N. Mohapatra, Phys. Lett. **B 329** (1994) 463

[LEN99] LENS collaboration, Letter of Intent, LNGS, Italy 1999.

[Loh85] W. Lohmann, R. Kopp, R. Voss, Energy loss of muons in the energy range 1–10000 GeV, CERN 85-03, Geneva 1985.

[Lou98] W.C. Louis, priv. comm.

[Ma99] E. Ma, Phys. Rev. Lett. **83** (1999) 2514 and hep-ph/9902392

[Mai96] B. Maier, PhD Thesis, University of Heidelberg 1996

[Mat94] S. Matsuki et al., Phys. Lett. **B 336** (1994) 573

[McL88] V. McLane, C.L. Dunford, P.F. Rose, Neutron cross sections, Volume 2, Academic Press Inc., 1988

[MSW85] S.P. Mikheyev, A.Yu. Smirnov, Yad. Fiz. **42** (1985) 1441 and L. Wolfenstein, Phys. Rev. **D 17** (1978) 2369

[Mic95] R. Michel et al., NIM **B 103** (1995) 183

[Min97] H. Minakata, O. Yasuda, hep-ph/9712291

[Min99] H. Minakata, H. Nunokawa, Phys. Rev. **D 59** (1999) 073004, Nucl. Phys **B 523** (1998) 597

[Moe91] M. K. Moe, Phys. Rev. **C 44** (1991) R931

[Moe94] M. K. Moe, Prog. Part. Nucl. Phys. **32** (1994) 247; Nucl. Phys. (Proc. Suppl.) **B 38** (1995) 36

[Moh86a] R.N. Mohapatra, Phys. Rev. **D 34** (1986) 3457

[Moh86b] R.N. Mohapatra, Phys. Rev. **D 34** (1986) 909

[Moh88] R.N. Mohapatra and E. Takasugi, Phys. Lett. **B 211** (1988) 192

[Moh91] R.N. Mohapatra, P.B. Pal, 'Massive Neutrinos in Physics and Astrophysics' (World Scientific, Singapore) 1991

[Moh92] R.N. Mohapatra, Unification and Supersymmetry (Springer: Heidelberg, New York) 1986 and 1992

[Moh94] R.N. Mohapatra, Progr. Part. Nucl. Phys. **32** (1994) 187

[Moh95] R.N. Mohapatra, S. Nussinov, Phys. Lett. **B 346** (1995) 75

[Moh96a] R.N. Mohapatra, A. Rasin, Phys. Rev. Lett. **76** (1996) 3490 and Phys. Rev. **D54** (1996) 5835

[Moh96b] R.N. Mohapatra, in [Kla96a] p. 44

[Moh97a] R. N. Mohapatra, Proc. *Neutrino 96*, Helsinki, 1996, World Scientific Singapore, 1997, p. 290

[Moh97b] R.N. Mohapatra, Proc. Int. School on Neutrinos, Erice, Italy, Sept. 1997, Progr. Part. Nuc. Phys. **40** (1998)

[Mon99] M. Moniez, in [DARK98] p. 425.

[Mue93] A. Müller, PhD Thesis, University of Heidelberg 1993

[Mut88] K. Muto, H.V. Klapdor, in 'Neutrinos (Springer: Heidelberg, New York) 1988, ed. H.V. Klapdor, p. 183

[Mut89] K. Muto, E. Bender, H.V. Klapdor, Z. Phys. **A 334** (1989) 177, 187.

[Nap73] V. di Napoli, Phys. Rev. C **8** (1973) 206

[Nar95] E. Nardi *et al.*, Phys. Lett. **B 344** (1995) 225

[NEM94] NEMO Collaboration, Nucl. Phys. (Proc. Suppl.) **B 35** (1994) 369

[Nor97] D. Normile, Science **276** (1997) 1795

[OCo88] J.S. O'Connell, F.J. Schima, Phys. Rev. D **38** (1988) 2277

[Päs96] H. Päs *et al.*, in [Kla96a] p. 130

[Päs97] H. Päs, M. Hirsch, H.V. Klapdor–Kleingrothaus, S.G. Kovalenko, in [Kla98] p. 884

[Päs99] H. Päs, M. Hirsch, H.V. Klapdor–Kleingrothaus, S.G. Kovalenko, Phys. Lett. **B 453** (1999) 194

[Päs99b] H. Päs, M. Hirsch, H.V. Klapdor–Kleingrothaus, Phys. Lett. **B 459** (1999) 450

[Pan96] O.Panella, in [Kla96a] p. 145

[Pan97a] O. Panella, in [Kla98] p. 339

[Pan96b] G. Pantis, F. Simkovic, J.D. Vergados, A. Faessler, Phys. Rev. **C 53** (1996) 695

[Pan99] O. Panella *et al.*, hep-ph/9903253v2

[Pan87] S. DePanfilis et al., Phys. Rev. Let. **59** (1987) 839

[PDG94] Particle Data Group, Phys. Rev. **D 50** (1994)

[PDG98] Particle Data Group, Eur. Phys. J. **C 3** (1998) 1

[Pel93] J. Peltoniemi, J. Valle, Nucl. Phys. **B 406** (1993) 409

[Pel95] J.T. Peltoniemi, preprint hep-ph/9506228

[Per98] S. Perlmutter et al., Nature **391** (1998) 51.

[Per92] M. Persic and P. Salucci, Mon. Not. R. Astron. Soc. **285** (1992).

[Pet94] S.T. Petcov, A.Yu. Smirnov, Phys. Lett. **B 322** (1994) 109

[Pet96] S. Petcov, in [Kla96a] p. 195

[Piq96] F. Piquemal *et al.*, in [Kla96a] p. 496

[Pri98] J.R. Primack, M.A.K. Gross, in Proc. Xth Recontrees de Blois 'The birth of galaxies', june 28- july 4, 1998 and astro-ph/9810204

[Rag94] R. S. Raghavan, Phys. Rev. Lett. **72** (1994) 1411

[Rag97] R.S. Raghavan, Phys. Rev. Lett. **78** (1997) 3618.

[Rau99] W. Rau, private communication.

[Rey81] J.L. Reyss, Y. Yokoyama and F. Guichard, Earth and Plan. Sci. Let. **53** (1981) 203

[Rie98] A. Riess et al., Astron. Journ. **116** (1998) 1009

[Riz96] T.G. Rizzo, hep/ph/9612440

[Roy92] D.P. Roy, Phys.Lett. **B 283** (1992) 270

[SAG99] SAGE collaboration, J.N. Abdurashitov et al., Phys. Rev. Lett. **83** (1999) 4686 astro-ph/9907131.

[Sch81] J. Schechter, J.W.F. Valle, Phys. Rev. **D 25** (1982) 2951

[Sik83] P. Sikivie, Phys. Rev. Lett. **51** (1983) 1415 and Phys. Rev. **D 49** (1985) 2988.

[Smi96] A. Yu. Smirnov, Proc. Int. Conf. on High Energy Physics, Warsaw 1996, hep-ph/9611465v2 (Dec 1996)

[Smi99] A. Yu. Smirnov, Proc. 5th International WEIN Symposium: A Conference on Physics Beyond the Standard Model (WEIN 98), Santa Fe, NM, June 14–21, 1998 ed. P. Herczeg, C.M. Hoffman and H. V. Klapdor–Kleingrothaus, p. 180 and hep-ph/9901208

[Sno97] SNO Collaboration, Proceedings of the 4th International Solar Neutrino Conference (Heidelberg, April 8-11 1997), edited by W. Hampel, (1997) 210

[Sou92] I.A. D'Souza. C.S. Kalman, Preons, Models of Leptons , Quarks and Gauge bosons as Composite Objects (World Scientific, Singapore) 1992

[Sta90] A. Staudt, K.Muto, H.V. Klapdor–Kleingrothaus, Europhys. Lett. **13** (1990) 31

[SK98] The Super-Kamiokande Collaboration, Y. Fukuda et al, Phys. Rev. Lett. **81** (1998) 1562.

[Suz97] A. Suzuki, priv. comm. 1997, and KAMLAND proposal, (in Japanese)

[Tak96] E.Takasugi, in [Kla96a] p. 165

[Tak97] E. Takasugi, in [Kla98] p. 360

[Tre95] V.I. Tretyak, Yu. Zdesenko, At. Data Nucl. Data Tables **61** (1995) 43

[Tur99] M. S. Turner, in *Physica Scripta*, Proceedings of the Nobel Symposium, Particle Physics and the Universe (Enkoping, Sweden, August 20-25, 1998) and hep-ph/9901109.

[Val96] J.W.F. Valle, in [Kla96a] p. 69

[Vis99] F. Vissani, JHEP **9906** (1999) 022 and hep-ph/9906525

[Vui93] J.-C. Vuilleumier et al., Phys. Rev. **D 48** (1993) 1009

[Wil92] C. M. Will, *Theory and Experiment in Gravitational Physics*, 2nd edition (Cambridge University Press, Cambridge, 1992).

[Whi93] S.D.M. White et al., Nature **366** (1993) 429

[Wol81] L. Wolfenstein, Phys. Lett **107 B** (1981) 77

[You95] Ke You et al., Phys. Lett. **B 265** (1995) 53

[Zde98] Yu. Zdesenko et al., in [DARK98] p. 738

[Zub98] K. Zuber, hep-ex/9810022.